## *Photoconductivity in conjugated polymers*

Sitch, Corin David

# Photoconductivity in Conjugated Polymers

**By**

**Corin David Sitch**



A thesis submitted to the Faculty of Science at the University of Durham for the degree of Master of Science.

Department of Physics

University of Durham

2001

# Declaration

The material in this thesis has not been submitted for examination for any degree or part thereof at the University of Durham or any other institution. The material contained in this thesis is the work of the author except where formally acknowledged by reference.

# Acknowledgements

I would like to thank my Mom and Dad without whom I would not have made it here. I would also like to say a big thanks to my wife who has kept me going and given me so much encouragement when I was ready to quit and become a postman.

Dr. Douglas Halliday and Dr. Andy Monkman have been a great help and have always been patient, even when I ask the same dumb questions again and again.

The condensed matter research group technicians, Dave and Norman, have always been very friendly and have been very helpful and never complained no matter what I broke. I would also like to thank the guys in the electrical workshop and the mechanical workshop.

I would also like to say thanks to all the members of the Organic Electroactive Materials Research Group for putting up with me for three years.

# Abstract

This thesis reports the results of photoconductivity experiments on films of the conjugated polymers poly(2-methoxy-5- (2'ethylhexyloxy)-1,4-phenylene vinylene) (MEH-PPV), poly(2,5-pyridinediyl) (PPY) and poly(9,9-bis(2-ethyl hexyl)fluorene-2,7-diyl) (PF2/6) sandwiched between gold and indium tin oxide on a glass substrate. The methods used to fabricate the sandwich structures, the photoconductivity methods used and the procedures used to normalise the data are described.

Results indicate that, at photon energies appropriate to the fundamental absorption of the particular polymer, the absorption of photons leads to the formation of excitons. These excitons can be extrinsically dissociated at an electrode to give free charge carriers. These free charge carriers then give rise to a photocurrent. At photon energies above the fundamental absorption of the conjugated polymer, free charge carriers are intrinsically generated in the bulk polymer. The polymer film thickness and the relative mobilities of electrons and holes in the conjugated polymers influence the spectral response of the photocurrent. In MEH-PPV, the hole mobility is one order of magnitude greater than the electron mobility. The effects of charge carrier mobility explain the temperature dependence of the photocurrent spectra for MEH-PPV samples. The charge carrier generation mechanism explains the electric field dependence of the photocurrent spectra for MEH-PPV samples. The electron mobility is greater than the hole mobility in PPY and this is confirmed by photoconductivity experiments. A comparison of the spectra obtained from photoconductivity experiments in PF2/6 and PPY suggest that excitations involving the nitrogen atom in the PPY molecule occur producing additional features in the photocurrent spectra.

# Table of Contents

# Chapter 1

# Introduction



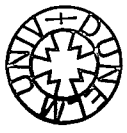

The discovery of electrical conductivity in the conjugated polymer polyacetylene in 1977 [1] sparked off a revolution in material science. Many advances have occurred in the last decade since the report of electroluminescence (EL) in poly(p-phenylenevinylene) (PPV) in 1990 [2]. A key feature of conjugated polymers is their ease of processibility. They can be processed from solution to give large area films. This has great potential value in the field of flat panel displays. Pioneer has produced monochrome displays and Philips, Pioneer, Uniax and Kodak have demonstrated multicolour displays. Chemical tuning of conjugated polymers can give a wide range of properties. For example, PPV has many derivatives that have been used in LED research. The use of conjugated polymers as the active layer in light emitting diodes (LED's) is well documented. A great deal of research has been done to increase our understanding of this application of conjugated polymers [2-16].

An understanding of transport mechanisms is essential to our understanding of conjugated polymers and in their development for optoelectronic device applications. The use of current-voltage measurements to investigate this aspect of conjugated polymers is well documented. Fowler-Nordheim tunnelling [12], Schottky injection [17], space charge limited conduction [16] and hopping [18] are a few of the current theories to explain the results observed but no consensus has been reached.

Photoconductivity measurements provide a means of probing the mechanisms of charge generation in these polymers. A description of charge generation in conjugated polymers using the semiconductor band model was applied to polyacetylene $(CH)_x$ by Su, Schreiffer and Heeger [19]. In the band model, absorption of a photon directly gives free charge carriers. Heeger and co-

workers cited the onset of photoconductivity with onset of absorption as evidence for the band model. The work by Barth *et al.* has increased our understanding of the effects of electrodes on optical carrier generation. They have shown that the absorption of a photon leads to the creation of an exciton that can be dissociated at an electrode to give free charge carriers. The exciton model accounts for the effects that Heeger and co-workers use to support the band model. It is now generally accepted that the exciton model is more appropriate than the band model– a point of contention for many years [20-27].

The present study involves the use of steady state photoconductivity experiments to elucidate the mechanisms of charge generation and transport in a number of conjugated polymers.

Chapter 2 gives a summary of the physics and chemistry applicable to the understanding of conjugated polymers. The first part of the chapter covers aspects of quantum theory and spectroscopy that are germane to the experimental work performed. The second part of the chapter covers molecular orbital theory and bonding including hybridisation and conjugation. The next part of the chapter covers benzene and the conjugated polymers used in this work. The last part of the chapter covers excitons and the present theories of charge generation and transport.

Chapter 3 covers the experimental techniques used in this investigation. The fabrication techniques used for sample preparation are presented. The method used for photoconductivity experiments and the data normalisation procedures are also presented.

The results of photoconductivity experiments on poly(2-methoxy-5-(2'ethylhexyloxy)-1,4-phenylene vinylene) (MEH-PPV) samples are discussed in

Chapter 4. This includes the photon energy, electric field and temperature dependence of the photocurrent. Photoconductivity experiments on poly(2,5-pyridinediyl) (PPY) samples are discussed in Chapter 5. Photoconductivity spectra of poly(9,9-bis(2-ethyl hexyl)fluorene-2,7-diyl) (PF2/6) and PPY are compared in chapter 6

The final chapter, Chapter 7, gives a summary of the experiments undertaken and the conclusions drawn. Ideas for further experiments are then given.

# References


1. C. Chiang, C.R. Fincher, Y.W. Park, A.J. Heeger, H. Shirakawa, E.J. Louis, S.C. Gau, and A.G. MacDiarmid, *Physical Review Letters*, **39** 1098-1101 (1977).
2. J.H. Burroughes, D.D.C. Bradley, A.R. Brown, R.N. Marks, K. Mackay, R.H. Friend, P.L. Burns, and A.B. Holmes, *Nature*, **347** 539-541 (1990).
3. P.W.M. Blom and M. Vissenberg, *Materials Science & Engineering R-Reports*, **27** 53-94 (2000).
4. A.R. Brown, D.D.C. Bradley, J.H. Burroughes, R.H. Friend, N.C. Greenham, P.L. Burn, A.B. Holmes, and A. Kraft, *Applied Physics Letters*, **61** 2793-2795 (1992).
5. S. Dailey, M. Halim, E. Rebourt, L.E. Horsburgh, I.D.W. Samuel, and A.P. Monkman, *Journal Of Physics-Condensed Matter*, **10** 5171-5178 (1998).
6. M. Deussen, M. Scheidler, and H. Bassler, *Synthetic Metals*, **73** 123-129 (1995).
7. M. Halim, I.D.W. Samuel, J.N.G. Pillow, and P.L. Burn, *Synthetic Metals*, **102** 1113-1114 (1999).
8. M. Halim, I.D.W. Samuel, J.N.G. Pillow, A.P. Monkman, and P.L. Burn, *Synthetic Metals*, **102** 1571-1574 (1999).
9. M. Halim, J.N.G. Pillow, D.W. Samuel, and P.L. Burn, *Advanced Materials*, **11** 371-374 (1999).
10. M. Lonergan, *Science*, **278** 2103-2106 (1997).

11. J.M. Lupton, I.D.W. Samuel, and A.P. Monkman, *Synthetic Metals*, **102** 1079-1080 (1999).

12. J.M. Lupton and I.D.W. Samuel, *Journal of Physics D-Applied Physics*, **32** 2973-2984 (1999).

13. G.G. Malliaras, J.R. Salem, P.J. Brock, and C. Scott, *Physical Review B-Condensed Matter*, **58** 13411-13414 (1998).

14. G.G. Malliaras, J.R. Salem, P.J. Brock, and J.C. Scott, *Journal Of Applied Physics*, **84** 1583-1587 (1998).

15. G.G. Malliaras and J.C. Scott, *Journal Of Applied Physics*, **83** 5399-5403 (1998).

16. R.N. Marks, D.D.C. Bradley, R.W. Jackson, P.L. Burn, and A.B. Holmes, *Synthetic Metals*, **57** 4128-4133 (1993).

17. G. Rikken, D. Braun, E.G.J. Staring, and R. Demandt, *Applied Physics Letters*, **65** 219-221 (1994).

18. C. Im, H. Bassler, H. Rost, and H.H. Horhold, *Journal of Chemical Physics*, **113** 3802-3807 (2000).

19. W.P. Su, J.R. Schrieffer, and A.J. Heeger, *Physical Review Letters*, **42** 1698 (1979).

20. S. Barth and H. Bassler, *Physical Review Letters*, **79** 4445-4448 (1997).

21. S. Barth, H. Bassler, H. Rost, and H.H. Horhold, *Physical Review B-Condensed Matter*, **56** 3844 (1997).

22. S. Barth, D. Hertel, Y.H. Tak, H. Bassler, and H.H. Horhold, *Chemical Physics Letters*, **274** 165-170 (1997).

23. S. Barth, H. Bassler, T. Wehrmeister, and K. Mullen, *Journal Of Chemical Physics*, **106** 321-327 (1997).

24. S. Barth, M. Deussen, and H. Bassler, *Philosophical Transactions of the Royal Society of London Series a-Mathematical Physical and Engineering Sciences*, **355** 749-761 (1997).

25. S. Barth, H. Bassler, U. Scherf, and K. Mullen, *Chemical Physics Letters*, **288** 147-154 (1998).

26. S. Barth, H. Bassler, S. Pfeiffer, and H. Horhold, *Macromolecular Chemistry and Physics*, **199** 717 (1998).

27. S. Barth, H. Bassler, D. Hertel, V.I. Nikitenko, and U. Wolf, *Pure and Applied Chemistry*, **71** 2067-2077 (1999).

# Chapter 2

# Theory

# 2.1 Introduction

This chapter provides a summary of aspects of spectroscopy appropriate to the study of optical transitions in conjugated polymers. Molecular orbital theory, aspects of excitons and polarons and charge generation, recombination and transport are also covered. The structure and absorption spectra of polymers used in this study are also discussed.

# 2.2 Optical Spectroscopy

Absorption of a photon in conjugated polymers leads to the creation of charge carriers that give rise to a photocurrent. An understanding of aspects of optical spectroscopy including elements of quantum theory and optical transitions is therefore essential to the analysis of photoconductivity spectra.

## 2.2.1 Quantum Theory

Quantum theory is the basis of our understanding of optical spectroscopy and it is therefore appropriate that the fundamentals of quantum theory are summarised.

Before Niels Bohr, it was thought that electrons orbited the nucleus in a similar manner to planets orbiting the Sun. The drawback to this theory is that, as the electron has a centripetal acceleration due to its motion, it ought to continuously emit electromagnetic radiation. It would thus lose energy and spiral into the nucleus. To overcome this problem, Bohr postulated that the electron

could only orbit the nucleus in certain stable orbits in which the electron does not emit energy. The orbital angular momentum was quantised and had values given by:

$$mvr = nh/2\pi \quad n = 1,2,3,4.....$$

**Equation 2-1**

where $h$ is Planck's constant.

There was no physical basis for this postulate except to overcome the difficulty described above but it worked to a reasonable degree of accuracy.

The dual nature of electrons and electromagnetic waves, which may be regarded as both waves and particles, was postulated by de Broglie in 1924 for electrons and by Einstein in 1905 for electromagnetic radiation. The wave particle duality is expressed as:

$$E = h\nu \text{ and } p = h/\lambda$$

**Equations 2-2 and 2-3**

where $E$ is the energy of the particle, $\nu$ is the frequency of the particle, $p$ is the momentum of the particle and $\lambda$ is the wavelength of the particle.

In 1927, Heisenberg postulated that there are certain variables that are impossible to measure simultaneously e.g. energy and time, position and momentum. Due to the act of observation, there is a fundamental uncertainty in measurements of these variables given by:

$$\Delta E \Delta t \approx h / 2\pi$$

$$\Delta p \Delta x \approx h / 2\pi$$

**Equations 2-4 and 2-5**

If a particle can be thought of in terms of a wave, it should be possible to formulate a wave equation. In 1926, Schrödinger developed an equation of motion which incorporated both particle and wave properties. The wave property of a particle of mass m, which has total energy $E$ and potential energy $V$ as expressed by the time independent Schrödinger equation is [1]:

$$\nabla^2 \psi + \frac{8\pi^2 m}{h}(E - V)\psi = 0$$

**Equation 2-6**

where $\psi$ is the wave function which describes the wave property of the particle and $\nabla^2$ is the Laplacian operator:

$$\nabla^2 = \frac{\partial^2}{\partial x^2} + \frac{\partial^2}{\partial y^2} + \frac{\partial^2}{\partial z^2}$$

**Equation 2-7**

On rearrangement of equation 2-6, we get:

$$\left(-\frac{h^2}{8\pi^2 m}\nabla^2 + V\right)\psi = E\psi$$

**Equation 2-8**

or

$$H\psi = E\psi$$

**Equation 2-9**

where

$$H = -\frac{h^2}{8\pi m^2}\nabla^2 + V$$

**Equation 2-10**

$H$ is known as the Hamiltonian operator and is a measure of the total energy of the particle. The two terms in the Hamiltonian give the kinetic and potential energy of the particle. The time dependent form of the Schrödinger wave equation for one dimension is:

$$-\frac{\partial^2\psi}{\partial x^2}\left(\frac{\hbar}{2m}\right) + V\psi = i\hbar\left(\frac{\partial\psi}{\partial t}\right)$$

**Equation 2-11**

The symbol $\psi$ represents a complex function that has real and imaginary parts. The interpretation of $\psi$ by Max Born in 1920 is that $|\psi|^2 dV$ represents the probability of finding an electron in a region of space. Since the electron also carries a charge, $\psi$ also represents the charge distribution.

## 2.2.2 Optical Transitions

In an atom or molecule, the electrons occupy orbitals surrounding the positive nucleus. When an atom or molecule absorbs a photon, the electric field component of the electromagnetic wave interacts with the electric dipole moment of the atom or molecule. This has the effect of exciting an electron to a higher energy orbital. The electric dipole moment of an atom or molecule $\mu$ is a vector quantity and is given by:

$$\boldsymbol{\mu} = \sum_i e_i \mathbf{r}_i$$

**Equation 2-12**

where $\boldsymbol{r}_i$ is the length of the vector from the origin to the $i$th atom. It is possible to determine the intensity of the transition by determination of the transition dipole moment $\mu_{nm}$, which is given by:

$$\mu_{nm} = \left\langle \psi_n \left| \boldsymbol{\mu} \right| \psi_m \right\rangle$$

**Equation 2-13**

where $\psi_n$ is the wavefunction of the initial state and $\psi_m$ is the wavefunction of the final state. In general, ordinary spectral lines arise from the interaction of an electric dipole oscillation with the electric vector of an electromagnetic wave.

However, transitions can also result from magnetic dipole and electric quadrupole interactions with electromagnetic radiation but with a much smaller probability.

The amount of radiation absorbed by a material is proportional to the number of molecules absorbing the radiation and is given by the Beer-Lambert law:

$$\log_{10} \frac{I_O}{I_T} \propto CL$$

**Equation 2-14**

where $I_O$ and $I_T$ are the intensity of the incident and transmitted radiation, $C$ is the concentration of the absorbing species and $L$ is the thickness of the absorbing layer. The term $\log_{10}(I_O / I_T)$ is called the absorbance $A$. Rewriting equation 2-14 gives

$$A = \varepsilon CL$$

**Equation 2-15**

The decadic extinction coefficient $\varepsilon$ is a function of the photon frequency and is related to the strength of the optical transition or the transition probability. A better measure of the transition intensity is obtained by integrating $\varepsilon$ over the whole of the absorption band. The integrated absorption coefficient of the material $\alpha$ is defined as:

$$\alpha = \int_{band} \varepsilon(\tilde{\upsilon})\, d\tilde{\upsilon}$$

**Equation 2-16**

where the integration is carried out over the whole absorption band as indicated in figure 2-1. The absorption coefficient $\alpha$ is related to the oscillator strength which is a measure of the strength of a transition compared to that of a free electron oscillating in three dimensions. The oscillator strength is given by:

$$f_{nm} = \left[\frac{4\varepsilon_O\, m_e\, c^2 \ln(10)}{N_A\, e^2}\right] \alpha$$

**Equation 2-17**

The value of the oscillator strength is approximately unity for an allowed transition. The oscillator strength is related to the transition dipole moment by:

$$f_{nm} = \left[\frac{8\pi^2 m_e c}{3e^2 h}\right] \tilde{\nu}_{nm} \left|\mu_{nm}\right|^2$$

**Equation 2-18**

where $\tilde{\nu}_{nm}$ is the frequency of the transition from $n$ to $m$.

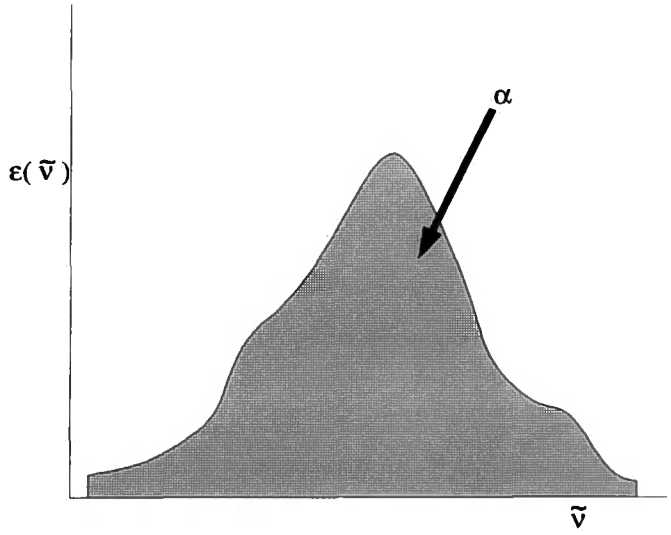


**Figure 2-1** *The integrated absorption coefficient for a typical molecule.*

The Bohr theory of the atom was adequate to determine the spectra of hydrogen but was inadequate when applied to more complicated atoms and molecules due to screening of the nucleus by inner electrons. Using the wave theory of Schrödinger and the Bohr theory, it was found necessary to use four quantum numbers to determine the allowed optical transitions. The four quantum numbers are: the principle quantum number, $n$, the orbital angular momentum quantum number, $l$, the magnetic orbital angular momentum quantum number, $m_l$ and the magnetic spin angular momentum quantum number $m_s$. These quantum numbers have the following restricted values:

$n = 1, 2, 3, \ldots .$

$l = 0, 1, 2, 3 \ldots ., (n\text{-}1)$

$m_l = 0, \pm 1, \pm 2, \ldots ., \pm l$

$m_s = \pm \frac{1}{2}$

The principal quantum number determines the allowed values of the quantized electron energy levels. The orbital angular momentum is quantized with values being determined by $l$. The angular momentum is a vector and therefore requires the specification of a direction. This direction has significance if an external magnetic field is applied to the system. The allowed orientations of the orbital angular momentum relative to the applied magnetic field are specified by the magnetic quantum number. Based on the theories of relativity and quantum mechanics and by experiment, it was determined that a fourth quantum number was needed. The electron spin is an internal property of the electron and has a value of ½. The electron spin is a vector and therefore requires the specification of a direction. This direction also has significance if an external magnetic field or other perturbation is applied to the system. The allowed orientations of the electron spin relative to the applied magnetic field are specified by the spin angular momentum quantum number, $\boldsymbol{s}$. The Pauli Exclusion Principle states that no two electrons can have the same set of quantum numbers. This means that only two electrons can occupy each orbital, one with $\boldsymbol{s} = +½$ (represented by ↑) and one with $\boldsymbol{s} = -½$ (represented by ↓).

The total orbital angular momentum of a molecule $\mathbf{L} = \boldsymbol{l}_1 + \boldsymbol{l}_2 + \boldsymbol{l}_3 + \boldsymbol{l}_4 \ldots \boldsymbol{l}_n$ where $\boldsymbol{l}_n$ is the angular momentum of the nth electron The total spin angular momentum of a molecule $\mathbf{S} = \boldsymbol{s}_1 + \boldsymbol{s}_2 + \boldsymbol{s}_3 + \boldsymbol{s}_4 \ldots \boldsymbol{s}_n$ where $\boldsymbol{s}_n$ is the spin angular momentum of the nth electron Since both **L** and **S** are vector quantities, the resultant total angular momentum $\mathbf{J} = \mathbf{L} + \mathbf{S}$.

The ordering of the elements in the periodic table can be accounted for by the use of the quantum numbers. Hydrogen has one electron and, in the ground state, $n = 1$ and $l = 0$. Two electrons can occupy this orbital ($\boldsymbol{s} = +½$ and $\boldsymbol{s} = -½$)

but, since hydrogen has only one electron, only one electron will occupy this orbital. Helium has two electrons and, in the ground state, both electrons will occupy the $n = 1$, $l = 0$ orbital which will now be full. For Lithium in the ground state, two electrons will occupy the $n = 1$, $l = 0$ orbital and the next electron will occupy the $n = 2$, $l = 0$ orbital. The electrons for the other elements will fill the orbitals in a similar fashion.

Optical transitions can occur between orbitals but do not occur indiscriminately. A series of selection rules are used to predict if an optical transition is allowed or forbidden. Analysis of the absorption spectra of hydrogen determined that $\Delta n$ is unrestricted. The basis of the selection rules for the other quantum numbers comes from the fact that the spin angular momentum of a photon depends on the polarisation of the photon. The evidence for this comes from the existence of left and right circularly polarised light. Electromagnetic theory shows that circularly polarised photons have a |spin| = 1. Right circularly polarised light corresponds to spin = -1 and left circularly polarised light corresponds to spin = +1. Linearly polarised light is an equal combination of left and right circularly polarised light. Particles with an integer spin are known as Bosons and particles with non-integer spin are known as Fermions. During optical transitions, total angular momentum **J** must be conserved. When an atom absorbs a photon, all the angular momentum of the photon is transferred to the electrons in the atom. When a photon is emitted, it carries away unit angular momentum. In either case, based on the conservation of momentum, the angular momentum cannot change by more than one unit. This can be summarised as $\Delta l = \pm 1$

It is possible to extend this idea to $\Delta m_l$. Suppose $m_l$ corresponds to some direction with respect to the propagation direction of a photon. An absorption of a left circularly polarised photon ($\boldsymbol{s}$ = +1) results in $\Delta m_l$ = +1, while emission results in $\Delta m_l$ = -1. For absorption / emission of right circularly polarised light, the opposite holds true. For absorption / emission of a linearly polarised photon, $\Delta m_l = 0$.

When a photon is absorbed by a full atomic or molecular level, one electron is excited to a higher energy level. The spin multiplicity of an excited state is given by $2\mathbf{S}+1$ where $\mathbf{S} = \mathbf{s}_1 + \mathbf{s}_2$ and the spin angular momenta of the two electrons is $\mathbf{s}_1$ and $\mathbf{s}_2$. For a closed shell molecule having a singlet ground state, if, on promotion of an electron to the excited state, the electron retains its spin, the spin multiplicity equals one and the state is said to be an excited singlet state. If, by some means, the electron spin is reversed then the spin multiplicity will equal three and the state is said to be a triplet state. The excited triplet state has a lower energy than the excited singlet state because the coulombic repulsion of the electrons forming the singlet is higher than the coulombic repulsion of the electrons forming the triplet (see figure 2-2).

Within the electronic energy levels, there are vibrational and rotational energy levels associated with the vibrations and rotations of the atom or molecule. The quantisation of vibrational energy levels is represented in figure 2-3. The Franck-Condon principle states that the internuclear separation can be regarded as fixed during an electronic transition and can be shown as vertical lines connecting the initial and final state in diagrams such as is shown for absorption in the configuration coordinate diagram in figure 2-3. Each vibrational level has an

associated wavefunction. During absorption, the particular vibronic level that the electron will be excited into corresponds to the wavefunction that has the greatest overlap with the wavefunction of the original state. This corresponds to the vertical line in figure 2-3. Vibrational relaxation from a higher energy vibronic level to a lower energy vibronic level is very fast ($\sim 10^{-13}$s).

Once in the excited state, there are a number of ways for the electron to lose the excess energy. Vibrational relaxation takes place resulting in the excited electron being in the lowest vibrational level of the excited state. The electron may decay to some vibrational level in the ground state emitting a photon. This process is called fluorescence.

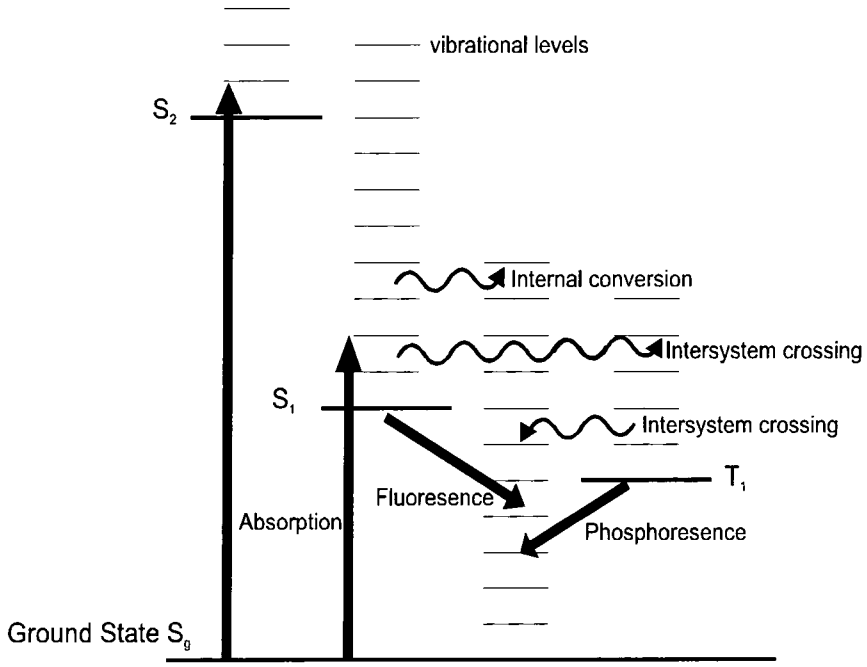


**Figure 2-2** *Photophysical processes. $S_g$ is the singlet ground state, $S_1$ is the 1st excited singlet state, $S_2$ is the 2nd excited singlet state and $T_1$ is the 1st excited triplet state.*

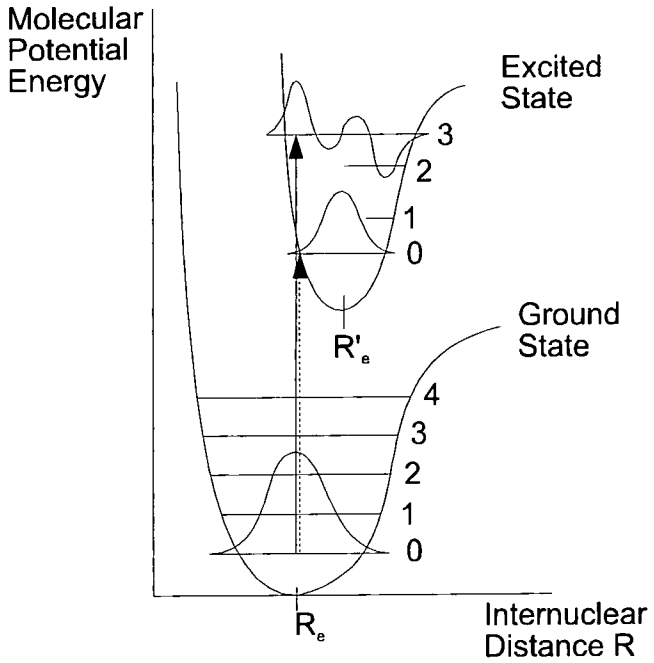


**Figure 2-3** *Basis of the Franck-Condon Principle from Atkins [2].*

The electron may undergo a spin transition resulting in the electron being in the excited triplet state. This is known as intersystem crossing and is caused by a redistribution of the total angular momentum **J**. This process is quantum mechanically forbidden but, if the energy difference between the excited singlet state and the excited triplet state is small, the process may be quite efficient. Once in the triplet state, the electron may emit a photon and return to some vibrational level in the singlet ground state. This process is termed phosphorescence and is also quantum mechanically forbidden. The probability of phosphorescence occurring is very small and the process takes much longer than fluorescence but is one of the few routes back to the ground state. These processes are shown in figure 2-2.

## 2.3 Conjugated Polymer Theory

The polymers used in this work are conjugated polymers. Conjugated polymers are polymers that have alternating single and double bonds in the polymer backbone. The structure of these polymers will influence their optical and physical properties. An understanding of how this conjugation arises and how these conjugated polymers differ from each other is essential if we are to tailor these polymers for industrial applications.

### 2.3.1 Molecular Orbitals

Atomic orbitals are solutions to the wave equation and describe the probability of finding an electron in a region of space surrounding an atom. These wave functions may have a positive or negative phase. The first four atomic orbitals are denoted *s*, *p*, *d* and *f* but the *s* and *p* orbitals have the most important role in organic chemistry. A molecular bond is formed by the overlap of atomic orbitals. Since the wavefunction of the atomic orbital can have either a positive or negative phase, two types of molecular bond may be formed and are known as bonding and antibonding molecular orbitals. The bonding orbital is formed by the addition of two atomic orbitals of the same phase. The antibonding orbital is formed by the addition of two atomic orbitals of differing phase. The sigma ($\sigma$) bond formed by the overlap of two *s* orbitals is shown in figure 2-4. This bond is symmetrical about a line joining the nuclei. If a *s* orbital overlaps with a *p* orbital, a sigma bond is formed. An example is an HF molecule. The pi ($\pi$) bond formed

by the overlap of two *p* orbitals is shown in figure 2-5. The bonding orbital has a lower energy than that of the atomic orbital.

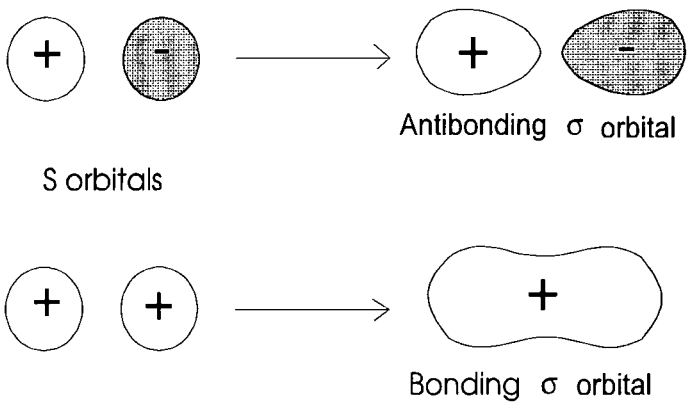


**Figure 2-4** *Formation of sigma bonding (σ) and antibonding (σ*) molecular orbital.*

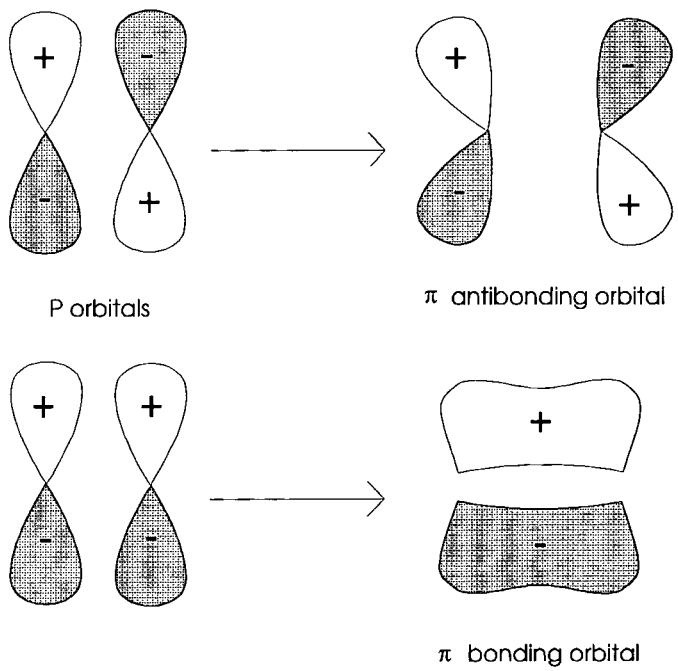


**Figure 2-5** *Formation of pi bonding (π) and antibonding (π*) molecular orbital.*

Sigma bonding electrons are found close to the nucleus and, usually, directly between the nuclei. The σ orbital has a lower energy than the σ* orbital.

When a photon is absorbed by a σ orbital, an electron is excited to a higher energy orbital and a rearrangement of the molecular wavefunction occurs (from the σ wavefunction to the σ* wavefunction). This results in severe coulombic repulsion between the nuclei (see figure 2-4). When a photon is absorbed by a π orbital, an electron is excited to a higher energy orbital and a rearrangement of the molecular wavefunction occurs (from the π wavefunction to the π* wavefunction). The π bonding electrons however, are further from the nucleus. Excitation of a π electron does not result in such severe coulombic repulsion between the nuclei due to shielding by the σ bonding electrons (see figure 2-5). The relative energies of the atomic orbitals and bonding and antibonding orbitals are shown in figure 2-6 for the hydrogen molecule that is formed by the addition of two *s* orbitals.

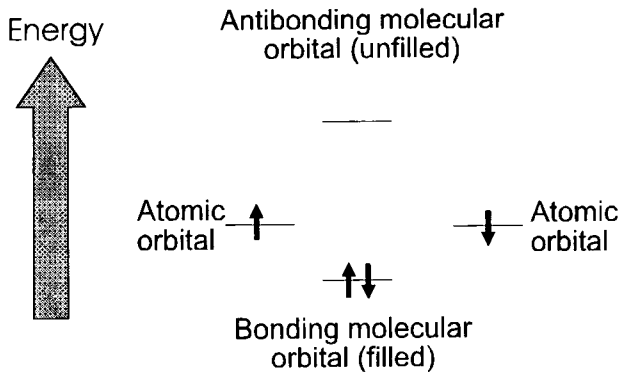


**Figure 2-6** *Relative energies of the atomic orbital of atomic hydrogen (H) and the molecular orbitals for the hydrogen molecule ($H_2$).*

## 2.3.2 Hybridisation

Hybridisation is the mixing or blending of atomic orbitals and is essential to our understanding of bonding in organic molecules. The ground state of carbon is $1s^2\ 2s^2\ 2p^2$. The 1*s* orbital is filled and is not used for bonding. The four

electrons in the second energy level are used for bonding, however, they are not used in the atomic form. These orbitals are mixed or hybridised when forming bonds with other elements. There are three different ways in which the carbon atom may be hybridised. The carbon must be in the excited state for hybridisation to occur. The excited state of carbon is $1s^2\ 2s^1\ 2p^3$. Combining the wavefunctions of the 2*s* orbital of carbon with three 2*p* orbitals is known as *sp*3 hybridisation and is used when carbon forms four single bonds e.g. methane. The *sp*3 hybridised orbitals point towards the corners of a tetrahedron and are shown in figure 2-7. Combining the wavefunctions of the 2*s* orbital of carbon with two of the three 2*p* orbitals is known as *sp*2 hybridisation. One *p* orbital remains unhybridised. This is shown in figure 2-8. In the ethylene molecule ($CH_2$=$CH_2$), two *sp*2 hybridised carbons bond together by the overlap of one *sp*2 orbital from each atom. This is a σ bond. Each carbon atom has two *sp*2 orbitals for bonding with hydrogen and also has a *p* orbital that forms a π bond between the carbon atoms. The π bond and the σ bond together make a double bond. A double bond is shorter than a single bond.

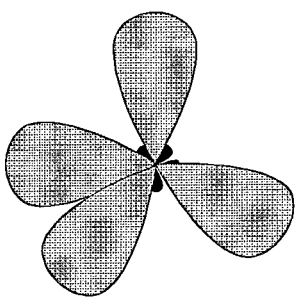

**Figure 2-7** *$sp^3$ hybridised carbon atom.*

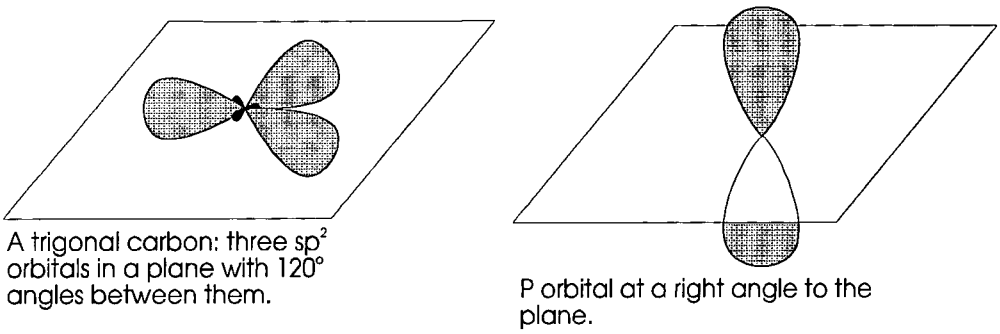


**Figure 2-8** *$sp^2$ hybridised carbon atom*

Combining the wavefunction of one 2*s* orbital of carbon with one of the three 2*p* orbitals is known as *sp* hybridisation. This is shown in figure 2-9. Two 2*p* orbitals remain unhybridised. An example of *sp* hybridisation is acetylene (CH≡CH). The two 2*p* orbitals form two $\pi$ bonds that are perpendicular to each other. With the $\sigma$ bond, a triple bond is formed.

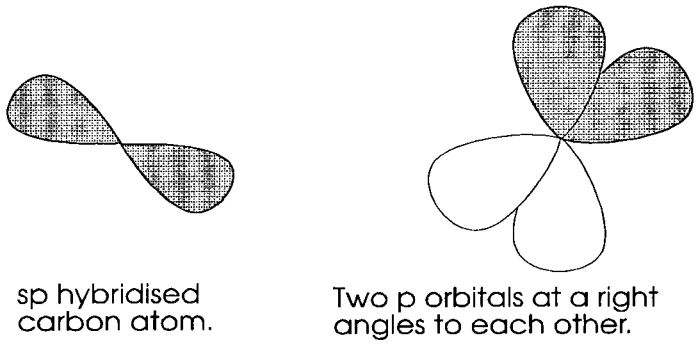


**Figure 2-9** *sp hybridised carbon atom with two p orbitals unhybridised.*

## 2.3.3 Conjugation

Conjugated polymers are long chain molecules with alternating single and double bonds. One of the simplest examples of a conjugated polymer is *trans*-polyacetylene (*trans*-PA). *Trans*-PA consists of a long chain of CH monomers.

Each carbon bonds with two other carbon atoms and one hydrogen atom as shown in figure 2-10. This leaves one unpaired electron per monomer to form a π bond. This structure can be considered as a one-dimensional metal where the CH monomer replaces the metal atom and metallic conductivity can take place.

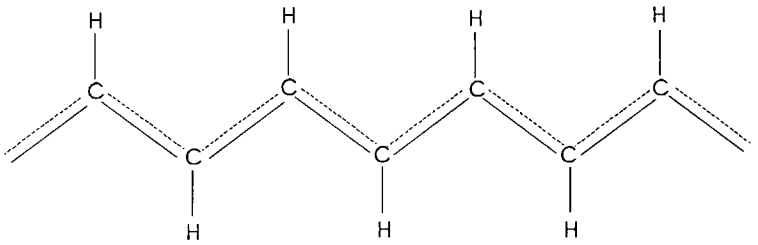


**Figure 2-10** *Metallic form of trans-PA.*

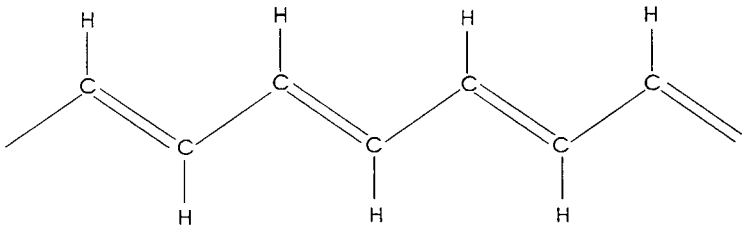


**Figure 2-11** *Dimerised form of trans-PA.*

The regular linear chain does not exist in any real system because it cannot be isolated from its environment and is thus susceptible to distortion. This distortion results in an alternating form of *trans*-PA (figure 2-11) that is lower in energy than the linear form. This distortion is known as the Peierls Distortion and the polymer is said to be dimerised. This also has the effect of opening up a band gap at the Fermi level. Conjugated polymers do not form very long chains such as in conventional polymers e.g. polyethylene. Defects, impurities and twists in the polymer backbone limit the conjugation length. The effective conjugation length is the average chain length over all chain segments for the complete sample.

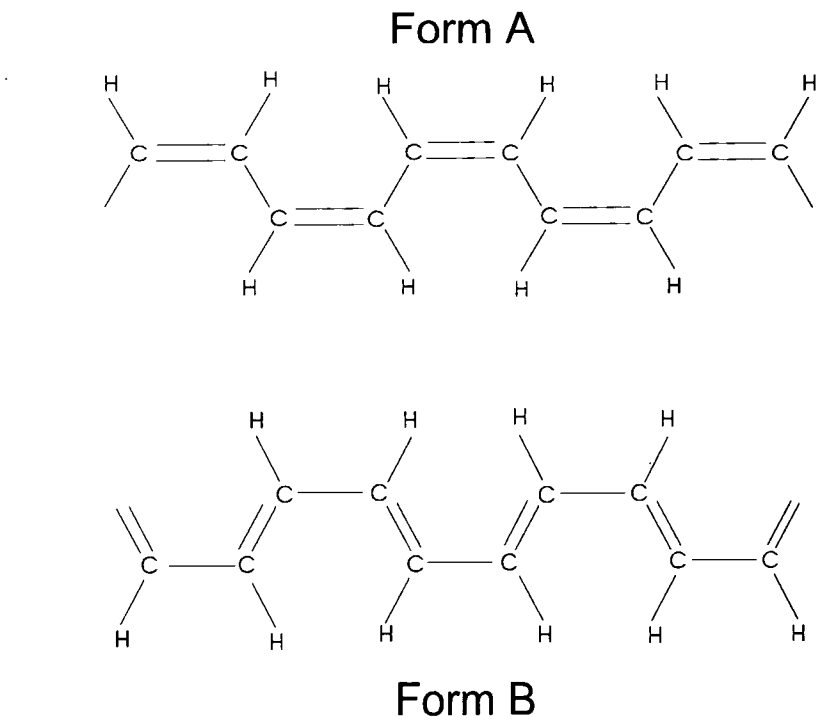


**Figure 2-12** *Dimerised forms of cis-PA. Form A has a lower energy than form B.*

There is a second isomer of PA known as *cis*-PA. There are two forms of the dimerised *cis*-PA but they are not isoenergetic. The structure of the dimerised *cis*-PA isomers are shown in figures 2-12.

## 2.4 Aromatic Conjugated Polymers

The polymers used in this work are aromatic conjugated polymers. The absorption spectra and structure of these polymers has a large effect on the photoconductivity spectra obtained and it is therefore relevant to examine these aspects.

### 2.4.1 Benzene

Many conjugated polymers have a structure involving a benzene ring. Benzene is a planar, cyclic, aromatic hydrocarbon with the molecular formula $C_6H_6$. Each carbon atom is $sp^2$ hybridised and is $\sigma$ bonded to one other carbon atom and a hydrogen atom. Perpendicular to the $\sigma$ bonds in the ring is a $p$ orbital. Each of these six $p$ orbitals can contribute one electron for $\pi$ bonding. The individual wavefunctions of benzene formed from the $p$ orbitals are shown in figure 2-13.

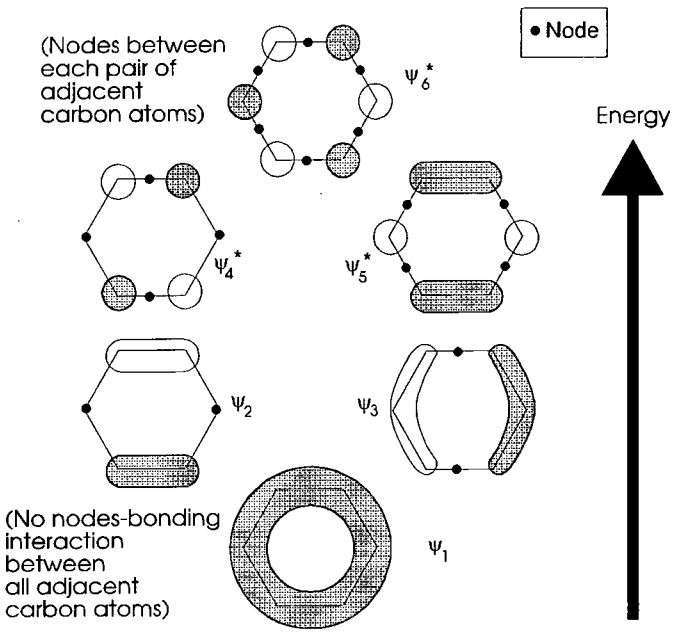


**Figure 2-13** *Wavefunctions of benzene.*

Each wavefunction can contain two electrons. There are six $\pi$ electrons in benzene so $\psi_1$, $\psi_2$ and $\psi_3$ are all filled and $\psi_4$, $\psi_5$ and $\psi_6$ are unfilled in the ground state. The three low energy molecular orbitals - $\psi_1$, $\psi_2$ and $\psi_3$ are the

bonding orbitals and the three high energy molecular orbitals - $\psi_4^*$, $\psi_5^*$ and $\psi_6^*$ are the antibonding orbitals. Two of the bonding orbitals - $\psi_2$ and $\psi_3$ have the same energy as do the antibonding orbitals $\psi_4^*$ and $\psi_5^*$. Such orbitals are said to be degenerate. To determine the overall wavefunction of the benzene atom, the occupied wavefunctions are added together.

## 2.4.2 MEH-PPV

Poly (2-methoxy-5- (2'ethylhexyloxy)-1,4-phenylenevinylene) (MEH-PPV) is a conjugated polymer similar to benzene. The structure of MEH-PPV, shown in figure 2-14, is based on a benzene ring with two side groups replacing hydrogen atoms and a vinylene group connecting the monomers together.

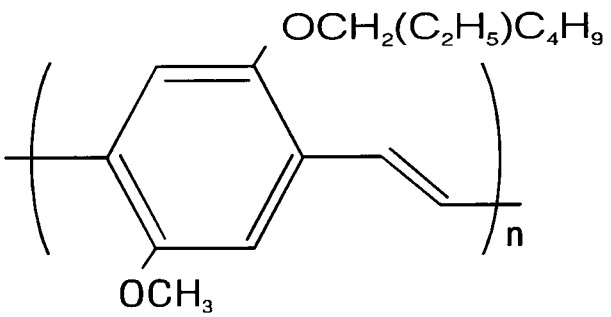


**Figure 2-14** *Structure of MEH-PPV.*

In the unexcited state, all the molecular orbitals up to and including the HOMO (highest occupied molecular orbital) are full and all the molecular orbitals above and including the LUMO (lowest unoccupied molecular orbital) are empty. The HOMO is also known as the $\pi_1$ level and the LUMO is also known as the $\pi_1^*$ level.

The absorbance spectrum of a thin film (100nm) of MEH-PPV and the energy level diagram of optical transitions in MEH-PPV are shown in figures 2-15 and 2-16 respectively. It is believed [3] that the peak at ~ 2.5eV is due to optical transitions between molecular orbitals delocalised along the polymer backbone.

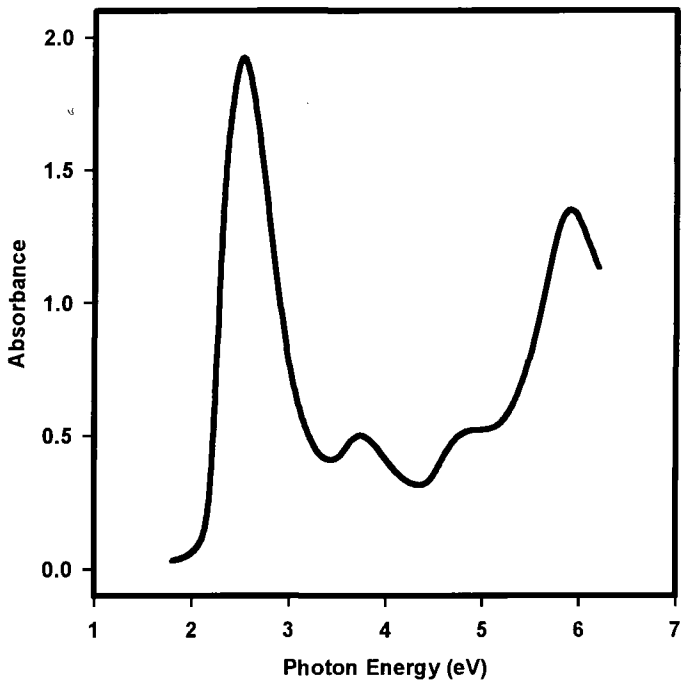


**Figure 2-15** *Absorbance spectrum of MEH-PPV.*

This transition is termed the $\pi_1$ to $\pi_1^*$ transition and is known as the fundamental absorption or the band gap. The peak at ~ 5.8eV arises from transitions to highly localised states originating from the molecular orbitals of benzene. This may be a transition from $\pi_2 \rightarrow \pi_2^*$ or a transition from $\pi_1 \rightarrow \pi_3^*$. The peaks at 3.7eV and 4.8eV are due to transitions from localised to delocalised states. Based on calculations on PPV [4], it is believed that the free electron continuum (conduction band) overlaps the $\pi_2^*$ and $\pi_3^*$ molecular levels, so that any excitations to the $\pi_2^*$ level or above results in the formation of free electrons.

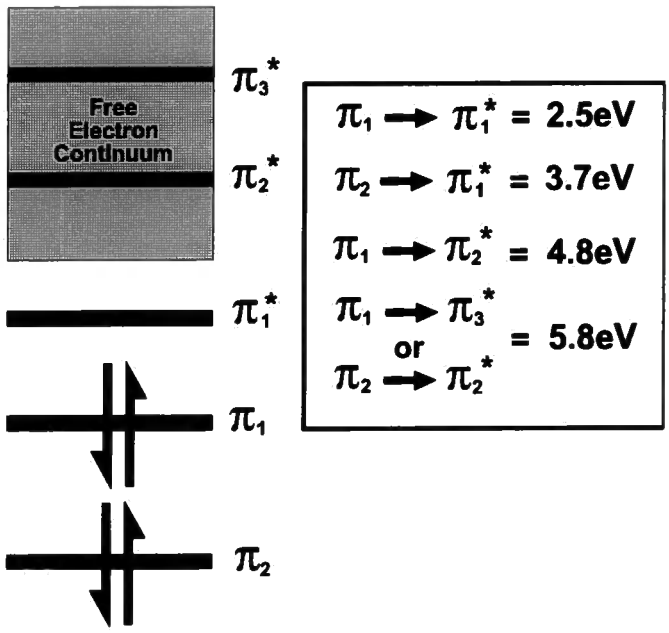


**Figure 2-16** *Energy level diagram of MEH-PPV.*

## 2.4.3 Poly (2,5-pyridinediyl)

The chemical formula of the Poly (2,5-pyridinediyl) (PPY) monomer is $C_5H_5N$. The structure of PPY, shown in figure 2-17, is very similar to benzene with a nitrogen atom replacing a CH group. The nitrogen atom has two extra electrons compared to the CH group that sit in the plane of the ring and act like a *s* orbital.

There are six ways in which two PPY monomers may join together. These are based on the position of the nitrogen atom and are shown in figure 2-18. In real systems, a mixture of the *trans*-head-to-head, *cis*-tail-to-tail and *trans*-tail-to-tail configurations are prevalent due to the coulombic repulsion of the lone pair of electrons of the nitrogen atom.

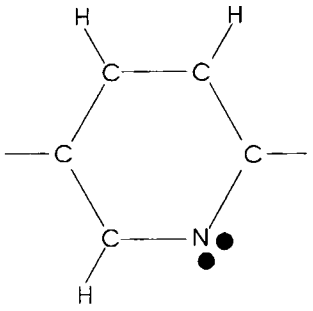


**Figure 2-17** *Structure of PPY monomer.*

The absorbance spectrum of PPY and an energy level diagram of the optical transitions of PPY are shown in figures 2-19 and 2-20 respectively. Electron transitions from localised to delocalised orbitals occur in the near ultraviolet (UV) and electron transitions from localised to localised orbitals occur at very high photon energy.

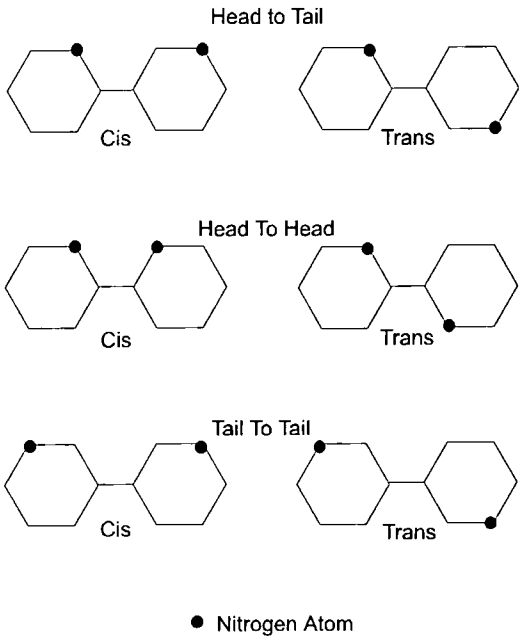


**Figure 2-18** *Possible bonding configurations of two PPY monomers.*

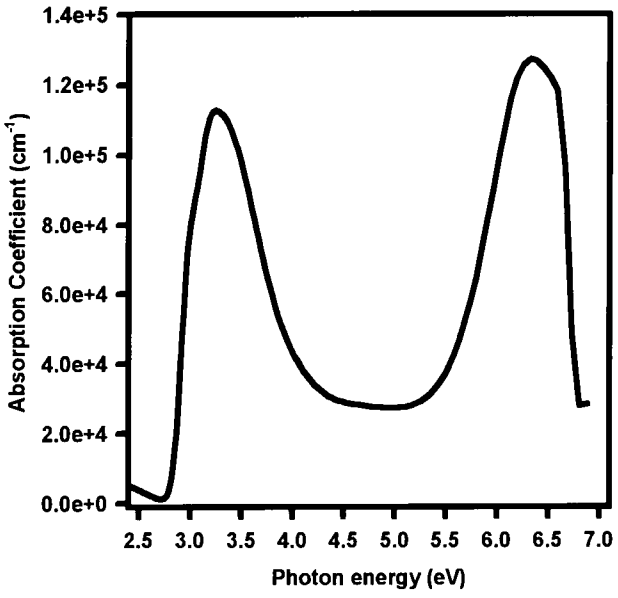


**Figure 2-19** *Absorption spectrum of PPY.*

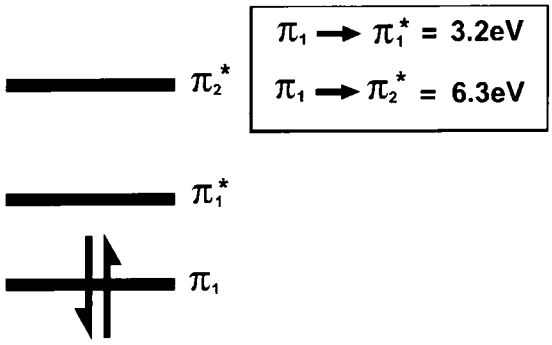


**Figure 2-20** *Energy level diagram of PPY.*

## 2.4.4 Polyfluorene

There are several variants of polyfluorene. Poly(9,9-bis(2-ethylhexyl)fluorene-2,7-diyl) (PF2/6) is a conjugated polymer that is similar to PPY. The chemical structure is shown in figure 2-21. The absorbance spectrum of PF2/6 is shown in figure 2-22. The effect of the side groups in PF2/6 is to

increase the solubility. The fundamental absorption peak in PF2/6 is at the same energy as PPY. There are two high energy peaks in PF2/6 but at a lower energy than the single high energy peak in PPY.

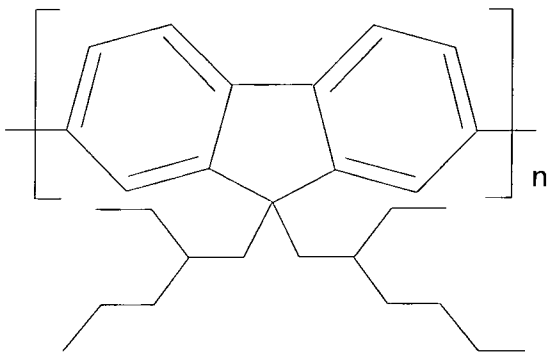


**Figure 2-21** *Chemical structure of PF2/6.*

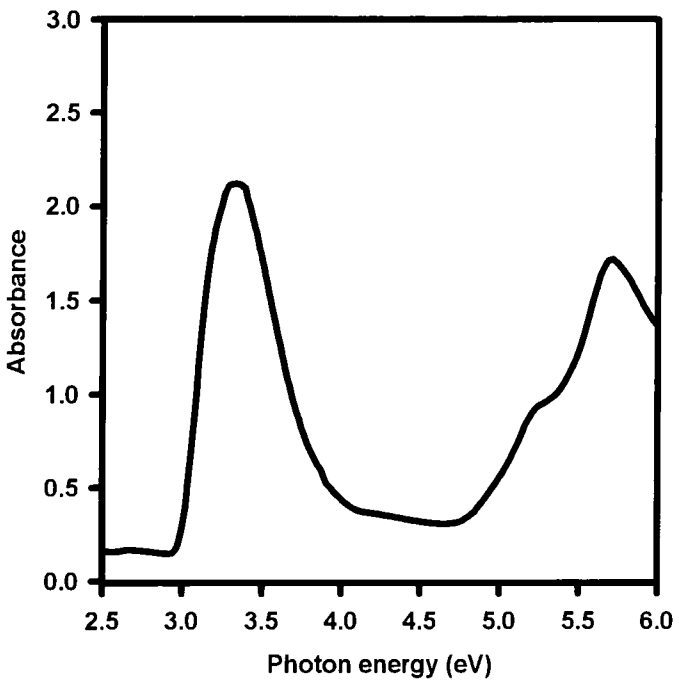


**Figure 2-22** *Absorbance spectrum of PF2/6.*

## 2.5 Charge Carrier Generation and Transport

The aim of this work is to elucidate the mechanisms of charge generation and transport in conjugated polymers. It is therefore appropriate to discuss aspects of charge carrier generation and transport mechanisms.

### 2.5.1 Excitons

An exciton is a coulombically bound geminate electron–hole pair. If the electron–hole pair are tightly bound (<5Å) then the exciton is called a Frenkel exciton. If the electron-hole pair are weakly bound (separation ~ 40-100Å) then the exciton is called a Wannier exciton or a Mott-Wannier exciton. If the electron is transferred to a neighbouring atom but still remains correlated to the hole, this is known as a charge transfer exciton. These are shown diagrammatically in figure 2-23.

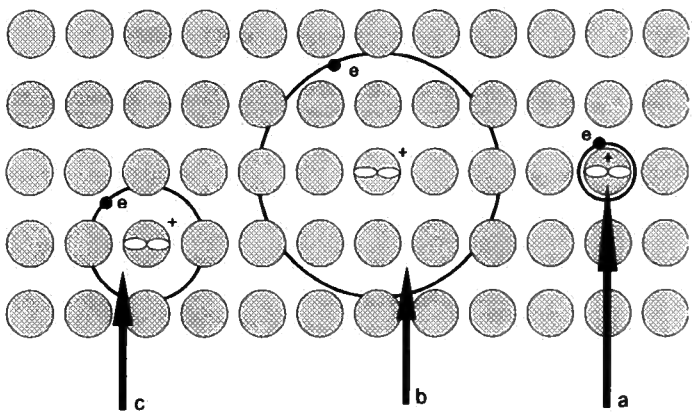


**Figure 2-23** *(a) Frenkel exciton, (b) Mott-Wannier exciton and (c) Charge-transfer exciton from Pope and Swenberg [5].*

In polymer devices, the exciton sits within a potential well formed by a superposition of the binding coulomb field and the external field (applied or due to the difference in work function of the electrodes). For the exciton to be dissociated, it must gain enough energy to escape this potential well. This energy is the exciton binding energy $E_{exc}$ and is given by:

$$E_{exc} = e^2 / 4\pi\varepsilon\varepsilon_o r_{exc}$$

**Equation 2-19**

where $r_{exc}$ is the separation of the electron and hole, $e$ is the charge on the electron, $\varepsilon$ is the relative permittivity of the polymer and $\varepsilon_o$ is the permittivity of free space. An exciton may be singlet (electron spin is opposite to the hole spin) or triplet (electron spin is the same as the hole spin). Optical formation of triplets can only occur through intersystem crossing.

## 2.5.2 Polarons

When an electron is added to a polymer chain, it is added to the lowest vibrational level in the LUMO band. It causes the chain to deform creating a characteristic pattern of bond deformation. With the bond deformation, there is also a change in the energy level structure. An energy level, with its two electrons of opposite spin, is pulled out of the HOMO band into the gap and the energy level with the added electron is pulled out of the LUMO band into the gap and an electron polaron (P-) is formed (see figure 2-24).

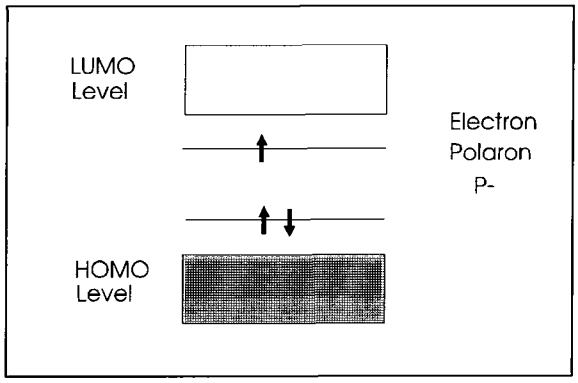


**Figure 2-24** *Electron polaron band structure.*

If an electron is removed from a polymer chain, a hole polaron (P+) is formed. This also causes a chain deformation. The lowest vibrational energy level from the LUMO band and the energy level in the HOMO band with only one electron are pulled into the gap. The hole polaron is shown in figure 2-25.

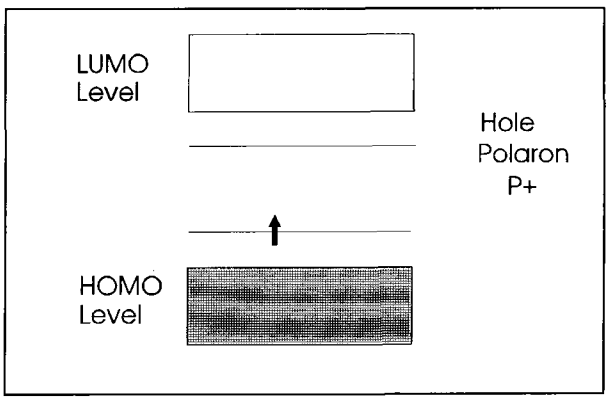


**Figure 2-25** *Hole polaron band structure.*

Having one half filled level, the P+ and P- polarons have spin ½. The energy interval between a polaron level and the nearest band edge and the band gap depends on the conjugation length.

If another electron is added to an electron polaron, an electron bipolaron (BP2-) is formed. This electron is added to the upper level of the electron polaron (see figure 2-26).

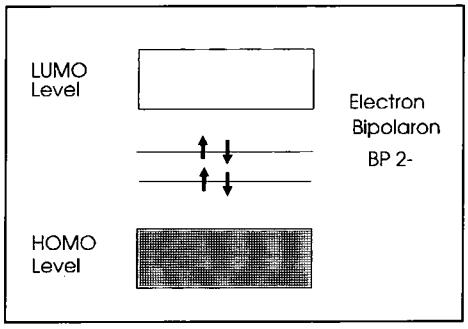


**Figure 2-26** *Electron bipolaron band structure.*

If another electron is removed from a hole polaron, a hole bipolaron (BP2+) is formed. (see figure 2-27).

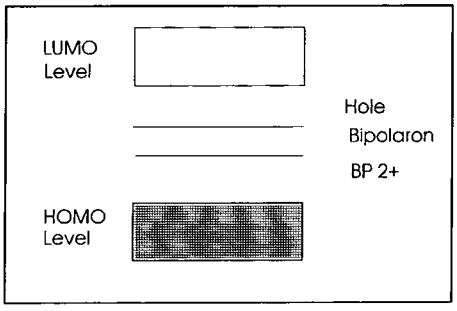


**Figure 2-27** *Hole bipolaron band structure.*

The bipolaron has spin 0. It must be noted that the polaron levels of P+ and P- are not in the same positions as BP2+ and BP2- due to the coulombic attraction and repulsion of the electrons in the gap with each other and the HOMO electrons.

## 2.5.3 Charge Carrier Generation

### 1) Exciton Formation

When two free charges of opposite sign (an electron and a hole) meet in a polymer, there is a probability that the electron will be bound to the hole as an exciton. The coulomb capture radius is the distance at which the kinetic energy of the electron is equal to the coulombic attractive potential energy and is given by:

$$r_c = e^2 / 4\pi\varepsilon\varepsilon_o k_B T$$

**Equation 2-20**

where ε is the dielectric constant of the material. The coulomb capture radius is a constant for a system of temperature T.

### 2) Recombination

The dielectric constant of conjugated polymers is low, typically between 2.5 and 3.5 compared to 11 for silicon. Conjugated polymers also have weak intermolecular coupling that results in a charge carrier mean free path not much greater than the intermolecular spacing. A dielectric constant of 3.5 gives a capture radius of 18nm at 295K. This is approximately 20-30 intermolecular spacings [6]. Even if a molecule were excited at very high photon energies, this would not be enough for the electron to escape therefore there must be other processes that allow dissociation of the exciton. Based on work by Haberkorn and Michel-Beyerle [7], Donovan and Wilson determined the probability of escaping

geminate recombination (recombination of a geminate pair) in 1D for a perfect chain with an external field $F$ [8]:

$$f^{1-D}(r_o, F) = \frac{\int_0^1 \exp(-2\xi t - (\eta / t))dt}{\int_0^\infty \exp(-2\xi t - (\eta / t))dt}$$

**Equation 2-21**

where $\zeta = eFr_o / 2k_BT$, $\eta = r_c / r_o$, $r_c$ is the coulomb capture radius and $r_o$ is the thermalisation distance. This is the distance from the hole that an electron will thermalise to after initial excitation. When $\zeta >> 1$, i.e. for high electric fields, the probability of escaping geminate recombination tends to unity. When $\eta >> 1$ and $\zeta << 1$, i.e. for small electric fields and large coulomb capture radius, the probability of escaping geminate recombination tends to zero. When a high energy photon is absorbed, the initial electron-hole separation increases and the probability of escaping geminate recombination increases.

The thermalisation distance is difficult to determine since it involves knowledge of the energy loss mechanism. It is assumed that the electron only loses energy via quasi-elastic collisions with the emission of phonons. At high electric fields ($F \geq 10^6$ $Vm^{-1}$) and at sufficiently large thermalisation distances ($r_o \geq$ 4nm), the field-induced increase in thermalisation distance $r_E$ can be approximated by the expression [9]:

$$r_E = \langle \mu \rangle F \tau_{th}$$

**Equation 2-22**

where $\langle\mu\rangle$ is an average electron mobility during the thermalisation process and $\tau_{th}$ is the thermalisation time. Due to electron drift during $\tau_{th}$, the initial population of thermalised electrons is shifted along the field and the thermalisation distance is increased by $r_E$. The total thermalisation distance therefore is equal to $r_o+r_E$.

Monte Carlo simulations on poly(phenylene vinylene) (PPV) [10] have yielded the following modification to the 1D theory to account for the possibility of dissociation due to hopping of one of the constituent charges of the exciton from one chain segment to another. In this modification, the exciton can be considered to be in a potential well with a Gaussian density of states (DOS) distribution due to disorder. In the presence of an electric field, the potential well will be modified and dissociation can take place more readily. This is shown diagrammatically in figure 2-28 (redrawn from reference [10]). $V(r)$ is the potential due to the coulombic attraction between the electron and hole and may be modified by an electric field such that the new potential is $V(r)-qFx$. $\rho_1$ is the DOS of the bound exciton and $\rho_2$ is the DOS of an electron hole pair that are spatially separated from each other and can be considered free charge carriers. During dissociation, the carrier must surmount the barrier $\Delta E$. The probability that the exciton will hop to a lower energy chain is $\nu_{hop}$. The probability of dissociation taking place will decrease. When an electric field is applied, $\rho_2$ is effectively lowered and the probability that the exciton may be dissociated ($\nu_{diss}$) will increase. Dissociation in the bulk polymer is known as intrinsic dissociation [11, 12].

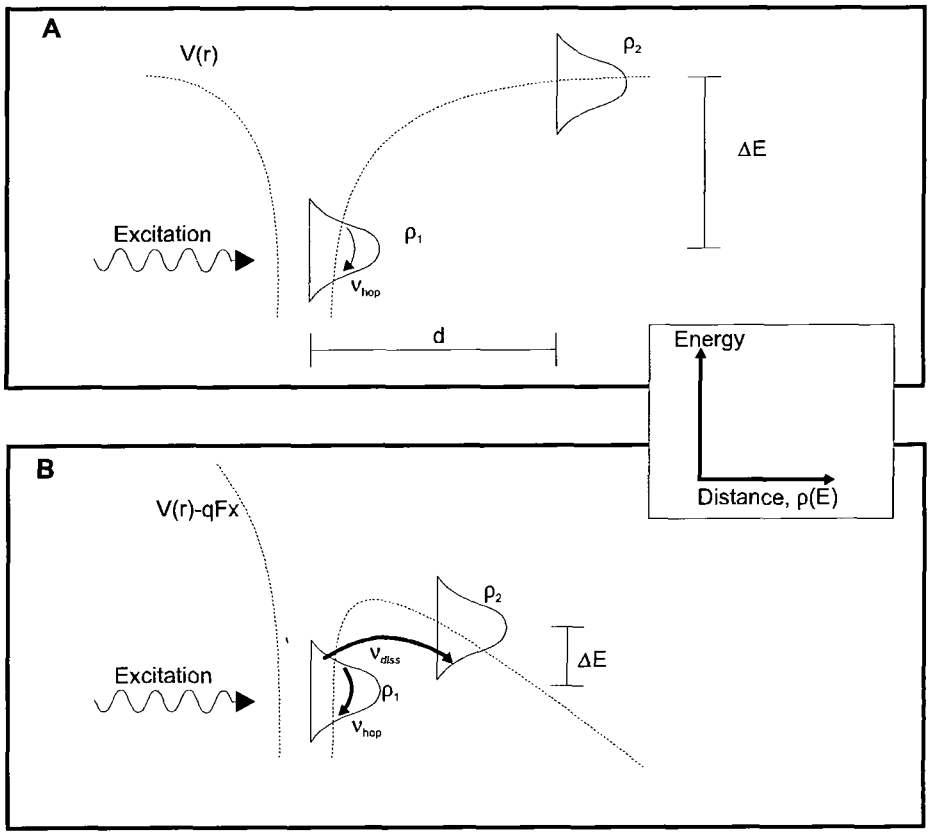


**Figure 2-28** *Scheme for intrinsic dissociation of excitons without (A) and with (B) an electric field.*

## 2.5.4 Charge Transport

Current-voltage experiments by Bozano and Carter [13] on MEH-PPV devices at high fields ($10^8$V/m) have shown that the motion of the charge carrier is space charge limited with the current density given by:

$$J = 9\varepsilon\mu E^2 / 8L$$

**Equation 2-23**

where $J$ is the current density, $\varepsilon$ is the permittivity of the polymer layer, $\mu$ is the charge carrier mobility, $E$ is the electric field across the device and $L$ is the

thickness of the polymer layer. The carrier mobility $\mu$ is described by a Poole-Frenkel like form:

$$\mu = (\mu_* e^{-\Delta/kT}) e^{\gamma\sqrt{E}}$$

**Equation 2-24**

where $\Delta$ is the activation energy, $\mu_*$ is the mobility prefactor and $\gamma$ is the electric field coefficient of the mobility due to the interaction between charge carriers and randomly distributed permanent dipoles in semiconducting polymers (equation 2-25) with $B$ and $T_o$ constant..

$$\gamma = \left(\frac{1}{kT} - \frac{1}{kT_o}\right) B$$

**Equation 2-25**

The transport mechanisms in conjugated polymers are not very well understood. Interchain interaction, coulomb interaction, screening, electron-phonon interaction, charge delocalisation, conjugation length and disorder play important parts in charge transport. Theoretical modelling has provided some insight into the effects of the above parameters on charge transport but has yet to describe these mechanisms completely [10, 14-19].

The work presented in this thesis contributes to our understanding of the charge generation and transport mechanisms in conjugated polymers.

# References


1. B.P. Straughan and S. Walker, *Spectroscopy Volume 1*. 1976: Chapman and Hall Ltd.
2. P.W. Atkins, *Molecular Quantum Mechanics 2nd Edition*. 1983: Oxford University Press.
3. S.J. Martin, D.D.C. Bradley, P.A. Lane, H. Mellor, and P.L. Burn, *Physical Review B-Condensed Matter*, **59** 15133-15142 (1999).
4. M. Rohlfing and S.G. Louie, *Physical Review Letters*, **82** 1959-1962 (1999).
5. M. Pope and C. Swenberg, *Electronic Processes in Organic Crystals*. 2nd ed. 1999: Oxford University Press.
6. S. Barth, D. Hertel, Y.H. Tak, H. Bassler, and H.H. Horhold, *Chemical Physics Letters*, **274** 165-170 (1997).
7. R. Haberkorn and M.E. Michel-Beyerle, *Chem. Phys. Lett.*, **23** 128-130 (1973).
8. K.J. Donovan and E.G. Wilson, *Philos. Mag. B*, **44** 31-45 (1981).
9. E. Silinsh and V. Capek, *Organic Molecular Crystals*. 1994: American Institute of Physics Press.
10. M. Scheidler, U. Lemmer, R. Kersting, S. Karg, W. Riess, B. Cleve, R.F. Mahrt, H. Kurz, H. Bassler, E.O. Gobel, and P. Thomas, *Physical Review B*, **54** 5536-5544 (1996).
11. S. Barth, H. Bassler, H. Rost, and H.H. Horhold, *Physical Review B-Condensed Matter*, **56** 3844 (1997).
12. S. Barth and H. Bassler, *Physical Review Letters*, **79** 4445-4448 (1997).

13. L. Bozano, S.A. Carter, J.C. Scott, G.G. Malliaras, and P.J. Brock, *Applied Physics Letters*, **74** 1132-1134 (1999).

14. V.I. Arkhipov, U. Wolf, and H. Bassler, *Physical Review B-Condensed Matter*, **59** 7514-7520 (1999).

15. S. Barth, U. Wolf, H. Bassler, P. Muller, H. Riel, H. Vestweber, P.F. Seidler, and W. Riess, *Physical Review B-Condensed Matter*, **60** 8791 (1999).

16. H. Bassler, *Physica Status Solidi B-Basic Research*, **175** 15-56 (1993).

17. P.W.M. Blom and M. Vissenberg, *Materials Science & Engineering R-Reports*, **27** 53-94 (2000).

18. S.V. Novikov and A.V. Vannikov, *Synthetic Metals*, **85** 1167-1168 (1997).

19. U. Wolf, V.I. Arkhipov, and H. Bassler, *Physical Review B-Condensed Matter*, **59** 7507-7513 (1999).

# Bibliography

## Spectroscopy and Quantum Theory

- C. H. J Wells, Introduction to Molecular Photochemistry, (Chapman and Hall Ltd.) 1972.
- R. P. Wayne, Principles and Applications of Photochemistry, (Oxford University Press) 1988.
- J. P. Simons, Photochemistry and Spectroscopy, (John Wiley & Sons Ltd.) 1971.
- D. A. Seanor, Electrical Properties of Polymers, (Academic Press) 1982.

- W. S. Struve, Fundamentals of Molecular spectroscopy (John Wiley & Sons Inc.) 1989.
- B. P. Straughan and S. Walker, Spectroscopy Volume 1 (John Wiley & Sons Inc.) 1976.
- Gilbert and J. Baggott, Essentials of Molecular Photochemistry (Blackwell Scientific Publications) 1991.
- P. W. Atkins, Molecular Quantum Mechanics 2nd Edition (Oxford University Press) 1983.


## Conjugated Polymers and Molecular Orbital Theory.


- N. S. Sariciftci, Primary Photoexcitations in Conjugated Polymers (World Scientific Publishing Co.) 1997.
- M. Pope and C. E. Swenberg, Electronic Processes in Organic Crystals and Polymers 2nd Edition (Oxford University Press) 1999.
- R. J. Fessenden and J. S. Fessenden, Organic Chemistry 6th Edition (Brooks/Cole Publishing Company) 1998.
- J. McMurry, Organic Chemistry 4th Edition (Brooks/Cole Publishing Company) 1996.
- H. S. Nalwa, Handbook of Organic Conductive Molecules and Polymers Volumes 1-4 (John Wiley & Sons Ltd.) 1997.
- E. A. Silinsh and V. Čápek, Organic Molecular Crystals (American Institute of Physics Press) 1994.

# Chapter 3

# Experimental Methods

# 3.1 Introduction

This chapter describes the methods used for sample fabrication. It also describes the method used to obtain the photocurrent spectra and the procedure used to normalise the spectra obtained.

# 3.2 Etching of Substrates (see figure 3-1)

Indium tin oxide (ITO) patterned substrates were prepared using the following procedure:

1. Glass substrates coated with a 125nm thick layer of indium tin oxide (ITO) (Balzers, $13\Omega\square^{-1}$) were cleaned in acetone for 4 minutes in an ultrasonic bath.
2. The substrates were then cleaned with propan-2-ol (IPA) in an ultrasonic bath for 4 minutes.
3. The area NOT to be etched was coated with an etch resistant PCB marker pen and allowed to stand until dry.
4. The substrate was then placed in concentrated HCl in an ultrasonic bath for approximately 4 minutes.
5. The substrate was then cleaned in acetone for 4 minutes in an ultrasonic bath then in IPA for 4 minutes in an ultrasonic bath. The substrate was then dried using dry nitrogen.
6. The conductivity of the surface of the substrate was then determined to ensure that the exposed area had been completely etched.

## 3.3 Sample Fabrication

Samples were fabricated in a sandwich configuration. The polymers used in the photoconductivity experiments were MEH-PPV, PPY and PF2/6. MEH-PPV was obtained from Covion, Dr. L. E. Horsburgh made PPY on-site and PF2/6 was obtained from Professor Scherf of the Max-Planck-Institut für Polymerforschung.

MEH-PPV was dissolved in Chlorobenzene (6mg MEH-PPV + 1ml Chlorobenzene), PPY was dissolved in Formic acid (40mg PPY + 1.5ml Formic acid) then filtered twice and PF2/6 was dissolved in toluene (10mg PF2/6 + 0.4ml toluene).

The solutions were then spin coated onto the patterned substrate at 2500 rpm for 2 minutes (for thin PPY and MEH-PPV films) or drop cast onto the patterned ITO substrate and left in air in a class 10,000 clean room for 12 hours (for thick MEH-PPV and PF2/6 films).

Semitransparent gold electrodes (12nm) were evaporated onto the samples as shown in figure 3-2 to complete the samples. The active area of the sample was the overlap between the Au electrode and the ITO electrode.

Wires were connected to the sample with silver paint as shown in figure 3-2b. Electrical connection to the ITO was achieved by scraping away a small amount of the polymer before connecting the wire using silver paint. It was ensured that the placement of the wire connected to the Au electrode did not interfere with illumination of the active area and that none of the silver paint overlapped the edge of the Au electrode.

## 3.4 Photoconductivity Experimental Methods

The experimental set-up for the photoconductivity experiments is shown in figure 3-3. The samples were placed in an Oxford Instruments Microstat and pumped down to approximately $10^{-2}$ mbar using a rotary pump which was left running while the sample was in the microstat. A tungsten (W) filament lamp was used for experiments up to 3eV and a xenon (Xe) arc lamp was used for measurements up to 5eV. A Keithley 2400 sourcemeter was used to simultaneously apply a bias and measure the photocurrent and dark current. The experiment was computer controlled. For each photon energy, the following method was used:

- A bias was applied to the sample for 10 seconds with no illumination.
- The dark current was then measured (average of 20 measurements).
- The active area of the sample was illuminated at the appropriate photon energy.
- The photocurrent was then measured (average of 20 measurements).
- The applied bias was then set to 0V.
- The active area of the sample was then illuminated with light at 1.6eV for 30 seconds.
- The sample was then left for 5 minutes with no illumination and zero bias.

Each scan from 1.8eV to 5eV with 0.02eV increments took approximately 16 hours.

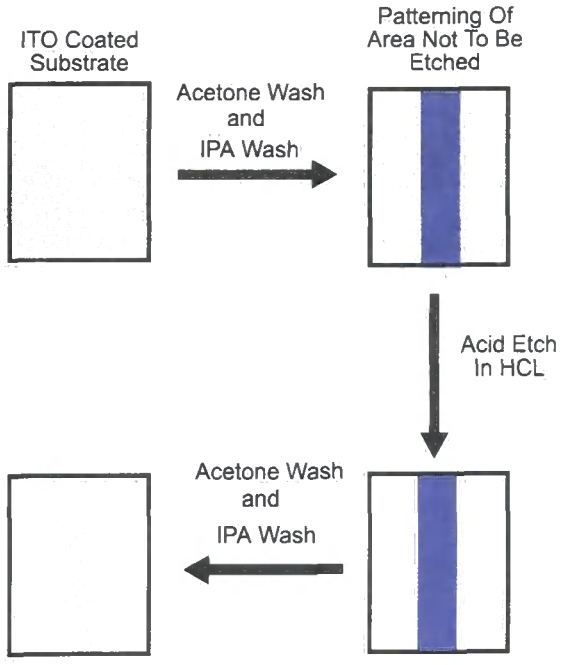


**Figure 3-1** *Etching of substrates.*

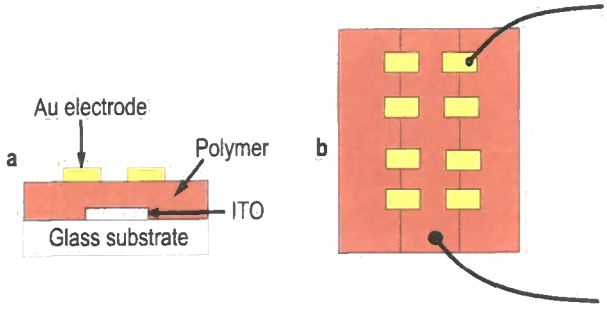


**Figure 3-2** *Sample configuration.*

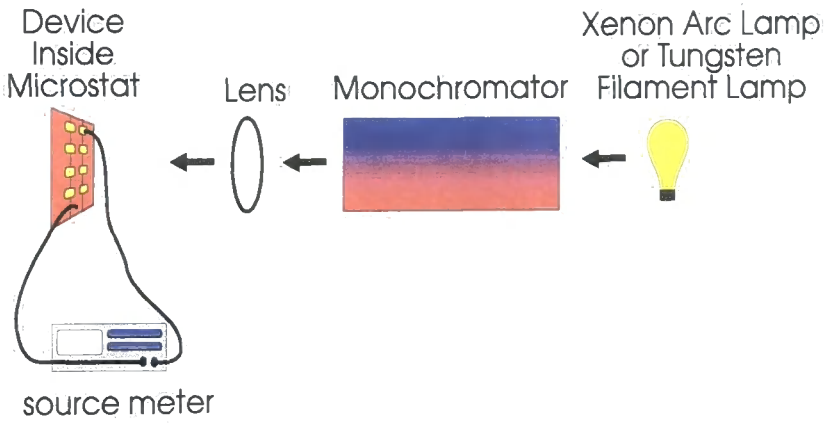


**Figure 3-3** *Experimental set-up for photoconductivity experiments.*

## 3.5 Normalisation of Data

The amount of light falling on the sample was measured using a UV enhanced silicon photodiode (SD 100, Advanced Photonix, Inc.). A quartz substrate with 12nm of Au or an ITO coated glass substrate was placed in front of the photodiode to simulate the effects of the electrode and substrate material. This data was then normalised for the response of the photodiode. The spectral response of the photodiode is shown in figure 3-4 (reproduced from the Advanced Photonix, Inc. catalogue). The normalisation curves (taking into account the photodiode response) for the Xe arc lamp for illumination through the Au electrode and for illumination through the semitransparent ITO electrode are shown in figures 3-5 and 3-6 respectively. The normalisation curves (taking into account the photodiode response) for the W lamp for illumination through the ITO electrode and for illumination through the Au electrode are shown in figure 3-7 and figure 3-8 respectively. The normalisation curves have been normalised so that the maximum value is 1. When illuminating through the ITO electrode, it was only possible to illuminate the sample at photon energies up to 3.7eV due to absorption by the ITO coated glass substrate. This can easily be seen in the absorption spectra shown in figure 3-9.

It is usually possible to determine the quantum efficiency of PC experiments but it was not possible in this case. This was because only part of the electrode was illuminated to reduce noise caused by illuminating across the ITO/Au boundary. This made the illuminated area impossible to determine and therefore, the quantum efficiency was also impossible to determine.

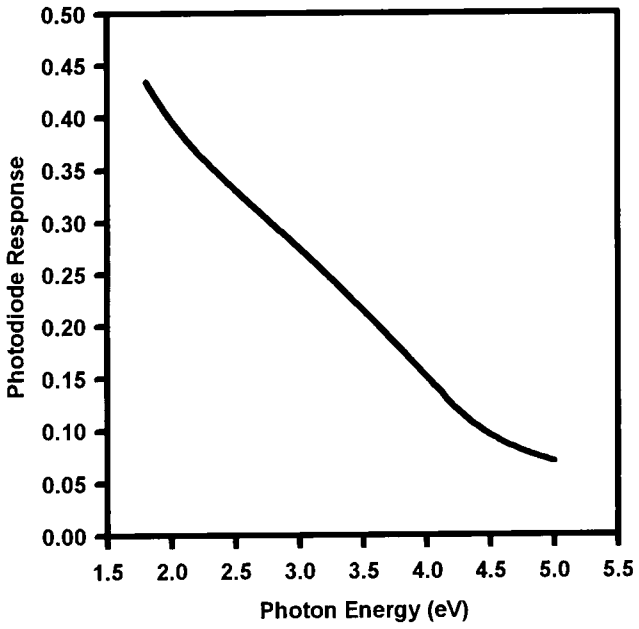


**Figure 3-4** *Spectral response of UV enhanced silicon photodiode.*

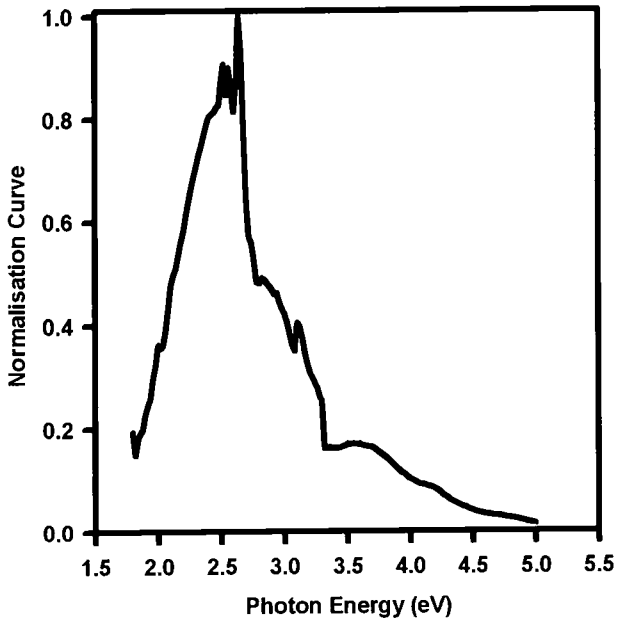


**Figure 3-5** *Normalisation curve for Xe arc lamp for illumination through a semitransparent Au layer.*

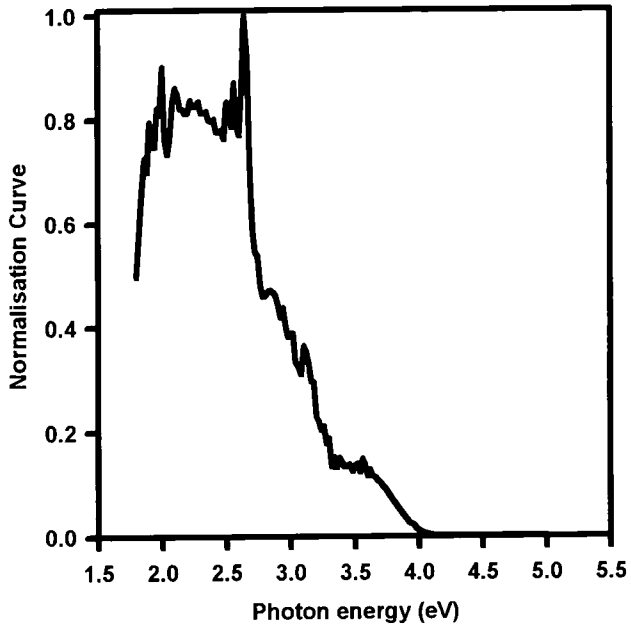


**Figure 3-6** *Normalisation curve for Xe arc lamp for illumination through the ITO coated substrate.*

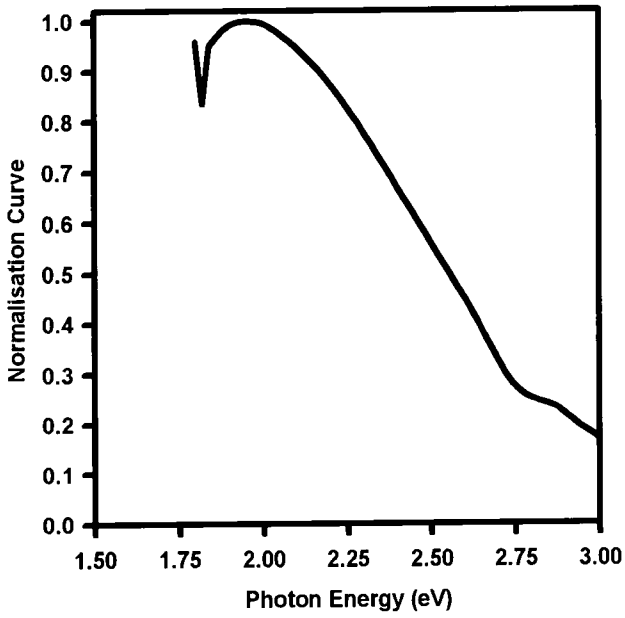


**Figure 3-7** *Normalisation curve for W lamp for illumination through the ITO coated substrate.*

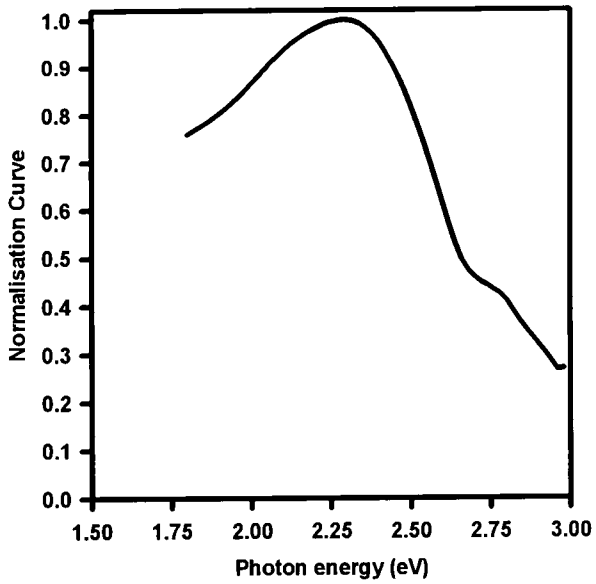


**Figure 3-8** Normalisation curve for W lamp for illumination through the Au electrode.

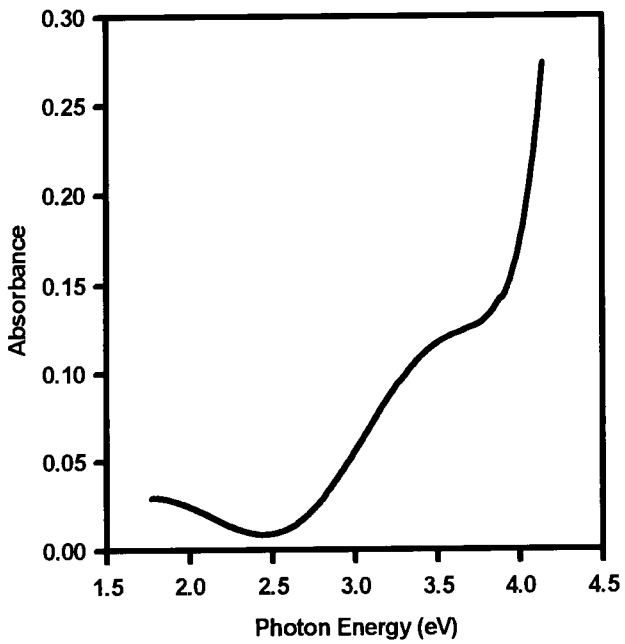


**Figure 3-9** *Absorption of an ITO coated glass substrate.*

# Chapter 4

# Photoconduction in MEH-PPV

# 4.1 Introduction

Photoconductivity in conjugated polymers is the measurement of the current produced in a polymer film sandwiched between two electrodes when illuminated by photons of a specific energy. Steady state photoconductivity measurements were made on poly(2-methoxy-5- (2'ethylhexyloxy)-1,4-phenylene vinylene) (MEH-PPV) films sandwiched between an ITO coated glass substrate and a semitransparent Au electrode. The method used to obtain the photoconductivity spectra is given in section 3.4 and the method used to normalise the spectra for the effects of the illumination source (Xe or W lamp) is given in section 3.5. For all spectra, the normalised photocurrent has been quoted for easy comparison between different experimental results.

Photoconductivity experiments have previously been performed on several conjugated polymers including MEH-PPV [1-5]. These experiments have been limited to illumination through only one electrode or for one electric field or over a small photon energy range. A comprehensive study of the effects of illumination direction, bias polarity, electric field strength, temperature and high photon energy has yet to be done for a single polymer. The results documented here rectify this situation.

Section 4.2 covers the effects of extrinsic dissociation of excitons (dissociation at the electrodes) to form charge carriers and how this is affected by the thickness of the polymer layer. The next section explains how aggregates and solvent affect the photoconductivity spectra. Section 4.4 discusses intrinsic charge carrier formation (charge carriers formed in the bulk polymer) and why this is only observed at high photon energies. Section 4.5 demonstrates how

curves were fitted to the intrinsic photocurrent spectra based on an understanding of the optical transitions in MEH-PPV. The next section discusses the effects of electric field and temperature on the charge generation mechanisms and compares the data with results obtained by Barth *et al* and Bozano who have made considerable contributions to this field. The chapter concludes with a summary.

## 4.2 Extrinsic Dissociation

This section explains how, when a photon is absorbed at photon energies appropriate to the fundamental absorption peak, an exciton is formed. This exciton can be dissociated at either electrode to give free charge carriers but only those charge carriers formed at the positive electrode can give rise to a photocurrent. The thickness of the polymer film, the charge carrier mobility, different illumination directions and bias polarities influence the photocurrent spectra.

Photoconductivity spectra were measured when the sample was illuminated through the ITO electrode for ITO negatively biased and positively biased. The photoconductivity spectra were also measured when the sample was illuminated through the Au electrode for Au negatively biased and positively biased. This was done for both thick film (7 microns) and thin film (170nm) MEH-PPV samples. The results are shown in figures 4-1 and 4-2 for thick and thin films respectively. These experiments were performed at 290K.

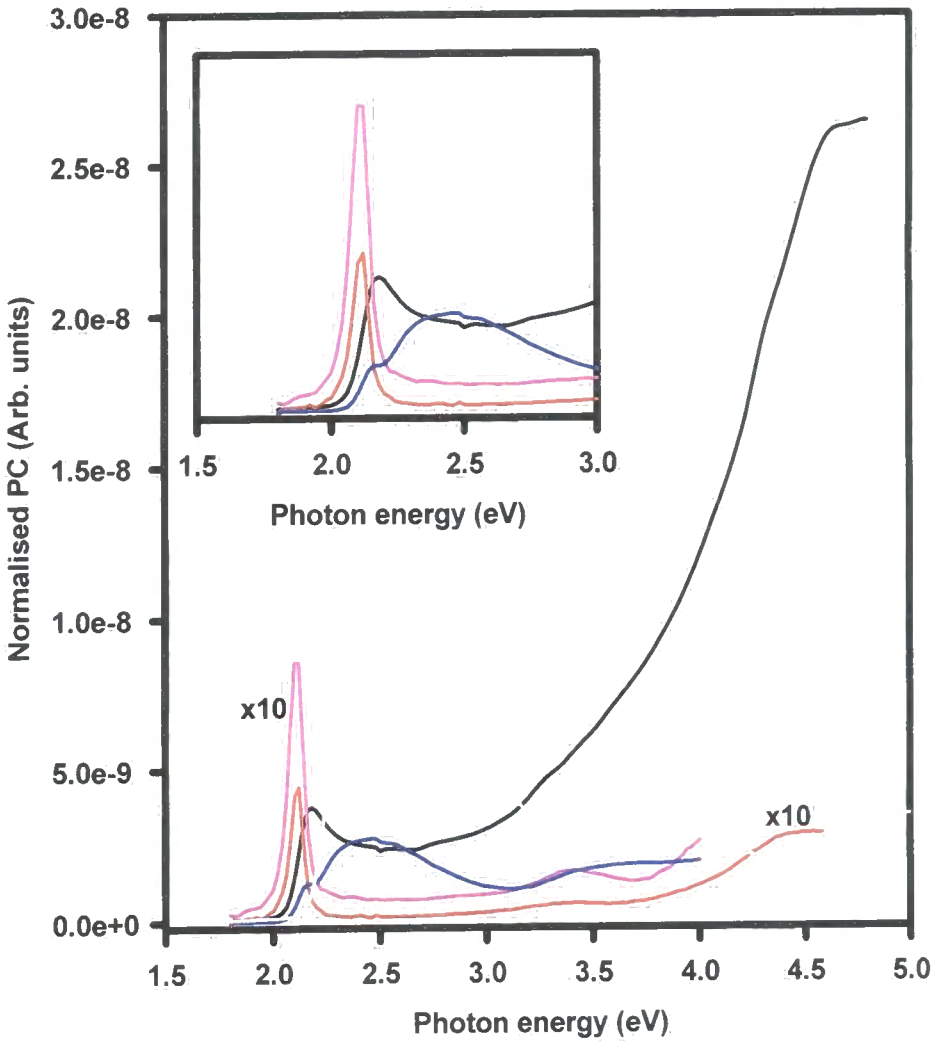


**Figure 4-1** *Photocurrent spectra for the thick film MEH-PPV sample (7 microns) illuminated through the positively biased Au electrode (black line), through the negatively biased Au electrode (red line), through the positively biased ITO electrode (blue line) and through the negatively biased ITO electrode (pink line). The spectra for illumination through the negatively biased ITO and negatively biased Au electrode have been multiplied by a factor of 10 to enable comparison with the other curves. The applied electric field was $5.7x10^6$ V/m. The absorbance spectrum of a 170nm MEH-PPV film is shown for reference (grey line, linear scale).*

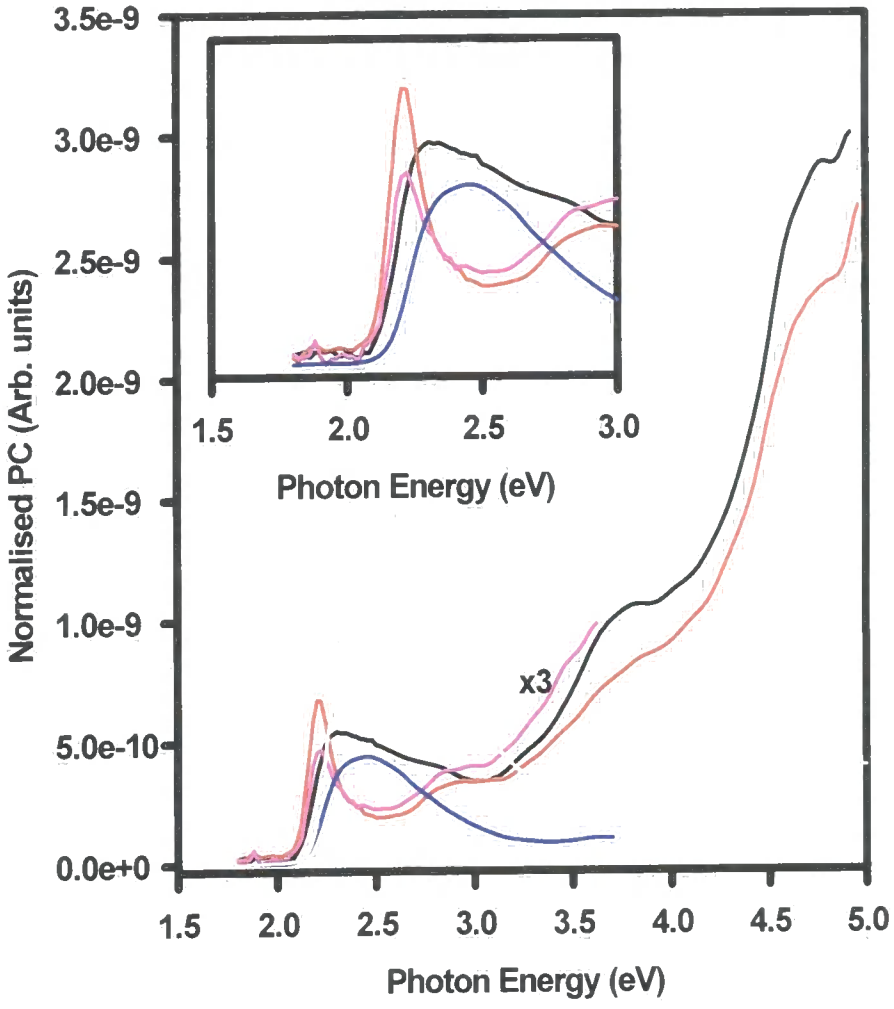


**Figure 4-2** *Photocurrent spectra for the thin film MEH-PPV sample (170nm) through the positively biased Au electrode (black line), through the negatively biased Au electrode (red line), through the positively biased ITO electrode (blue line) and through the negatively biased ITO electrode (pink line). The spectrum for illumination through the negatively biased ITO electrode has been multiplied by a factor of 3 to enable comparison with the other curves. The applied electric field was $5.9x10^6$ V/m. The absorbance spectrum of a 170nm MEH-PPV film is shown for reference (grey line, linear scale).*

For illumination through the positively biased Au electrode of the thick film MEH-PPV sample (black line, figure 4-1), the PC peaks at 2.18eV then decreases slightly before increasing rapidly with photon energy. There is evidence for peaks between 3eV and 4.8eV.

For illumination through the negatively biased Au electrode of the thick film MEH-PPV sample (red line, figure 4-1), the PC peaks at 2.15eV at the fundamental absorption edge of MEH-PPV. The PC has maxima when absorption in MEH-PPV is at a minimum (2.15eV, 3.3eV and 4.5eV) and has minima when absorption in MEH-PPV is at a maximum (2.5eV and 3.7eV).

For illumination through the positively biased ITO electrode of the thick film MEH-PPV sample (blue line, figure 4-1), there is a small peak at 2.18eV, a large peak at 2.5eV and a feature at 3.7eV. The peak at 2.5eV corresponds to a maximum in the absorption spectrum of MEH-PPV.

For illumination through the negatively biased ITO electrode of the thick film MEH-PPV sample (pink line, figure 4-1), there is a peak at 2.15eV at the fundamental absorption edge of MEH-PPV and a peak at 3.3eV. The PC spectrum is a minimum at maximum MEH-PPV absorption and is a maximum at minimum MEH-PPV absorption. The peaks in the PC spectrum for illumination through the negatively biased ITO electrode (pink line) correspond exactly to peaks in the PC spectrum when the sample is illuminated through the negatively biased Au electrode (red line).

For illumination through the positively biased Au electrode of the thin film MEH-PPV sample (black line, figure 4-2), the PC peaks at ~ 2.2eV then decreases with a minimum at 3eV. The PC then increases rapidly with photon energy with peaks at 3.7eV and 4.8eV. These peaks correspond to peaks in the absorption

spectrum of MEH-PPV. For illumination through the negatively biased Au electrode of the thin film MEH-PPV sample (red line, figure 4-2), there is a peak at 2.2eV at the fundamental absorption edge of MEH-PPV. The PC decreases with a minimum in the PC at maximum absorption in MEH-PPV (2.5eV). There is a peak at 3eV and peaks at 3.7eV and 4.8eV. The peaks at 3.7eV and 4.8eV are at the same photon energy as peaks in the PC spectrum for illumination through the positively biased Au electrode (black line, figure 4-2). For illumination through the positively biased ITO electrode of the thin film MEH-PPV sample (blue line, figure 4-2), there is a peak in the PC spectrum at 2.5eV corresponding closely to maximum absorption in MEH-PPV. For illumination through the negatively biased ITO electrode of the thin film MEH-PPV sample (pink line, figure 4-2), there is a peak at 2.2eV at the fundamental absorption edge and at 3eV. These peaks correspond to minima in the absorption spectrum of MEH-PPV. The PC then starts to increase as photon energy increases.

For illumination through the negative electrode (either Au or ITO) for both thick and thin films, there is a peak at the fundamental absorption edge. As absorption in the polymer increases, the photocurrent decreases with a minimum in the photocurrent at maximum absorption. This is known as the antibatic effect. When a photon is absorbed, a free charge carrier is created via a process that will be discussed later and a photocurrent is produced. Since the PC is a maximum when the absorption in MEH-PPV is a minimum (but not zero), this suggests that charge carriers are created from photons absorbed at the back (not illuminated) electrode which is positively biased.

For illumination through the positively biased Au electrode in both thick and thin MEH-PPV samples, there is a photocurrent response between 2eV and

3eV. This response is the result of two peaks at ~ 2.2eV and 2.5eV. The peak at 2.5eV corresponds to a maximum in the absorption spectrum of MEH-PPV. For illumination through the positively biased ITO electrode in both thick and thin MEH-PPV samplés, the PC spectra follows the absorption spectrum of MEH-PPV. This is known as the symbatic effect. This suggests that a photon is being absorbed to create a free charge carrier but does not indicate where this free charge is being created. However, if charge carriers are being produced at the positively biased electrode, illuminating through the positively biased electrode would result in the PC spectra being the same shape as the absorption spectra.

Extrinsic dissociation of an exciton formed at the positive electrode accounts for the antibatic and symbatic effects observed in the thick and thin MEH-PPV samples for illumination below 3.1eV as follows. If an exciton is formed close to the positively biased electrode, the electron may find it energetically favourable to hop via defect states to the electrode in accordance with Monte Carlo simulations of Scheidler and Lemmer (see section 2.12 and [6]). The hole is swept through the polymer under the influence of the electric field [7] and a photocurrent is produced. The coulombic binding energy for excitons not formed near the electrode is too great for dissociation to occur at these photon energies. For excitons dissociated near the negative electrode, the electron does not have a large enough mobility to reach the positive electrode and becomes trapped creating a space charge layer. This will decrease the electric field observed by the charge carriers. This is supported by mobility measurements in MEH-PPV [8].

In conclusion, below 3.1eV, a photon is absorbed and an exciton created. The exciton requires defects that are in abundance at the electrode to dissociate

and this process is known as extrinsic dissociation. If the absorbance of the polymer is large and the sample is illuminated through the negatively biased electrode, only excitons dissociated at the positively biased back electrode can give rise to a photocurrent. The photocurrent spectrum peaks when absorption in the polymer is small (but not zero) and this is known as the antibatic response. If the sample is illuminated through the positively biased electrode where the photocurrent spectrum follows the absorption spectrum of the polymer and is known as the symbatic response. The effect of the absorbance of the polymer on the photocurrent spectra is known as the inner filter effect.

## 4.3 Low Energy Enhancement Mechanisms

For illumination through: i) the positively biased ITO electrode of the thick film sample, ii) the positively biased Au electrode of the thick film sample and iii) the positively biased Au electrode of the thin film sample, there is a low energy peak in the photocurrent spectrum at 2.18eV. This peak is not observed for illumination through the positively biased ITO electrode of the thin film MEH-PPV sample.

Harrison et al have measured the PC spectra for MEH-PPV films sandwiched between Al and ITO electrodes up to photon energies of 2.6eV [3]. They also observe enhancement of the low energy peaks in the PC spectra. They ascribe these low energy peaks as the result of diffusion of excitons, extended lifetime of the exciton and the effects of aggregates.

A distribution of lengths of conjugated segments gives rise to the possibility of diffusion of excitons from shorter segments (higher energy) to

longer segments (lower energy). There are few sites that it is energetically probable for the exciton to then diffuse to once it has diffused to a longer segment. An exciton on a long segment may thus have a lifetime up to three orders of magnitude longer than excitons on shorter segments [3].

This extended lifetime could account for enhancement of the low energy peak if exciton dissociation only occurs for the small fraction of excitons on the longest segments that happen to be situated close to a dissociation site such as an electrode [3].

The effects of solvent on the formation of aggregates in films has been studied by Nguyen *et al* [9]. Aromatic solvents such as chlorobenzene have a preferential interaction with the aromatic backbone of the polymer chain and the chains adopt a rigid and open conformation in solution. With the backbone open and exposed, it is easily possible for the $\pi$ electrons on one chain to overlap with those on another chain and aggregation of the polymer chains can occur. Nonaromatic solvents such as tetrahydrofuran (THF) have a preferential interaction with the polymer side groups. The polymer chains in THF are tightly coiled and aggregation is improbable. There is experimental evidence that these aggregates remain even after the formation of films from solution [9]. The effect of these aggregates in solution is to red shift the absorption spectrum [9]. Excitons formed on aggregates in the polymer film will have a lower energy than excitons formed on single chains. The density of states (DOS) of excitons formed on aggregates will be lower in the coulombic potential well caused by the attraction between the electron and hole than the DOS of excitons formed on single chains (see figure 4-3).

Harrison *et al* believe that separation of the positive and negative charge carriers forming the exciton during dissociation may be much easier when the exciton is formed on an aggregate. An exciton formed on an aggregate may exist across neighbouring chains if the chains are close enough together. The quantum efficiency of photocarrier generation of these interchain excitons is thus greater than the photocarrier generation quantum efficiency of intrachain excitons [3].

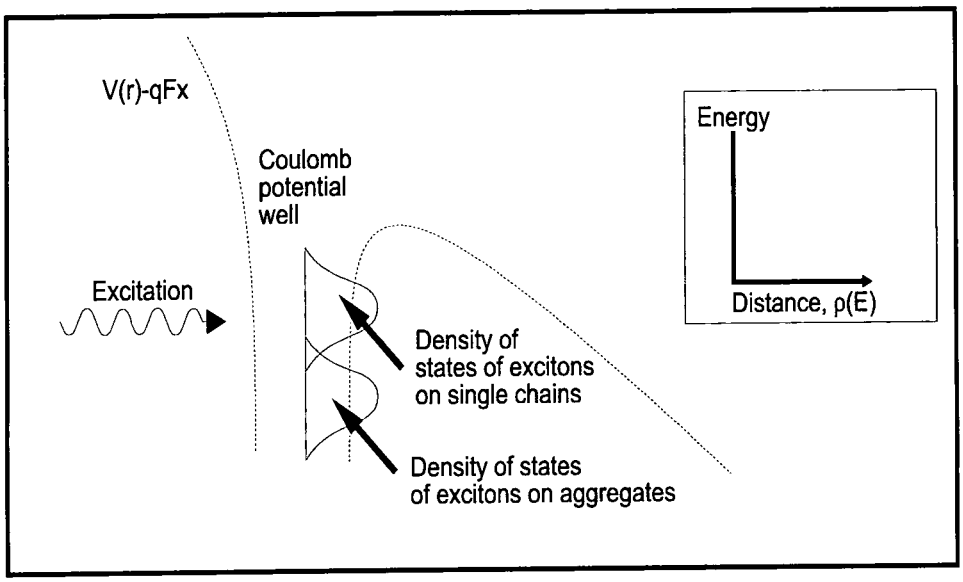


**Figure 4-3** *Diagram showing the DOS of excitons on aggregates compared to the DOS of excitons on single chains.*

## 4.4 Intrinsic Photocurrent

Extrinsic dissociation accounts for features observed in the photocurrent spectra for photon energies below approximately 3.1eV. In this section, it will be shown that the features observed above 3.1eV can be explained by intrinsic photogeneration of charge carriers (carriers formed in the bulk polymer). It is not known if an exciton is formed upon absorption then dissociated to give free

charge carriers or if free charge carriers are formed initially upon absorption. The applicability of initial exciton formation has no effect on the experimental data but will have impact on computer simulation of this process.

Barth *et al* believe that, for absorption above the fundamental transition, an electron is excited to a molecular orbital leaving a hole. This electron then loses energy and becomes bound to the hole forming an exciton. The energy lost by the electron is transferred to the polymer segment creating a vibronic heat bath. The exciton can then use some of the energy from the vibronic heat bath to dissociate and create free charge carriers [4].

Rohlfing *et al* have performed many body calculations on PPV (polyphenylenevinylene), a polymer very similar to MEH-PPV [10]. The structure of PPV is shown in figure 4-4. The absorption spectrum of PPV is almost identical to that of MEH-PPV (see figure 4-5). Their calculations show that the peaks at 3.7eV and 4.8eV are due to transitions from localised to delocalised states. When a photon is absorbed, it excites an electron to a higher energy level leaving a hole. The electron may recombine with the hole, become coulombically bound to the hole or become a free charge carrier (see section 2-13). The bottom of the conduction band or free electron continuum is the energy that an electron needs to avoid coulombic recapture with a hole. Based on calculations on PPV [10], it is believed that the conduction band overlaps the $\pi_2^*$ and $\pi_3^*$ molecular levels so that any excitations to the $\pi_2^*$ or $\pi_3^*$ level result in the formation of free electron-hole pairs (see figure 4-6). A photon with energy of 3.7eV may excite an electron from $\pi_2 \rightarrow \pi_1^*$ or excite electrons from the $\pi_1$ level into the conduction band. Charge carrier generation at these photon energies

depends on the position of the bottom of the conduction band and the width of the density of states function of the $\pi_2$* level.

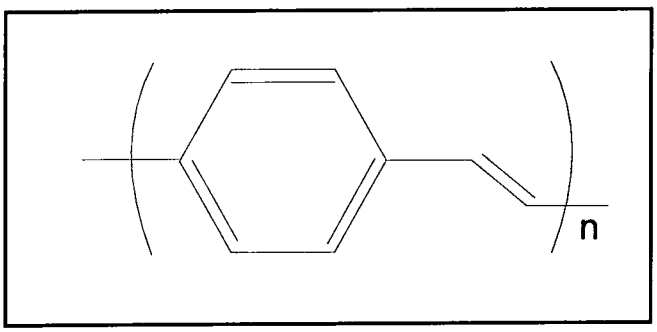


**Figure 4-4** *Structure of PPV.*

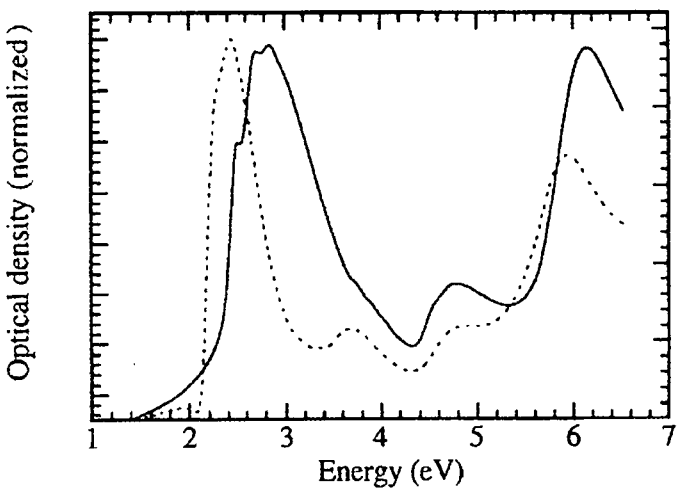


**Figure 4-5** *Absorption spectrum of PPV (solid line) and MEH-PPV (dashed line) reproduced from* [11].

The theory of Barth *et al* [4] is probable if the thermalisation time is much quicker than the electron transfer time. Experiments performed on Ru dye molecules in a colloidal anatase $TiO_2$ film give an electron transfer time of < 25fs [12]. The electron transfer time in perylene has been measured to be between 40fs and 80fs [13]. These electron transfer times are much quicker than the

thermalisation time (1ps for conjugated polymers [14]). In this case, it is more probable that, upon absorption, the electron gains enough energy from the photon to overcome the coulombic attraction of the hole. This supports the calculations of Rohlfing *et al.* The free charge carriers must still be formed from optical transitions between molecular orbitals in the polymer.

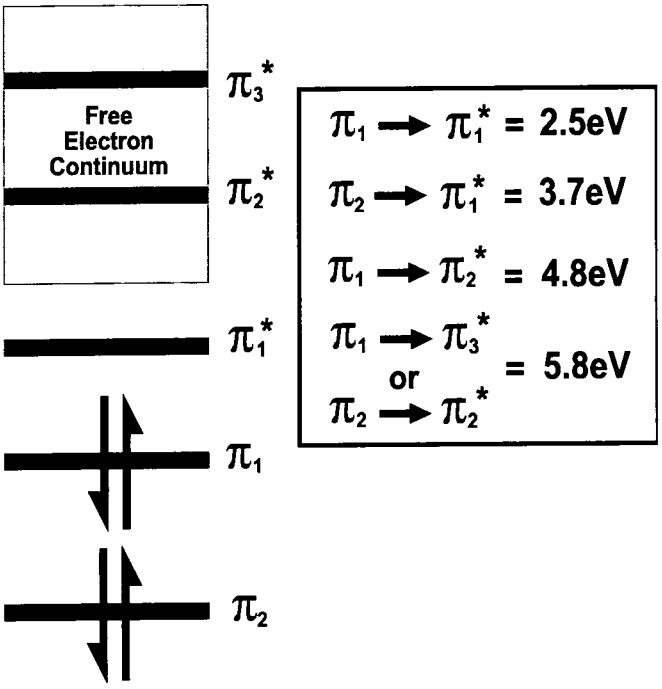


**Figure 4-6** *Energy level diagram of MEH-PPV.*

For illumination above 3.1eV through the positively biased and negatively biased Au electrode in the thin film sample (figure 4-2) and for illumination through the positively biased Au electrode in the thick film sample (figure 4-1), it can be seen that the PC increases with photon energy. This effect is not observed for illumination through the ITO electrode because it is impossible to illuminate the sample through the ITO electrode at photon energies above ~ 4eV due to absorption by the glass substrate.

In the thick MEH-PPV sample, the PC increases when illuminating through the positively biased Au electrode but not when illuminating through the negatively biased Au electrode (figure 4-1). This is due to the difference in mobility of the charge carriers. Bozano *et al* [8] have measured the mobility of electrons and holes in MEH-PPV at various electric fields at 200K and 300K. Their data suggests that electron and hole mobility increase with temperature and electric field (see section 2-14). At the electric fields and temperatures used for PC measurements discussed in this work, the electron mobility is at least an order of magnitude lower than the hole mobility. At 300K and an electric field of $5.8 \times 10^{6}$V/m, the electron mobility is $1.48 \times 10^{-4}$m$^2$/Vs and the hole mobility is $1.46 \times 10^{-3}$m$^2$/Vs respectively. For charge carriers generated intrinsically in the bulk polymer, the hole will be attracted to the negative electrode and the electron will be attracted to the positive electrode. If the electron cannot reach the positive electrode, it will become trapped and a space charge layer will be formed. This will decrease the total electric field experienced by the hole and decrease the distance that the hole can travel and the photocurrent will decrease. The closer the charge carriers are generated to the positive electrode, the higher the probability that the electron can reach the positive electrode and the photocurrent will increase. If the MEH-PPV film is thin then the electron has a high probability of reaching the positive electrode no matter where the charge carriers are generated.

Illumination through the negatively biased Au electrode for the thick MEH-PPV film (red line, figure 4-1) shows antibatic peaks at 3.4eV and 4.5eV. If the MEH-PPV film is thick and charge carriers are formed close to the negatively biased electrode, the electron has a low probability of reaching the

positive electrode. This explains why, in thick MEH-PPV films, high energy photocurrent is only observed for illumination through the positively biased electrode.

For illumination through the negatively biased and positively biased Au electrode in the thin MEH-PPV film sample, there are peaks in the photocurrent spectra at 3.9eV and 4.8eV (figure 4-2). There are no observable peaks in the photocurrent spectrum for illumination through the positively biased Au electrode in the thick MEH-PPV film sample for photon energies above 3eV (black line, figure 4-1). There may be underlying peaks contributing to this feature but they are not resolvable.

The experiments performed above also give an estimate of the exciton binding energy. This is defined as the energy difference between the onset of absorption and the onset of intrinsic photoconduction. For MEH-PPV, the exciton binding energy can be estimated to be approximately 1eV. A layer of SiO evaporated between the ITO substrate and the polymer or evaporated between the Au layer and the polymer would remove extrinsic effects due to the energy level alignment between the SiO, the polymer and the electrode material. A more accurate value for the exciton binding energy could then be obtained.

In conclusion, above 3.1eV, absorption of a photon produces free charge carriers in the bulk polymer. These charge carriers can migrate through the polymer and give rise to a photocurrent. The electron mobility and polymer layer thickness dictates the magnitude of the photocurrent.

## 4.5 Peak Fitting of Intrinsic Photocurrent

Absorption in molecular systems is related to the DOS function. The DOS for molecular orbitals is Gaussian in shape. Dipole transitions are Lorentzian in shape and inhomogeneous broadening is Gaussian in shape therefore a Gaussian-Lorentzian convolution was used to give more flexibility in the shape of the fitted peaks. Gaussian-Lorentzian peaks were fitted to the intrinsic photocurrent spectra at 3.41eV, 3.76eV, 4.71eV and 5.88eV. A Gaussian-Lorentzian convolution was used to give more variability in the shape of the fitted peaks so that a more statistically accurate fit could be obtained. The peaks at 3.76eV, 4.71eV and 5.88eV correspond to peaks that are easily observable in the absorption spectrum of MEH-PPV (figure 2-15). There is no evidence of a molecular level in the absorption spectrum of MEH-PPV corresponding to the fitted peak at 3.41eV. It may however be a vibronic in the fundamental absorption peak of MEH-PPV and may then be included when fitting peaks to the PC spectra. An example of the fitted peaks for illumination through the positively biased Au electrode at 290K is shown in figure 4-7.

All fitted peaks produced statistically accurate fits ($r^2$>0.99995). It was found that small changes in the width and height of the fitted peaks still produced excellent fits to the data but produced large changes in the area under the fitted peaks which is proportional to the DOS of the optical transition. It can be seen that the fitted peaks are very broad and that the intensity does increase with photon energy. It was impossible to determine if the intensity increased linearly or exponentially with photon energy.

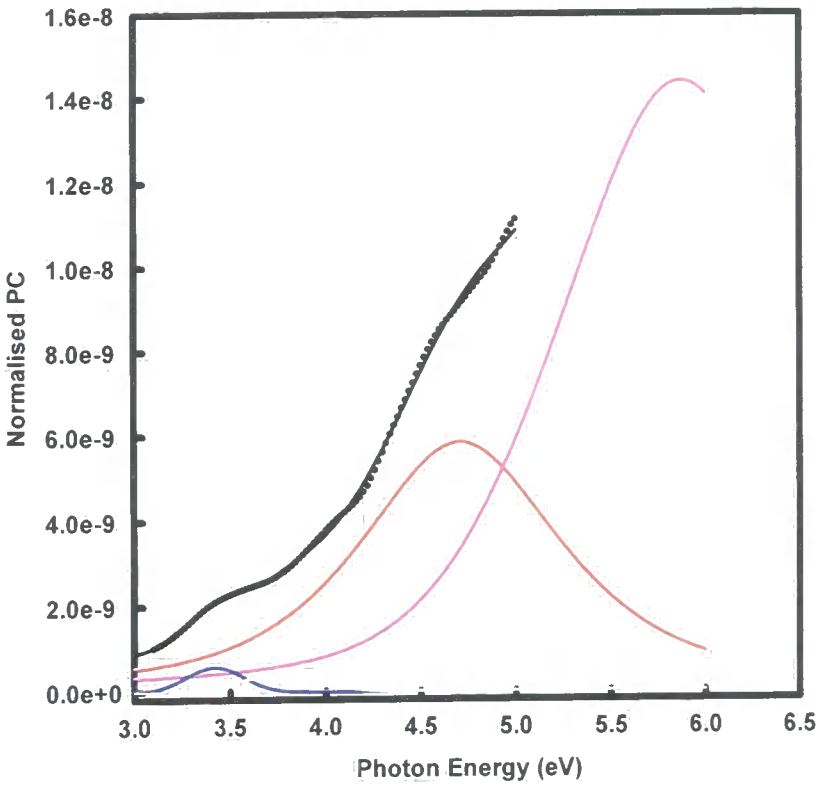


**Figure 4-7** *Data for illumination through Au electrode of thick film sample with Au electrode at +4V (symbols), fitted peaks (blue, pink, grey and red lines) and fitted line (black line)(from figure 4-12).*

## 4.6 Electric Field and Temperature Effects

In this section, the temperature and electric field dependence of the photocurrent at different photon energies will be discussed. The effects of charge carrier mobility will be discussed and a comparison with Onsager's theory of exciton dissociation will be made.

The electron and hole mobility at various electric fields and temperatures has been measured by Bozano *et al* [8]. The carrier mobility $\mu$ is given by equation 4-1 and 4-2:

$$\mu = \mu_o(T)e^{\gamma\sqrt{E}}$$

**Equation 4-1**

$$\gamma = \left(\frac{1}{k_B T} - \frac{1}{k_B T_o}\right) B$$

**Equation 4-2**

where $\mu_o$ is the zero field mobility, $E$ is the electric field across the device, $\gamma$ is the electric field coefficient, $T$ is the temperature and $T_o$ and $B$ are constants. The constants $T_0$ and B, obtained from [8] are given in table 4-1 and the values for $\mu_o$ for various temperatures are given in table 4-2. Using equations 4-1 and 4-2 and the data in tables 4-1 and 4-2, the electric field and temperature dependence of the electron and hole mobility can be calculated. The electric field and temperature dependence of the electron and hole mobility are shown in figures 4-8 and 4-9 respectively.

| **Constant** | | **Holes** | **Electrons** |
|---|---|---|---|
| B | $eV(m/V)^{1/2}$ | $2.3x10^5$ | $2.6x10^5$ |
| $T_o$ | K | 600 | 880 |

**Table 4-1** *Coefficients for equation 4-2 from* [8].

| Temperature (K) | $\mu_o$ for electrons ($cm^2/Vs$) | $\mu_o$ for holes ($cm^2/Vs$) |
|---|---|---|
| 200 | 1.8e-12 | 2.3e-11 |
| 210 | 8.0e-12 | 7.0e-11 |
| 220 | 1.7e-11 | 2.0e-10 |
| 230 | 4.0e-11 | 5.0e-10 |
| 240 | 8.0e-11 | 1.1e-9 |
| 250 | 1.5e-10 | 2.2e-9 |
| 260 | 2.5e-10 | 4.8e-9 |
| 270 | 5.0e-10 | 1.0e-8 |

**Table 4-2**

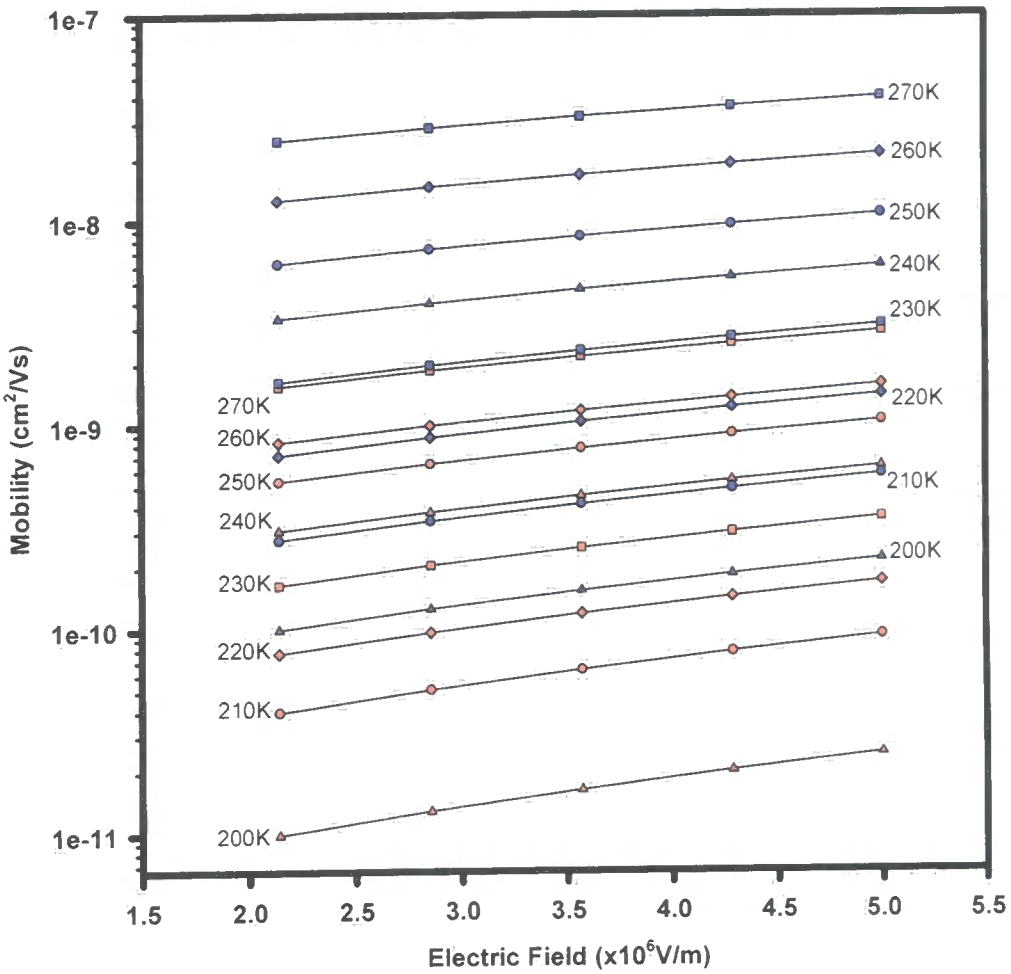


**Figure 4-8** Calculated electric field dependence of electron mobility (red symbols) and hole mobility (blue symbols).

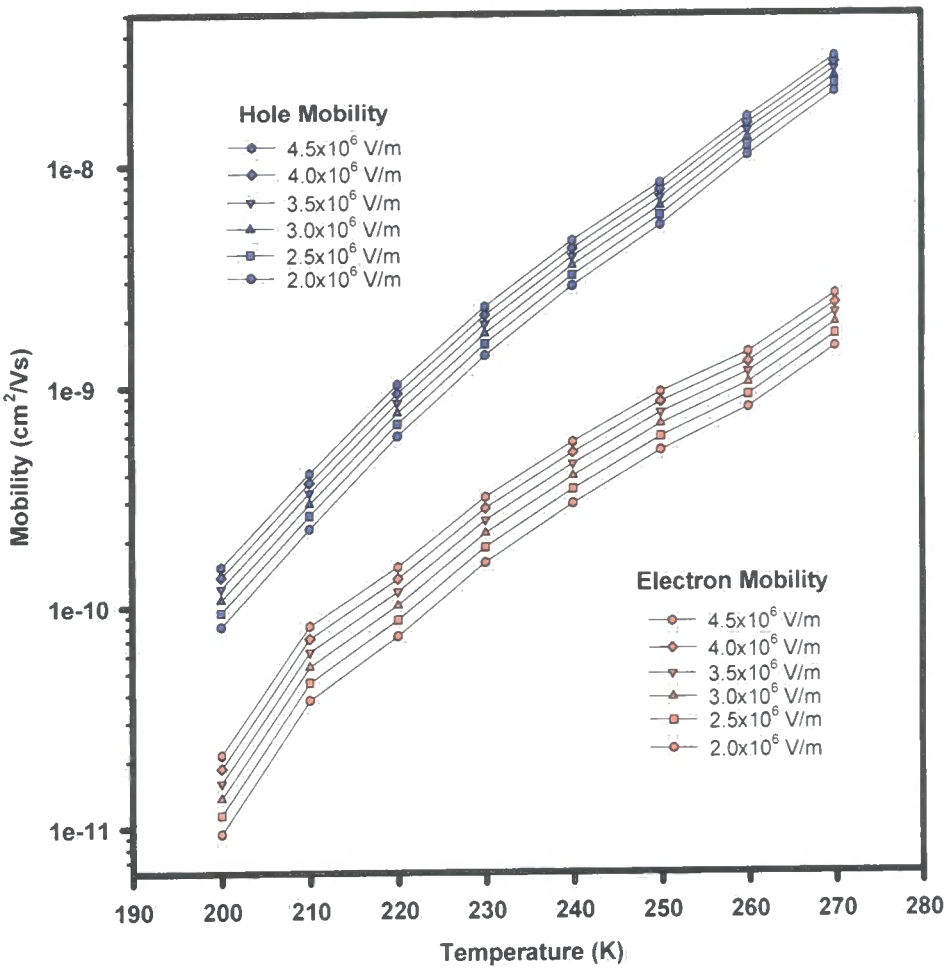


**Figure 4-9** Calculated temperature dependence of electron and hole mobility.

The field assisted ionisation of carrier pairs produced by the absorption of radiation was investigated by Onsager [15]. The Onsager theory of dissociation was modified by Pai and Enck to explain the effects of electric field, excitation wavelength and temperature dependence of photogeneration in amorphous selenium [16]. The first few terms of an infinite sum for the charge carrier generation efficiency is given by [16]:

$$\phi(r_o,E)=\phi_o e^{-r_c(T)/r_o}\left[1+\left(\frac{e}{kT}\right)\frac{1}{2!}r_c E+\left(\frac{e}{kT}\right)^2\frac{1}{3!}r_c\left(\frac{1}{2}r_c-r_o\right)E^2+\left(\frac{e}{kT}\right)^3\frac{1}{4!}r_c\left(r_o^{\,2}-r_o r_c+\frac{1}{6}r_c^{\,2}\right)E^3\right]$$

**Equation 4-3**

where $r_o$ is the initial intrapair distance, $E$ is the electric field, $\phi_o$ is the primary dissociation yield and $r_c$ is the distance at which the Coulomb energy is equal to $kT$ and is given by equation 4-4.

$$r_c(T)=\frac{e^2}{4\pi\varepsilon\varepsilon_o kT}$$

**Equation 4-4**

where $\varepsilon$ is the relative permittivity of the material and $\varepsilon_o$ is the permittivity of free space. A value for the primary dissociation yield $\phi_o$ can be obtained by extrapolating $\phi$ at $T\rightarrow\infty$. A field independent primary dissociation yield must be assumed for the determination of the initial intrapair distance using this formalism.

Barth *et al* have successfully used this formalism to determine an initial intrapair distance of 1.2nm for PPV-ether at 3.4eV [5].

The electric field dependence of the photocurrent spectra at 200K and 290K for a 7 micron thick MEH-PPV film are shown in figures 4-10 and 4-11 respectively.

The perturbations in the photocurrent spectra between 2.5eV and 2.7eV shown in the inset in figures 4-10 and 4-11 are due to sharply varying features in the output of the Xe arc lamp.

The PC at 3.5eV, 4.0eV and 4.5eV as a function of electric field at 290K and 200K, obtained from figures 4-10 and 4-11, are shown in figure 4-12. It can be seen that the PC increases linearly with electric field and that, at 200K, a higher electric field is needed to produce the same photocurrent obtained at 290K.

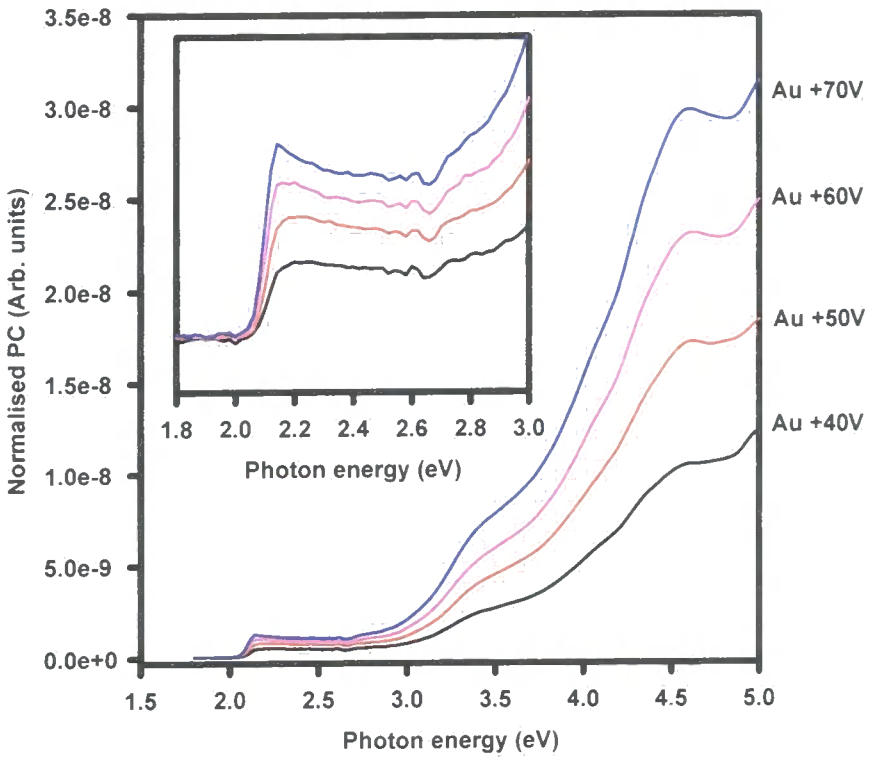


**Figure 4-10** *Electric field dependence of PC spectra at 200K for illumination through the positively biased Au electrode. Polymer thickness = 7 microns.*

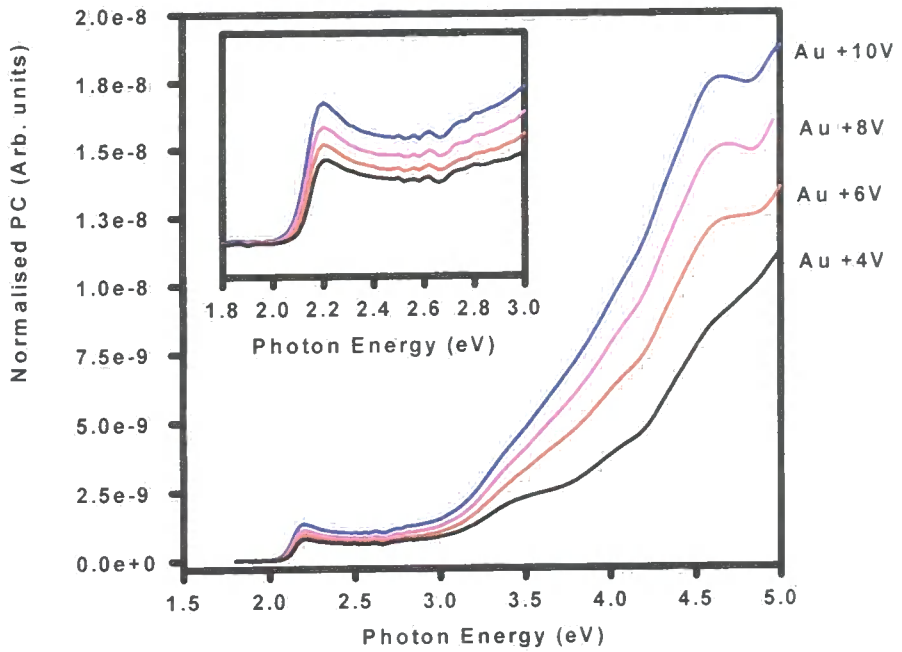


**Figure 4-11** *Electric field dependence of PC spectra at 290K for illumination through the positively biased Au electrode. Polymer thickness = 7 microns.*

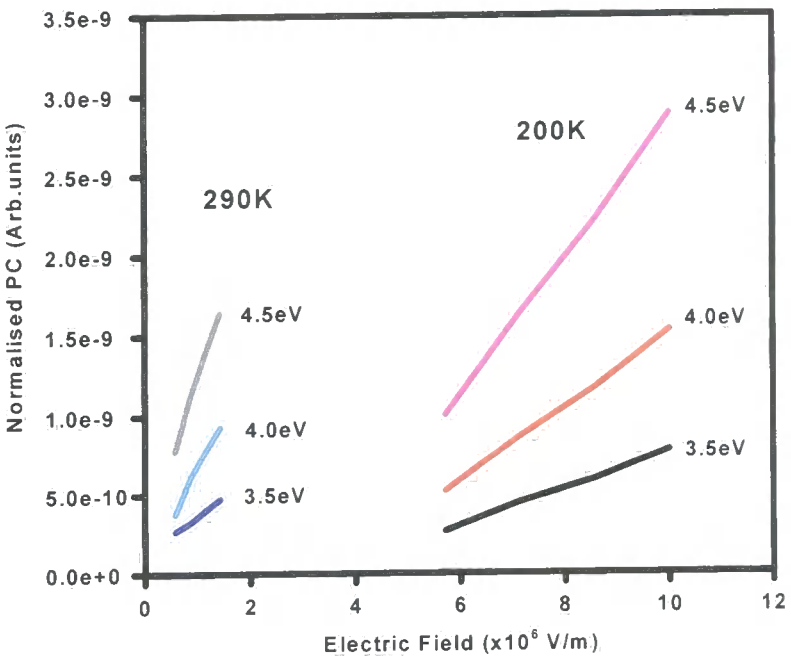


**Figure 4-12** *Electric field dependence of PC at various photon energies at 290K and 200K. Illumination was through the positively biased Au electrode of the thick film MEH-PPV sample.*

The electric field dependence for illumination at 2.5eV through the positively biased Au electrode at temperatures ranging from 250K to 290K is shown in figure 4-13. The electric field dependence for illumination at 2.5eV through the positively biased ITO electrode at these temperatures is shown in figure 4-14.

At 2.5eV, the photocurrent response is due to extrinsic dissociation at the electrodes and therefore the results shown in figures 4-13 and 4-14 will tell us the effect of temperature and electric field for extrinsic dissociation. The temperature dependence for illumination through the positively biased Au electrode is small. The temperature dependence for illumination through the positively biased ITO electrode is much larger.

It has been suggested that, during operation of an ITO/MEH-PPV/metal sample (i.e. when an electric field is applied), oxygen from the ITO electrode diffuses into the MEH-PPV. Carbonyl species (a group in which a carbon atom is double bonded to an oxygen atom) may form in MEH-PPV as shown in figure 4-15 [17]. Carbonyl formation produces a loss of conjugation in the polymer backbone and an interfacial layer is produced between the ITO and the MEH-PPV. Charge mobility through this interfacial layer will be lowered and the interfacial layer can be thought of as a barrier to charge transport. This explains the effects of temperature and electric field observed for illumination through the positively biased ITO electrode at 2.5eV.

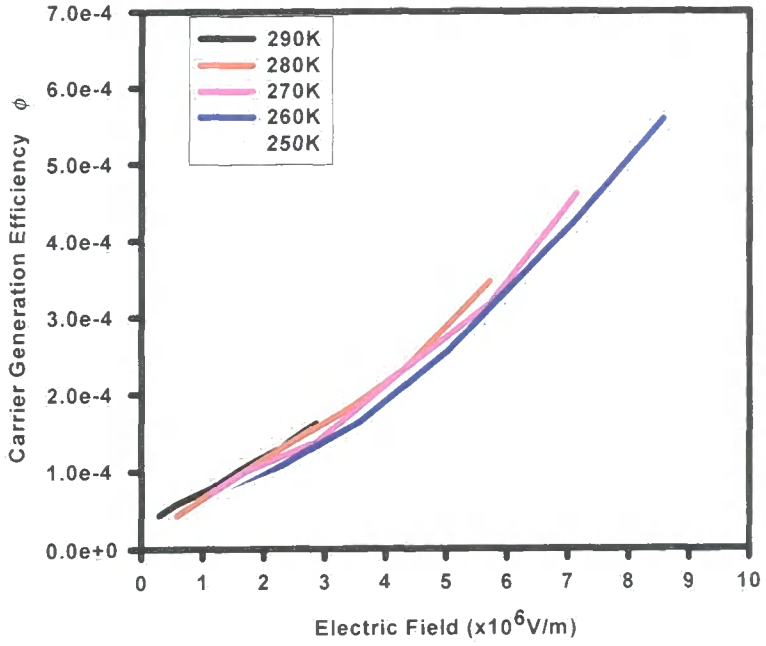


**Figure 4-13** *Electric field dependence for illumination at 2.5eV through the positively biased Au electrode of the thick film MEH-PPV sample.*

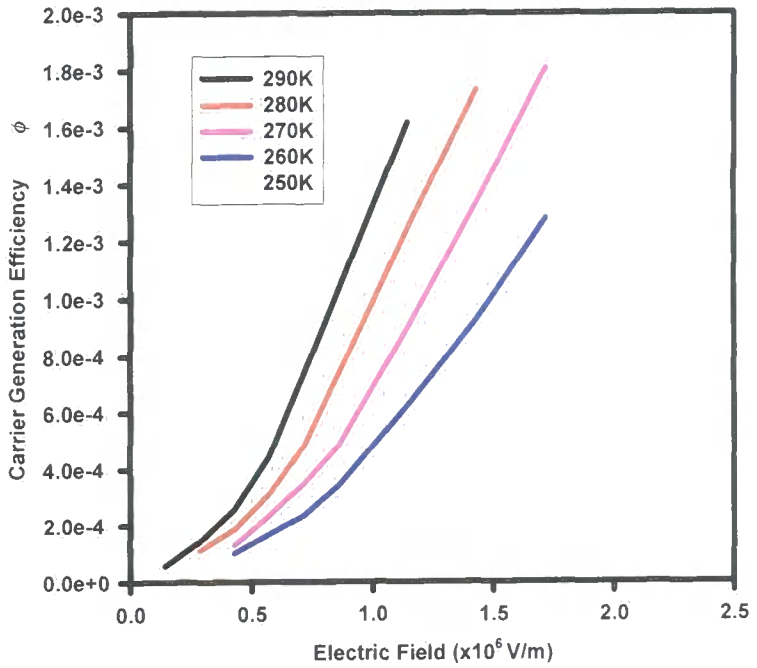


**Figure 4-14** *Electric field dependence for illumination through the positively biased ITO electrode of the thick film MEH-PPV sample at 2.5eV.*

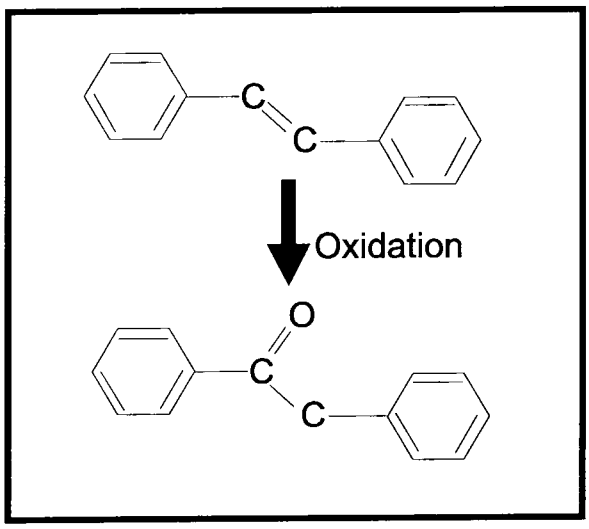


**Figure 4-15** *Oxidation of MEH-PPV and loss of conjugation by formation of a carbonyl group.*

Because the oxidation process occurs during operation, this implies that, during sample construction, the MEH-PPV will not be oxidised at the air/MEH-PPV interface as no electric field is applied. The photocurrent for illumination at 2.5eV through the positively biased ITO electrode is much greater than for illumination at 2.5eV through the positively biased Au electrode at comparable fields. This is because, even though there is an interfacial layer at the ITO/MEH-PPV interface, there are more impurities and defects at the ITO/MEH-PPV interface than at the Au/MEH-PPV interface to aid dissociation as discussed in section 4.3.

The temperature dependence for illumination at 4eV through the positively biased Au electrode at various electric fields is shown in figure 4-16. There are two regimes in the temperature dependence data with a discontinuity at 245K. It is believed that, below 245K, ring torsion in the MEH-PPV chain becomes frozen.

There is no evidence in the literature to support this hypothesis for MEH-PPV but experiments on polyaniline (Pani) give a ring torsion freezing temperature of 193K [18].

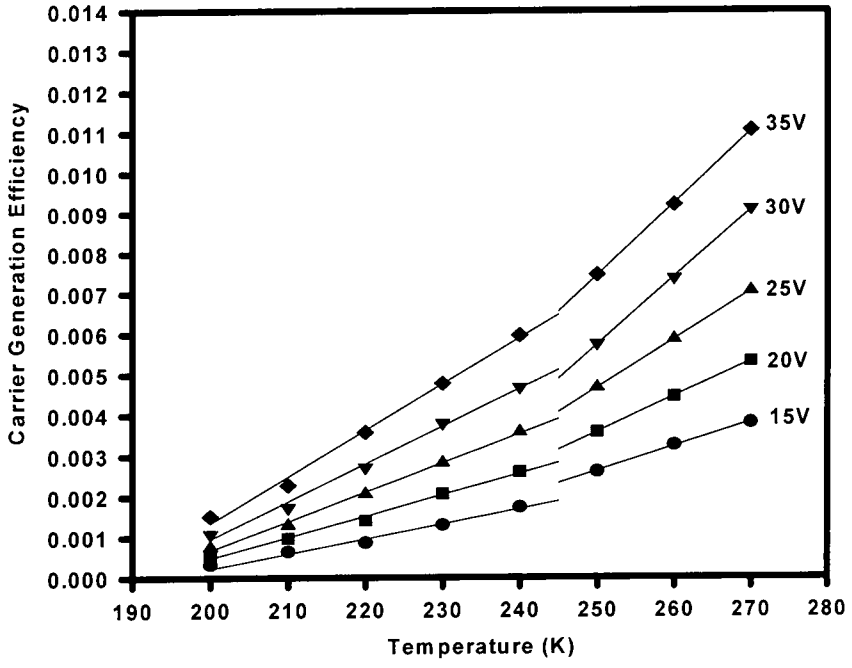


**Figure 4-16** *Temperature dependence for illumination at 4eV through the positively biased Au electrode at various applied voltages. Sample thickness is 7microns.*

Using the formalism of Pai and Enck based on Onsagers theory of exciton dissociation described above, it is possible to estimate the initial intrapair distance ($r_o$). A plot of the carrier generation efficiency against 1000/T gives a value for the primary dissociation yield $\phi_0$ defined as the carrier generation efficiency at infinite temperature. This value can be used with equation 4-3 to obtain the initial intrapair distance.

The temperature dependence of the carrier generation efficiency for illumination through the positively biased Au electrode at 4eV is shown in figure 4-17.

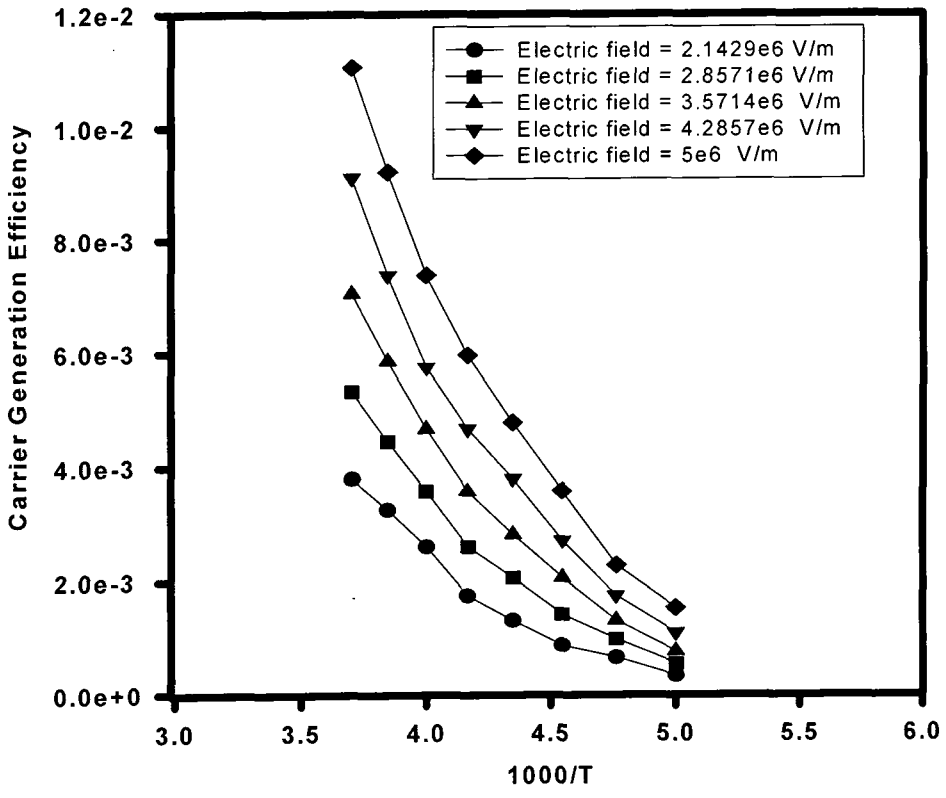


**Figure 4-17** *Temperature dependence of the carrier generation efficiency for illumination through the positively biased Au electrode at 4eV for determination of the primary dissociation yield* $\phi_o$.

From the data obtained for MEH-PPV for illumination through the Au electrode at 4eV, values for the primary dissociation yield varied from 0.05 to 0.68. These values are shown in table 4-3. This variation may be due to the electric field and temperature dependence of the charge carrier mobility discussed above. Using an average value of 0.35 for the primary dissociation yield obtained from the data shown in table 4-3, it was possible to fit the electric field dependence of the photocurrent using equation 4-3. The temperature dependence

of the initial intrapair distance is shown in figure 4-18. The initial intrapair distance is linear with temperature with a discontinuity due to ring torsion freezing.

| Temperature (K) | Primary Dissociation Yield |
|---|---|
| 200 | 0.05 |
| 210 | 0.12 |
| 220 | 0.18 |
| 230 | 0.31 |
| 240 | 0.42 |
| 250 | 0.48 |
| 260 | 0.56 |
| 270 | 0.68 |

**Table 4-3** *Values for the primary dissociation yield at 4eV.*

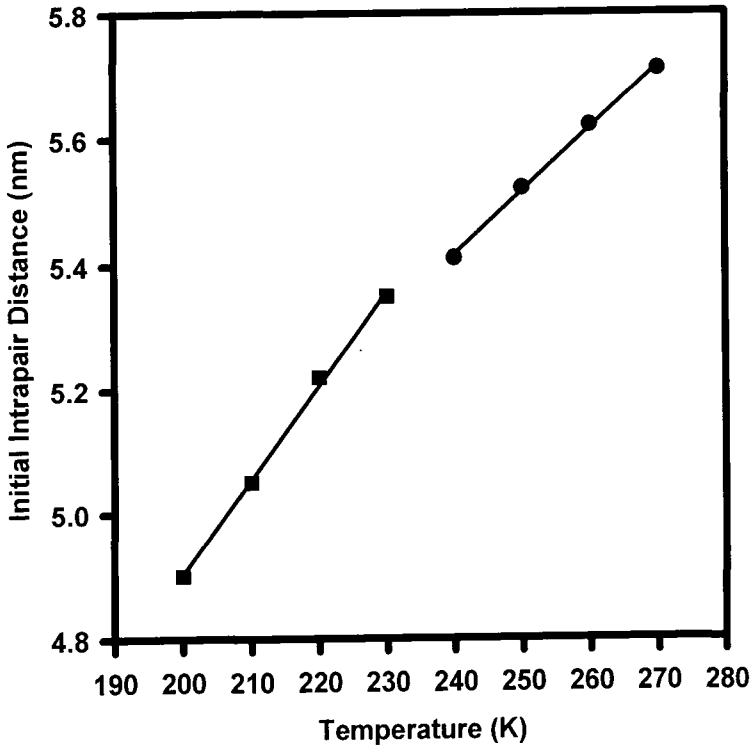


**Figure 4-18** *Temperature dependence of the initial intrapair distance.*

These values compare well with those obtained for poly(2,5-pyridinediyl) (3.33nm) [2] and for PPV-amine (1.05nm) [4].

## 4.7 Summary

In conclusion, it has been determined that excitons may be dissociated extrinsically at the electrodes at low photon energies. At high photon energies, free charge carriers are generated but only holes contribute to the photocurrent due to low electron mobility in MEH-PPV. Onsager's theory gives a good fit to the electric field dependence of the data and the temperature dependence of the initial intrapair distance has been obtained.

# References


1. A. Kohler, D.A. dosSantos, D. Beljonne, Z. Shuai, J.L. Bredas, R.H. Friend, S.C. Moratti, and A.B. Holmes, *Synthetic Metals*, **84** 675-676 (1997).
2. F. Feller and A. Monkman, *Applied Physics Letters*, **76** 664-666 (2000).
3. M.G. Harrison, J. Gruner, and G.C.W. Spencer, *Physical Review B-Condensed Matter*, **55** 7831-7849 (1997).
4. S. Barth and H. Bassler, *Physical Review Letters*, **79** 4445-4448 (1997).
5. S. Barth, H. Bassler, H. Rost, and H.H. Horhold, *Physical Review B-Condensed Matter*, **56** 3844 (1997).
6. M. Scheidler, U. Lemmer, R. Kersting, S. Karg, W. Riess, B. Cleve, R.F. Mahrt, H. Kurz, H. Bassler, E.O. Gobel, and P. Thomas, *Physical Review B*, **54** 5536-5544 (1996).
7. S. Barth, D. Hertel, Y.H. Tak, H. Bassler, and H.H. Horhold, *Chemical Physics Letters*, **274** 165-170 (1997).
8. L. Bozano, S.A. Carter, J.C. Scott, G.G. Malliaras, and P.J. Brock, *Applied Physics Letters*, **74** 1132-1134 (1999).
9. T.Q. Nguyen, V. Doan, and B.J. Schwartz, *Journal of Chemical Physics*, **110** 4068-4078 (1999).
10. M. Rohlfing and S.G. Louie, *Physical Review Letters*, **82** 1959-1962 (1999).
11. S.J. Martin, D.D.C. Bradley, P.A. Lane, H. Mellor, and P.L. Burn, *Physical Review B-Condensed Matter*, **59** 15133-15142 (1999).

12. T. Hannappel, B. Burfeindt, W. Storck, and F. Willig, *Journal of Physical Chemistry B*, **101** 6799-6802 (1997).

13. B. Burfeindt, C. Zimmermann, S. Ramakrishna, T. Hannappel, B. Meissner, W. Storck, and F. Willig, *Zeitschrift Fur Physikalische Chemie-International Journal of Research in Physical Chemistry & Chemical Physics*, **212** 67-75 (1999).

14. M. Pope and C. Swenberg, *Electronic Processes in Organic Crystals*. 2nd ed. 1999: Oxford University Press.

15. L. Onsager, *Phys. Rev. B.*, **54** 554 (1938).

16. D. Pai and R. Enck, *Phys. Rev. B*, **11** 5163-5174 (1975).

17. J.C. Scott, S.A. Carter, S. Karg, and M. Angelopoulos, *Synthetic Metals*, **85** 1197-1200 (1997).

18. A.J. Milton and A.P. Monkman, *Journal of Physics D-Applied Physics*, **26** 1468-1474 (1993).

# Chapter 5

# Photoconduction in PPY

# 5.1 Introduction

In this chapter, the results of PC experiments on thin film poly(2,5-pyridinediyl) (PPY) samples will be discussed. In the previous chapter, extrinsic dissociation of excitons and intrinsic charge carrier generation in MEH-PPV samples were discussed. It is reasonable to assume that both extrinsic dissociation of excitons and intrinsic charge carrier generation will be applicable to PC in PPY as well as MEH-PPV. The results presented in this chapter confirm this expectation. The onset of extrinsic effects has to occur at photon energies appropriate to the fundamental absorption of PPY (the polymer must absorb photons to produce a photocurrent). The onset of intrinsic charge carrier generation must occur at a higher photon energy than the fundamental absorption edge of PPY but the exact photon energy at which this onset will occur cannot be predicted based on PC experiments on MEH-PPV. This is due to the different energy level structure in PPY.

In the previous chapter, it was verified that holes have a higher mobility than electrons in MEH-PPV and this explained the PC spectra obtained when the sample was illuminated through the ITO or Au electrode with the illuminated electrode positively or negatively biased. In MEH-PPV, the symbatic effect is observed when the positively biased electrode is illuminated. The antibatic effect is observed when the negatively biased electrode is illuminated.

Current-voltage measurements on PPY samples have shown that electrons have a higher mobility than holes [1]. This difference implies that, in PPY, the antibatic effect should be observed for illumination through the positively biased electrode and the symbatic effect should be observed for illumination through the negatively biased electrode in contrast to MEH-PPV.

Steady state photoconductivity experiments have previously been performed on a range of other conjugated polymers [2-8]. A number of experiments have been performed on PPY [1, 9-13]. PPY is an important polymer because it is an electron transporter [13] and has great potential for many applications including LED devices and field effect transistors. Steady state photoconductivity experiments have previously been performed on PPY samples up to 4eV [14, 15]. Since the fundamental absorption peak is at 3.2eV, only extrinsic effects have been observed. If intrinsic effects are to be observed, then photoconductivity measurements at higher photon energies must be made. In this work, photoconductivity measurements up to 5eV were made on a 120nm thick PPY film sandwiched between an ITO coated glass substrate and a semitransparent Au electrode. Previous experiments have shown that no photocurrent is observed for films greater than ~ 300nm. It is assumed that this is due to the low carrier mobility (Feller, MSc thesis, 1999).

## 5.2 Experimental Data

Steady state photoconductivity measurements were made on PPY films sandwiched between an ITO coated glass substrate and a semitransparent Au electrode. The method used to obtain the photoconductivity spectra is given in section 3.4 and the method used to normalise the spectra for the effects of the illumination source (Xe or W lamp) is given in section 3.5.

The photoconductivity spectra for illumination through the Au electrode and illumination through the ITO electrode with the illuminated electrode positively biased and the illuminated electrode negatively biased for a thin film

PPY sample (120nm) are shown in figure 5-1. Experiments were performed at 290K.

For illumination through the positively biased ITO electrode (blue line, figure 5-1), there is a feature at 3eV. For illumination through the negatively biased ITO electrode (pink line, figure 5-1), there are two features close together at 3.05eV and 3.3eV. It was not possible to obtain PC spectra at photon energies greater than 3.7eV when the sample was illuminated through the ITO electrode due to absorption by the glass substrate.

For illumination through the positively biased Au electrode (black line, figure 5-1), there is a feature at 3eV. This feature occurs at the same photon energy as a feature when the sample is illuminated through the positively biased ITO electrode. There are also features at 3.8eV and 4.7eV. These features are weaker than the feature at 3eV.

For illumination through the negatively biased Au electrode (red line, figure 5-1), there are two features very close together at 3.05eV and 3.3eV. The photocurrent then increases with a feature at 4.7eV. The features at 3.05eV and 3.3eV occur at the same energy as features when the sample is illuminated through the negatively biased ITO electrode. The feature at 4.7eV occurs at almost the same energy as a feature when the sample is illuminated through the positively biased Au electrode.

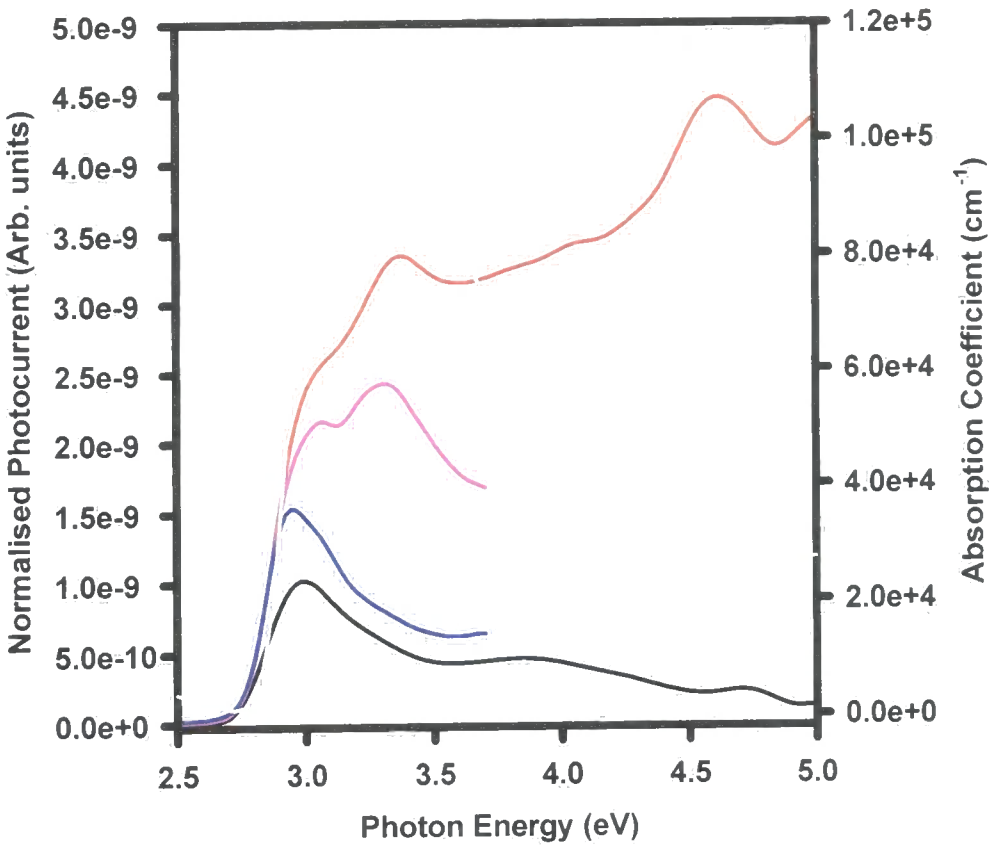


**Figure 5-1** *Photocurrent spectra for the thin PPY film (120nm) illuminated through the positively biased Au electrode (black line), through the negatively biased Au electrode (red line), through the positively biased ITO electrode (blue line) and through the negatively biased ITO electrode (pink line). The applied electric field was 16.7x10$^6$V/m. The absorption spectrum of a 120nm PPY film is shown for reference (grey line).*

## 5.3 Peak Fitting

The aim of this section is to determine the energies of the peaks for the PC spectra when illuminated through the negatively biased Au electrode (red line, figure 5-1). The energies of these peaks can then be compared to the fitted peaks for the absorption spectrum of a 100nm PPY film.

It can be seen that peaks in the PC spectrum for illumination through the negatively biased ITO electrode and for illumination through the positively biased Au electrode are also observed in the PC spectra for illumination through the negatively biased Au electrode.

By fitting peaks to the PC spectrum for illumination through the negatively biased ITO electrode and the PC spectrum for illumination through the positively biased Au electrode, it is possible to determine the energies of the peaks for illumination through the negatively biased Au electrode. The energies of these peaks can then be used to fit the absorption spectrum of PPY. It is not necessary to determine the energies of peaks fitted to the spectrum for illumination through the positively biased ITO electrode since the spectrum is almost identical to the spectrum for illumination through the positively biased Au electrode.

Electric dipole transitions are Lorenzian in shape and inhomogeneous broadening is Gaussian in shape therefore a Gaussian-Lorentzian convolution was used to give more flexibility in the shape of the fitted peaks. The fitted peaks for illumination through the negatively biased ITO electrode are shown in figure 5-2 and occur at 2.92eV, 3.08eV, 3.24eV, 3.40eV and 3.62eV. The fitted peaks for illumination through the positively biased Au electrode are shown in figure 5-3 and occur at 2.92eV, 3.08eV, 3.24eV, 3.40eV, 3.84eV and 4.74eV. The energy

difference between the first four peaks is 160meV. The significance of this energy difference will be discussed later.

Using the positions of these peaks, it is now possible to fit peaks to the spectra obtained when the sample is illuminated through the negatively biased Au electrode. These fitted peaks are shown in figure 5-4 and occur at 2.92eV, 3.08eV, 3.24eV, 3.4eV, 3.65eV, 4.08eV, 4.39eV and 4.6eV. The peak at 3.65eV corresponds closely to a fitted peak at 3.62eV for illumination through the negatively biased ITO electrode.

To determine the applicability of the above peak positions, peaks were fitted to the absorption spectra of a thin PPY film (120nm). The fitted peaks are shown in figure 5-5. The fitted peaks for the absorption spectrum occur at 2.93eV, 3.08eV, 3.23eV, 3.40eV, 3.65eV, 4.07eV, 4.39eV and 4.59eV. These compare well with the fitted peaks for the PC spectra.

The energy of the fitted peaks for the absorption spectra of PPY and the PC spectra is shown in table 5-1. The origin of the peaks at 2.92eV, 3.08eV, 3.24eV and 3.40eV is discussed in section 5.3. The origin of the peaks above 3.5eV is discussed in section 5.4.

## 5.4 Extrinsic Effects

The four fitted peaks at 2.92eV, 3.08eV, 3.24eV and 3.40eV have an energy separation of 160meV. This is the vibrational energy of a C=N bond [16] which implies that the nitrogen has a significant effect on the spectra of PPY.

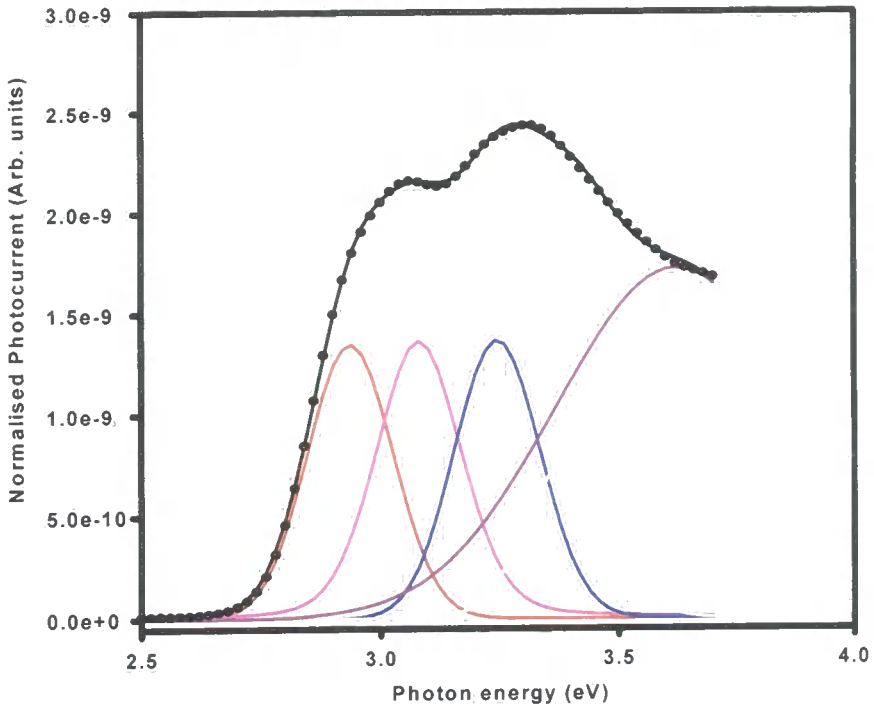


**Figure 5-2** *Data for illumination through negatively biased ITO electrode (symbols), fitted line (black line) and fitted peaks (coloured lines).*

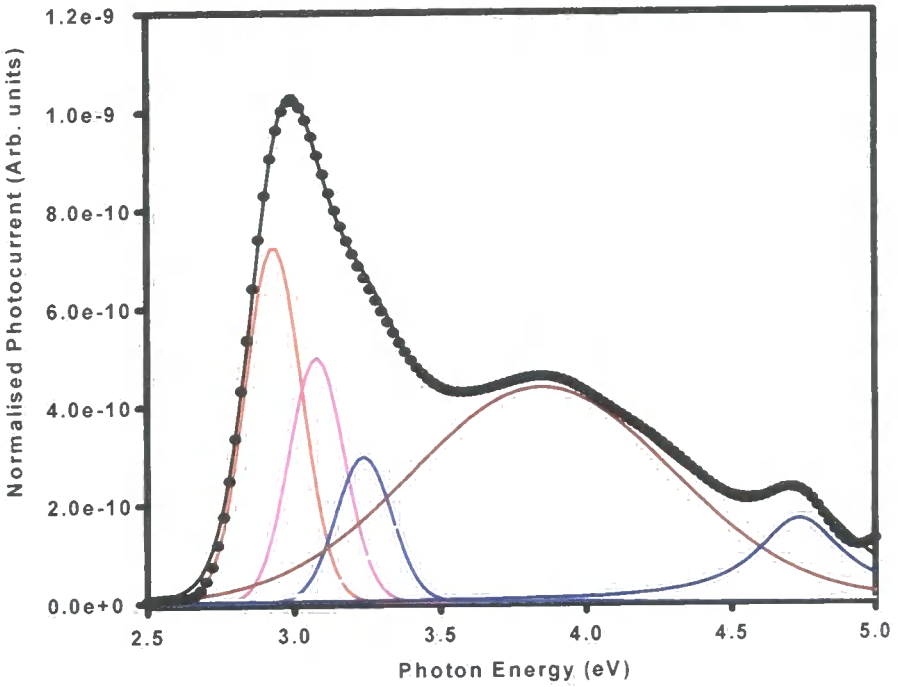


**Figure 5-3** *Data for illumination through positively biased Au electrode (symbols), fitted line (black line) and fitted peaks (coloured lines).*

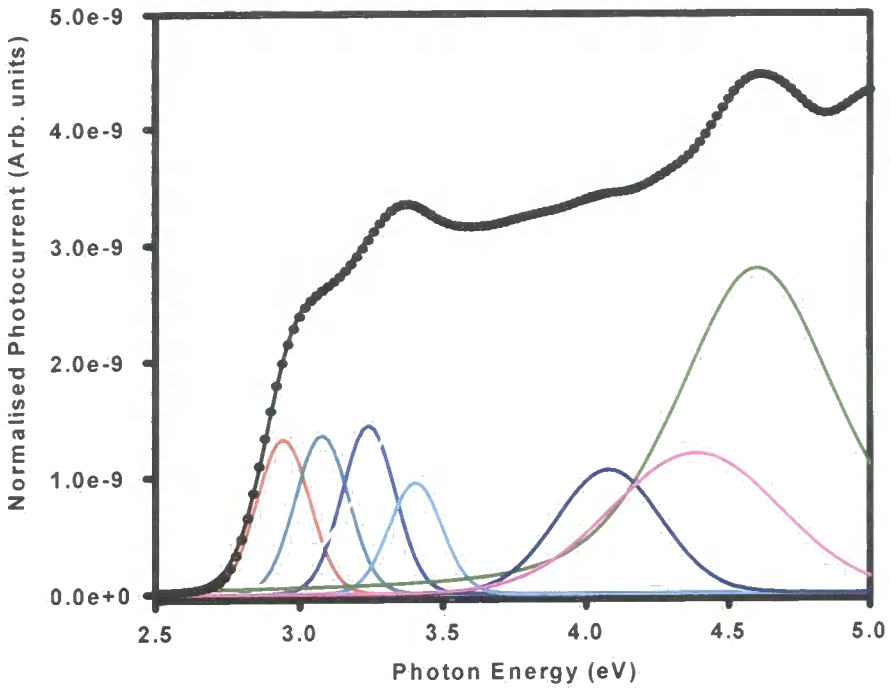


**Figure 5-4** *Data for illumination through negatively biased Au electrode (symbols), fitted line (black line) and fitted peaks (coloured lines).*

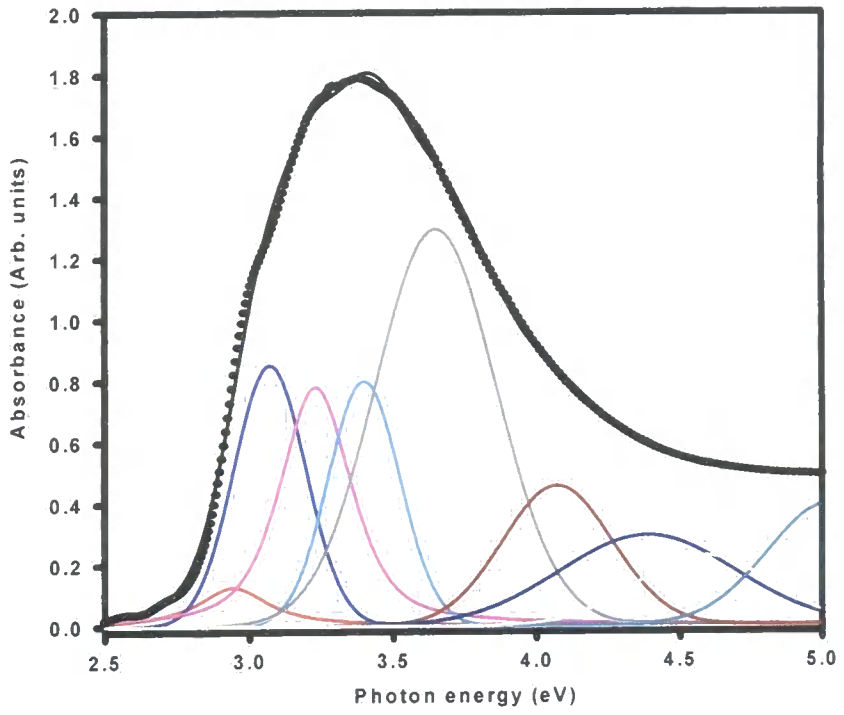


**Figure 5-5** *Data for absorbance spectra of 100nm thick PPY film (symbols), fitted line (black line) and fitted peaks (coloured lines).*

| Peak energy for illumination through positively biased Au electrode (eV) | Peak energy for illumination through negatively biased ITO electrode (eV) | Peak energy for illumination through negatively biased Au electrode (eV) | Peak energy for absorption spectrum of 120nm thick PPY film (eV) |
|---|---|---|---|
| 2.92 | 2.92 | 2.92 | 2.93 |
| 3.08 | 3.08 | 3.08 | 3.08 |
| 3.24 | 3.24 | 3.24 | 3.23 |
| 3.40 | 3.40 | 3.40 | 3.40 |
| | 3.62 | 3.65 | 3.65 |
| 3.84 | Not Applicable | 4.08 | 4.07 |
| | Not Applicable | 4.39 | 4.39 |
| 4.74 | Not Applicable | 4.60 | 4.59 |

**Table 5-1** *Peak energies for fitted peaks.*

The peak at 2.92eV is much weaker in the absorption spectrum of PPY compared to the PC spectra. This may be due to the formation of low energy excitons on aggregates. These excitons can be dissociated by impurities in the same manner as excitons formed on aggregates in MEH-PPV (see section 4.3).

The PC feature observed at 2.5eV to 3.5eV when the sample is illuminated through the positively biased Au electrode (black line, figure 5-1) is broad but does not follow the fundamental absorption peak of PPY. This feature is the same for illumination through the positively biased ITO electrode (blue line, figure 5-1). This is the antibatic response.

For illumination through the negatively biased ITO electrode (red line, figure 5-1), the photocurrent spectrum follows the absorption spectrum of PPY.

This is the symbatic response. The shape of the feature between 2.5eV and 3.5eV for illumination through the negatively biased Au electrode (red line, figure 5-1) suggests that this is also a symbatic response.

In contrast to photoconductivity spectra in MEH-PPV, the symbatic response is observed for illumination through the negatively biased electrode and the antibatic response is observed for illumination through the positively biased electrode. This suggests that, when an exciton is dissociated near the negatively biased electrode, the positively charged constituent (the hole) is transferred to the electrode. This leaves an electron that has a high enough mobility to traverse the sample and reach the positively biased electrode resulting in a photocurrent. If the exciton is dissociated near the positively biased electrode, the hole does not have a high enough mobility to reach the negatively biased electrode and a photocurrent is not observed. Experiments by Yamamoto *et al* indicate that PPY is more easily n-doped (reduced) than p-doped (oxidised) in spite of the electron lone pair on the nitrogen atom [17]. This means that the electron mobility will be higher than the hole mobility and is thus confirmed by PC experiments.

## 5.5 Intrinsic Effects

Above 3.5eV, the photocurrent increases with photon energy for illumination through the negatively biased Au electrode (red line, figure 5-1). For illumination through the positively biased Au electrode (black line, figure 5-1) above 3.5eV, the photocurrent decreases with photon energy. These two PC spectra can be compared to the spectra for illumination through the positively biased and negatively biased Au electrode of the thick MEH-PPV film (figure 4-

1). In the thick film MEH-PPV sample (7 microns), the intrinsic photocurrent increased with photon energy for illumination through the positively biased Au electrode but not for illumination through the negatively biased electrode. In the thin film MEH-PPV sample (170nm), the intrinsic photocurrent increases with photon energy for illumination through both the positively biased and negatively biased Au electrode above 3.5eV. These effects are tabulated in table 5-2.

In MEH-PPV, it was concluded that this effect was due to the electron being trapped before being able to reach the positive electrode. A space charge layer would be formed which would decrease the electric field in the polymer and thus reduce the photocurrent. Using this theory on the intrinsic photocurrent in PPY suggests that a hole would be trapped rather than an electron and that the electron mobility is much greater than the hole mobility in PPY compared to MEH-PPV where the hole mobility is greater than the electron mobility.

| PC Above 3.5eV For Thin Film MEH-PPV Sample. | | PC Above 3.5eV For Thick Film MEH-PPV Sample. | | PC Above 3.5eV For Thin Film PPY Sample. | |
|---|---|---|---|---|---|
| Illuminated Through Au Positively Biased | Illuminated Through Au Negatively Biased | Illuminated Through Au Positively Biased | Illuminated Through Au Negatively Biased | Illuminated Through Au Positively Biased | Illuminated Through Au Negatively Biased |
| PC Increases | PC Increases | PC Increases | PC Decrease | PC Decreases | PC Increases |

**Table 5-2** Comparison of intrinsic PC for thick and thin MEH-PPV and thin PPY samples.

Peak fitting of the PC spectra shows a feature at 4.74eV for illumination through the positively biased Au electrode and at 4.6eV for illumination through the negatively biased Au electrode.

Ellipsometry experiments have been performed on PPY [18]. These studies measure the rotation of the plane of polarisation upon reflection when the sample is illuminated with polarised light. The extinction coefficient (proportional to absorbance) can then be determined. These studies reveal that PPY films are highly anisotropic and this explains the features at 4.74eV and 4.6eV. The ordinary extinction coefficient (extinction coefficient parallel to the PPY chain) reproduced from [18] is shown in figure 5-6. The extraordinary extinction coefficient (extinction coefficient perpendicular to the PPY chain and across neighbouring chains) reproduced from [18] is shown in figure 5-7. It can be seen that there is a peak at 4.7eV in the extraordinary extinction coefficient that is absent in the ordinary extinction coefficient and the peaks in the PC spectra at 4.74eV and 4.6eV can therefore be ascribed to excitations perpendicular to the chain.

A close examination of the raw data reveals that the energy difference between the peaks at 4.6eV and 4.74eV is due to smoothing of the data for illumination through the positively biased Au electrode. At high photon energies, the number of photons emitted by the Xe arc lamp is less than the number of photons emitted at low photon energies. This means that the measured PC at high photon energies will be less than the measured PC at low photon energies.

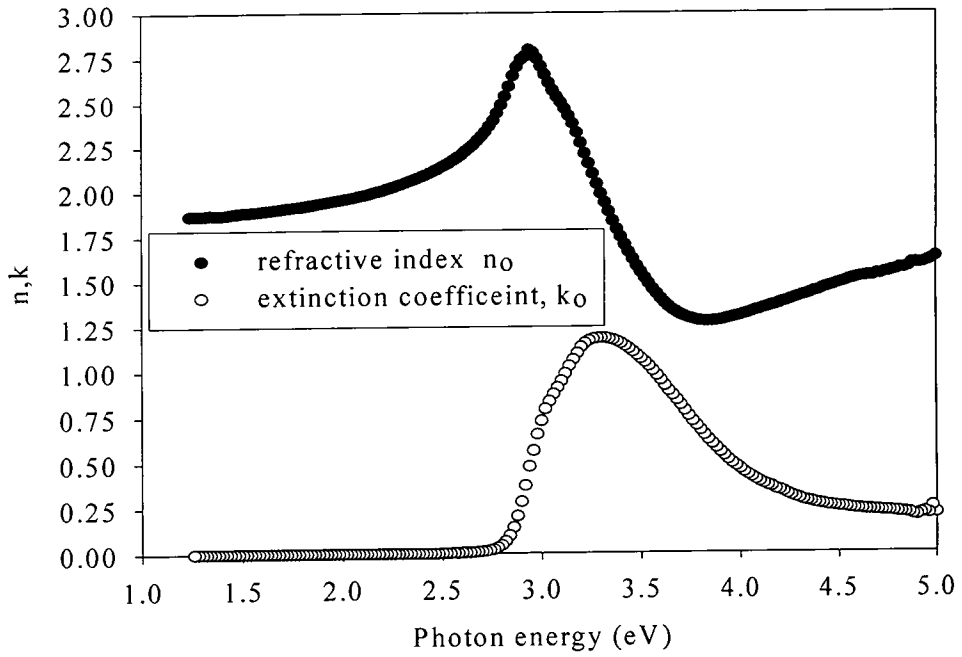


**Figure 5-6** *Ordinary refractive index and ordinary extinction coefficient from [18].*

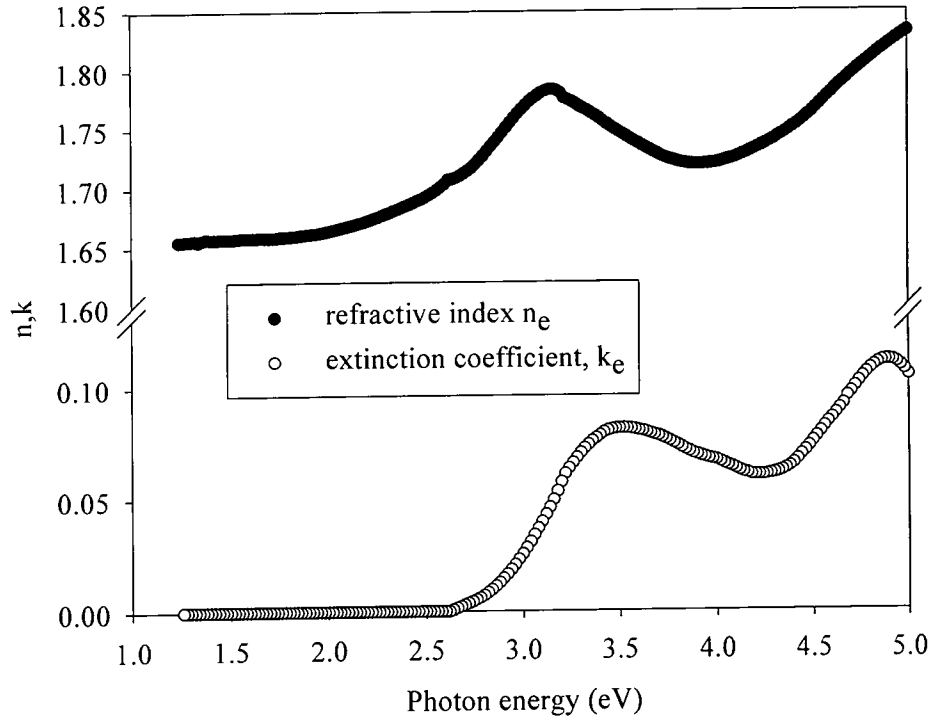


**Figure 5-7** *Extraordinary refractive index and extraordinary extinction coefficient from [18].*

The signal to noise ratio at high photon energies for illumination through the positively biased Au electrode is much less than the signal to noise ratio at high photon energies for illumination through the negatively biased Au electrode. The number of charge carriers formed when the sample is illuminated through the positively biased electrode is lower than the number of charge carriers formed when the sample is illuminated through the negatively biased electrode. This is due to trapping of holes creating a space charge layer as mentioned above.

The high photon energy data for illumination through the positively biased Au electrode was smoothed using a fast Fourier transform.

These effects make normalisation and smoothing of the PC data obtained at high photon energies for illumination through the positively biased Au electrode more difficult than for illumination through the negatively biased Au electrode or for the low energy PC data. There is therefore a greater uncertainty in the position of the peak at 4.74eV for illumination through the positively biased Au electrode.

There are two distinct features in the absorption spectrum of PPY. One occurs at 3.2eV and the other occurs at 6.2eV (see figure 2-19). Based on the data obtained for PPY, it is not possible to determine the origin of transitions between the features at 3.2eV and 6.2eV (except the feature at 4.7eV mentioned above). However, a comparison of the PC spectra obtained from PPY samples with PC spectra obtained for PF2/6 samples will resolve this issue. This comparison will be made in the next chapter.

An accurate value for the onset of intrinsic photoconduction would give a value for the exciton binding energy but cannot be obtained from this data due to extrinsic effects. An estimate of the exciton binding energy is 0.5eV.

## 5.6 Summary

The PC spectra of a 120nm PPY film sandwiched between Au and ITO has been measured. It has been determined that the electron mobility is much greater than the hole mobility. This is in contrast to MEH-PPV. Peaks have been fitted to the fundamental optical excitation in the PC spectra and the fundamental absorption peak. The vibronic energy separation of the fundamental absorption peak was measured to be 160meV and suggests that the nitrogen atom has a significant effect on the PC spectra. A comparison between PPY and PF2/6 will be made in the next chapter and the effect of the nitrogen atom on the PC spectra will be discussed. As with MEH-PPV, impurities have the effect of aiding dissociation of excitons formed on aggregates and an increase in the intensity of the low energy PC peak of the fundamental optical excitation is observed.

# References


1. J.M. Lupton, I.D.W. Samuel, and A.P. Monkman, *Synthetic Metals*, **102** 1079-1080 (1999).
2. S. Barth, H. Bassler, H. Rost, and H.H. Horhold, *Physical Review B-Condensed Matter*, **56** 3844 (1997).
3. H. Bassler, *Macromolecular Symposia*, **104** 269-284 (1996).
4. N. Chawdhury, A. Kohler, M.G. Harrison, D.H. Hwang, A.B. Holmes, and R.H. Friend, *Synthetic Metals*, **102** 871-872 (1999).
5. T.K. Daubler, D. Neher, H. Rost, and H.H. Horhold, *Physical Review B-Condensed Matter*, **59** 1964-1972 (1999).
6. M.G. Harrison, J. Gruner, and G.C.W. Spencer, *Physical Review B-Condensed Matter*, **55** 7831-7849 (1997).
7. A. Kohler, D.A. dosSantos, D. Beljonne, Z. Shuai, J.L. Bredas, R.H. Friend, S.C. Moratti, and A.B. Holmes, *Synthetic Metals*, **84** 675-676 (1997).
8. S.B. Lee, K. Yoshino, J.Y. Park, and Y.W. Park, *Physical Review B*, **61** 2151-2158 (2000).
9. H.D. Burrows, M.D. Miguel, A.P. Monkman, L.E. Horsburgh, I. Hamblett, and S. Navaratnam, *Journal of Chemical Physics*, **112** 3082-3089 (2000).
10. F. Feller and A.P. Monkman, *Synthetic Metals*, **116** 149-152 (2001).
11. L.J. Hartwell, M.E. Vaschetto, L.E. Horsburgh, and A.P. Monkman, *Synthetic Metals*, **101** 807-808 (1999).

12. A.P. Monkman, M. Halim, I.D.W. Samuel, and L.E. Horsburgh, *Journal of Chemical Physics*, **109** 10372-10378 (1998).

13. A.P. Monkman, M. Halim, S. Dailey, I.D.W. Samuel, and L. Horsbrugh, *Synthetic Metals*, **101** 253-254 (1999).

14. F. Feller and A.P. Monkman, *Physical Review B*, **61** 13560-13564 (2000).

15. F. Feller and A. Monkman, *Applied Physics Letters*, **76** 664-666 (2000).

16. A.P. Monkman, M. Halim, S. Dailey, I.D.W. Samuel, and L. Horsbrugh, *Synthetic Metals*, **101** 253-254 (1999).

17. T. Yamamato, *J. Am. Chem. Soc.*, **116** 4832-4845 (1994).

18. A. Monkman, *Society of Plastic Engineers*, **57** 109-117 (1999).

# Chapter 6

# Photoconduction in PF2/6

# 6.1 Introduction

Photoconductivity experiments have been performed on a different variation of polyfluorene (poly(9,9-dioctyl)fluorene) [1]. In this chapter, a comparison will be made between poly(9,9-bis(2-ethylhexyl)fluorene-2,7-diyl) (PF2/6) and PPY. The conjugated backbone structure of PF2/6 is similar to PPY. The chemical structures of the PPY and PF2/6 molecules are shown in figures 6-1 and 6-2 respectively. The main difference between PF2/6 and PPY is that, in PPY, a nitrogen atom has replaced a CH group. The presence of the nitrogen atom should affect the optical and electronic properties of PPY. The second difference between PF2/6 and PPY is that PF2/6 has a large side group whereas PPY has no sidegroups. This will influence the packing and order of the polymers when spin coated onto a substrate. The absorbance spectra of PPY and PF2/6 are also similar and are shown in figure 6-3. The fundamental absorption peaks of both PPY and PF2/6 occur at 3.5eV. Higher energy absorption peaks (above 5eV) of PPY and PF2/6 do not occur at the same energies.

The first part of this chapter is a comparison of the experimental data obtained from the PC spectra of PPY and PF2/6. The second part discusses extrinsic charge carrier generation. The third section discusses intrinsic charge carrier generation. The effects of the nitrogen atom in PPY will then be discussed. The main effect of the nitrogen atom is the addition of peaks in the PC spectra of PPY that are absent in the PC spectra of PF2/6.

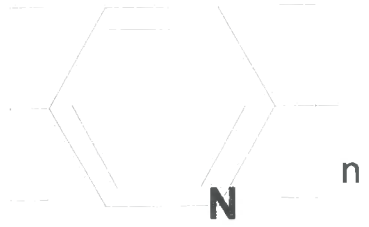


**Figure 6-1** *Chemical structure of PPY molecule.*

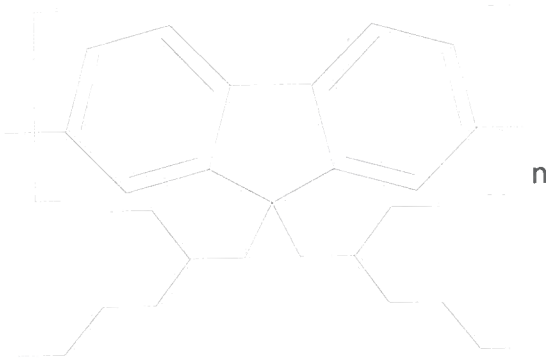


**Figure 6-2** *Chemical structure of PF2/6 molecule.*

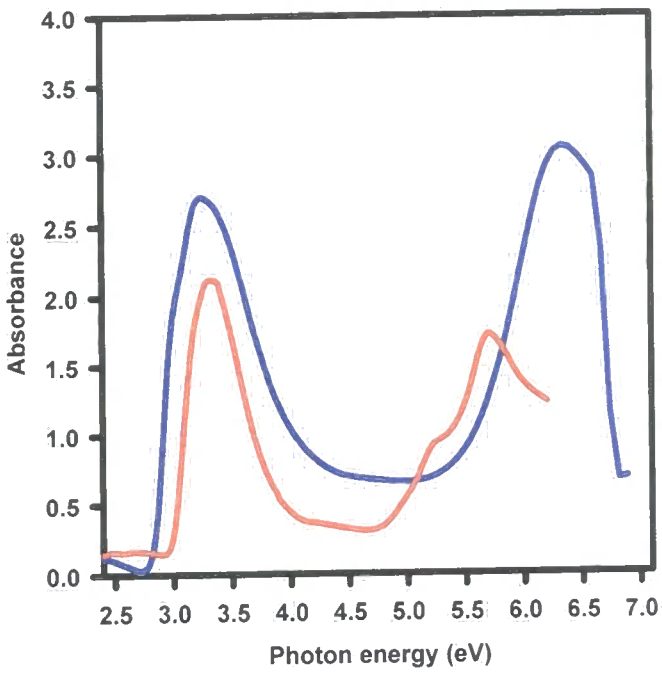


**Figure 6-3** *Absorbance spectrum of PPY (blue line) and PF2/6 (red line).*

## 6.2 Experimental Data

Steady state photoconductivity measurements were made on PF2/6 films sandwiched between an ITO coated glass substrate and a semitransparent Au electrode. The method used to obtain the photoconductivity spectra is given in section 3.4 and the method used to normalise the spectra for the effects of the illumination source (Xe or W lamp) is given in section 3.5.

The photoconductivity spectra for illumination through the Au electrode and illumination through the ITO electrode with the illuminated electrode positively biased and the illuminated electrode negatively biased for a thick film PF2/6 sample (6 microns) are shown in figure 6-4. Experiments were performed at 290K. No response to light was observed for thin film PF2/6 samples (120nm). A large dark current was measured. This may indicate that injection of charge carriers was giving rise to a current much larger than the photocurrent.

For illumination through the positively biased Au electrode (red line, figure 6-4), there are broad features at 3.2eV and 4.75eV. For illumination through the negatively biased Au electrode (black line, figure 6-4), there is a sharp feature at 2.8eV and a broad feature at 4.65eV. For illumination through the positively biased ITO electrode (pink line, figure 6-4), there is one broad feature at 3.2eV.

For illumination through the negatively biased ITO electrode (blue line, figure 6-4), there is one sharp feature at 2.8eV. It was not possible to obtain PC spectra at higher photon energies for illumination through the ITO electrode due to absorption by the glass substrate. These features are summarised in table 6-1 ("Not Applicable" indicates that it was not possible to obtain PC spectra at photon

energies appropriate to the peak being observable due to absorption of the glass substrate).

The spectra for photoconductivity in a thin film PPY sample shown in figure 5-1 has been reproduced in figure 6-5 so that the spectra for the thin film PPY sample and the thick film PF2/6 sample can be compared. Features observed in the PC spectra of PPY are summarised in table 6-2 and will be discussed in sections 6.3, 6.4 and 6.5.

| **Illumination Through Positively Biased Au Electrode** | **Illumination Through Negatively Biased Au Electrode** | **Illumination Through Positively Biased ITO Electrode** | **Illumination Through Negatively Biased ITO Electrode** |
|---|---|---|---|
| | 2.8eV | | 2.8eV |
| 3.2eV | | 3.2eV | |
| 4.75eV | 4.65eV | Not Applicable | Not Applicable |

**Table 6-1:** Features observed in PF2/6 spectra.

| **Illumination Through Positively Biased Au Electrode** | **Illumination Through Negatively Biased Au Electrode** | **Illumination Through Positively Biased ITO Electrode** | **Illumination Through Negatively Biased ITO Electrode** |
|---|---|---|---|
| 2.75 to 3.5eV | | 2.75 to 3.5eV | |
| | 2.8 to ~3.7eV | | 2.8 to ~3.7eV |
| ~3.8eV | ~3.8eV | Not Applicable | Not Applicable |
| 4.74eV | 4.6eV | Not Applicable | Not Applicable |

**Table 6-2:** *Features observed in PPY spectra.*

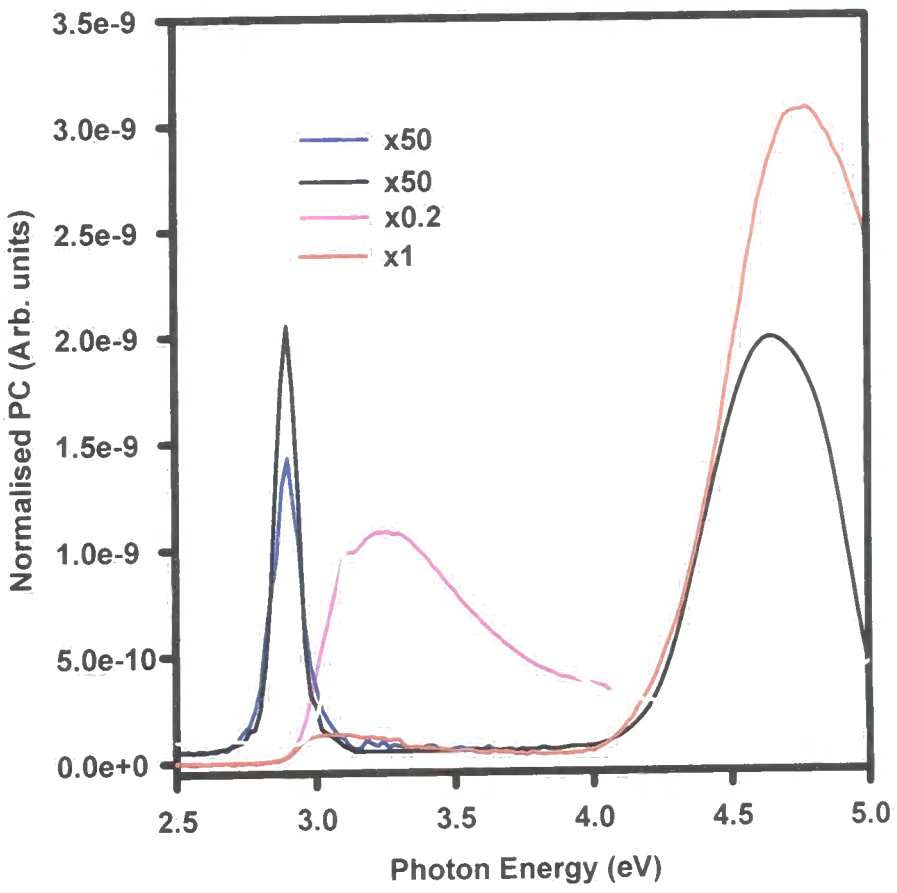


**Figure 6-4** *Photocurrent spectra for the thick PF2/6 film (6 microns) illuminated through the positively biased Au electrode (red line), through the negatively biased Au electrode (black line), through the positively biased ITO electrode (pink line) and through the negatively biased ITO electrode (blue line). The absorbance spectrum of a 120nm PF2/6 film is shown for reference (grey line, linear scale). The applied electric field was $11.7 \times 10^6$ V/m. The spectra have been multiplied by different factors (0.2 or 50) so that a comparison can be made between the spectra.*

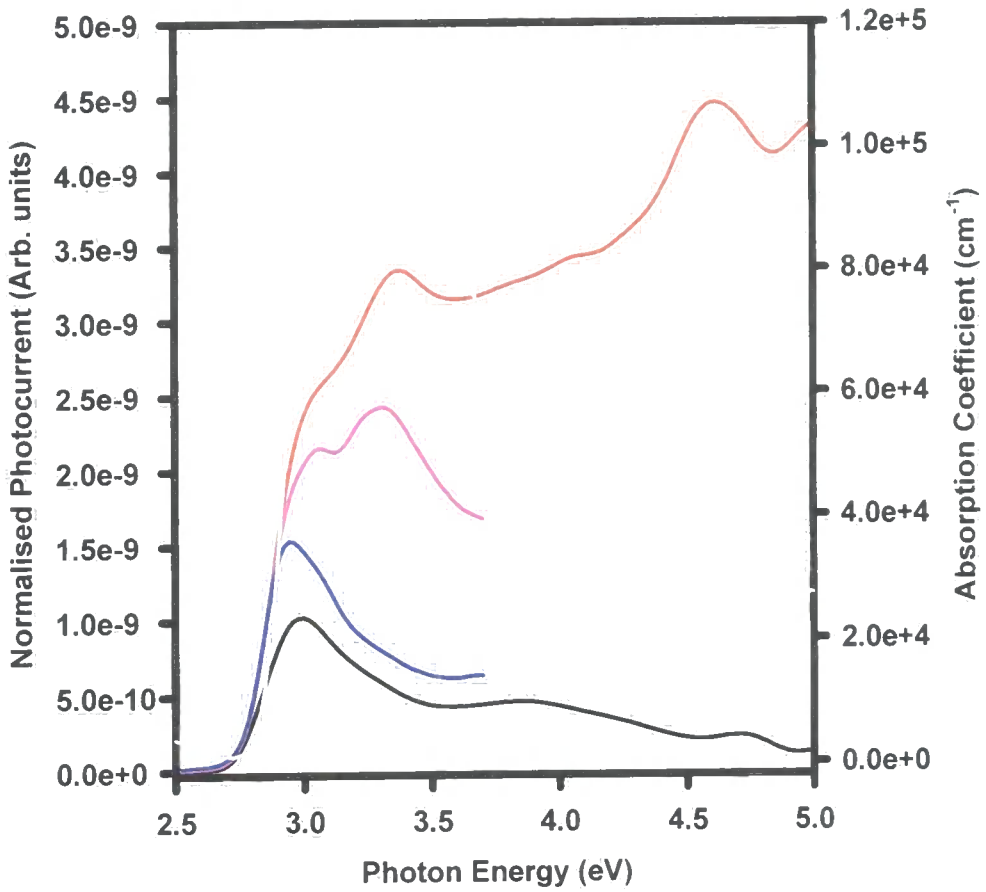


**Figure 6-5** *Photocurrent spectra for the thin PPY film (120nm) illuminated through the positively biased Au electrode (black line), through the negatively biased Au electrode (red line), through the positively biased ITO electrode (blue line) and through the negatively biased ITO electrode (pink line). The absorbance spectrum of a 120nm PPY film is shown for reference (grey line). The applied electric field was $16.7 \times 10^6$ V/m (reproduced from figure 5-1).*

## 6.3 Extrinsic Effects

For illumination through both the negatively biased ITO and Au electrode of the PF2/6 sample, there is a sharp peak 2.8eV. This occurs at the fundamental absorption edge of PF2/6. For illumination though both the positively biased ITO and Au electrode, the PC spectra follows the fundamental absorption peak of PF2/6. Based on effects already observed in PPY and MEH-PPV, it can be inferred that, for illumination through the negatively biased Au or ITO electrode, the sharp peak at 2.8eV is the antibatic effect and is due to absorption by the polymer film. For illumination through the positively biased Au or ITO electrode, the broad peak at 3.2eV is the symbatic response. This suggests that the hole mobility in PF2/6 is greater than the electron mobility.

The electron mobility in PF2/6 has not been measured. It has been determined that the hole mobility in PF2/6 is of the order of $10^{-4}$ $cm^2/Vs$ at electric fields of the order of $10^5$ V/cm at room temperature [2, 3]. The hole mobility in PF2/6 is three orders of magnitude greater than the hole mobility in MEH-PPV and four orders of magnitude greater than the electron mobility in MEH-PPV at similar electric fields and temperatures [4]. Experiments by Yamamoto *et al* indicate that PPY is more easily n-doped (reduced) than p-doped (oxidised) in spite of the electron lone pair on the nitrogen atom [5]. This means that the electron mobility in PPY will be higher than the hole mobility and is confirmed by PC experiments. The relative electron and hole mobilities of PPY, MEH-PPV and PF2/6 are summarised in table 6-3.

| MEH-PPV | PPY | PF2/6 |
|---|---|---|
| Hole Mobility Greater Than Electron Mobility | Electron Mobility Greater Than Hole Mobility | Hole Mobility Greater Than Electron Mobility |

**Table 6-3** *Comparison of electron and hole mobility in MEH-PPV, PPY and PF2/6 inferred from PC data.*

The symbatic peak for illumination through the positively biased ITO electrode is 40 times greater than the symbatic peak for illumination through the positively biased Au electrode. This can be attributed to impurities sinking to the ITO interface during the drop casting process. These impurities will aid exciton dissociation as discussed in section 4.3 for MEH-PPV samples. There is a small peak at 3.1eV in the symbatic response for illumination through the positively biased ITO electrode. This can be attributed to the formation of aggregates during the drop casting process. Excitons formed on these aggregates will have a lower energy than those formed elsewhere. Impurities will also aid dissociation of these excitons as discussed in section 4.3 for MEH-PPV samples.

## 6.4 Intrinsic Effects

For illumination through the positively biased Au electrode of the PF2/6 sample (red line, figure 6-4), there is a peak at 4.75eV. For illumination through the negatively biased Au electrode of the PF2/6 sample (black line, figure 6-4), there is a peak at 4.65eV. For illumination through the negatively biased Au

electrode of the PPY sample (red line, figure 6-5), there is a peak at 4.60eV. For illumination through the positively biased Au electrode of the PPY sample (black line, figure 6-5), there is a peak at 4.74eV.

The origin of the feature at ~4.7eV for PPY was discussed in section 5.5. It was determined that this feature was due to intrinsic excitations perpendicular to the polymer chain, possibly from one chain to another. This effect must be the same for PF2/6 as for PPY since the peaks occur at almost the same energy.

The energy difference between the peaks at 4.60eV and 4.74eV for PPY is due to smoothing of the data for illumination through the positively biased Au electrode. This was discussed in section 5.5. This effect also accounts for the energy difference between the peaks at 4.75eV and 4.65eV for PF2/6.

In the case of PF2/6, the signal to noise ratio at high photon energies for illumination through the negatively biased Au electrode is much less than the signal to noise ratio at high photon energies for illumination through the positively biased Au electrode.

The intensity of the peak at 4.75eV for illumination through the positively biased Au electrode is 80x greater than the intensity of the peak at 4.65eV for illumination through the negatively biased Au electrode. Based on results obtained from PPY and MEH-PPV, it has been determined that, when a high energy photon is absorbed, free charge carriers are generated (intrinsic carrier generation). The intrinsic PC spectra for the 6 micron thick film PF2/6 sample is very similar to the PC spectra for the thick film (7 microns) MEH-PPV sample. The intrinsic PC spectra for illumination through the positively biased Au electrode for the thick film MEH-PPV sample is much larger than for illumination through the negatively biased Au electrode (see figure 4-1). This effect can

therefore be attributed to the difference in carrier mobility as discussed in section 4.4 for MEH-PPV samples.

## 6.5 PPY and PF2/6 – The Nitrogen Atom

Analysis of the PC spectra of PPY of PF2/6 samples indicates that there is a feature at 3.8eV in the PC spectra of PPY that is absent from the PC spectra of PF2/6. It is believed that this feature is due to transitions involving the electron lone pair in the PPY molecule.

Quantum chemical calculations on PPY indicate that the lowest transition involving the nitrogen lone pair is the $n \rightarrow \pi_1^*$ transition and occurs at more than 1eV above the $\pi_1 \rightarrow \pi_1^*$ transition [6-8]. Semiempirical quantum chemical calculations on the *trans*- head to head and *trans*- head to tail bonding configurations (see section 2.4.3) suggest that transitions involving the nitrogen atom occur at 4.6eV and 5.2eV [9].

The nitrogen lone pair is not conjugated with the $\pi$ cloud surrounding the chain but sticks out perpendicular to it. It is therefore probable that transitions involving the lone pair are interchain.

Using the data obtained from the PC spectra for PPY and PF2/6 samples it is now possible to determine the optical transitions of both PPY and PF2/6. Energy level diagrams for PPY and PF2/6 are shown in figures 6-6 and 6-7 respectively. Blue lines indicate that the transition was observed in the absorption spectrum of the polymer, red lines indicate that the transition was observed in the PC spectra and blue and red lines together indicate that the transition was observed in both the absorption spectrum and the PC spectrum.

The energy and origin of all the transitions in PPY are shown in table 6-4. The energy and origin of all the transitions in PF2/6 are shown in table 6-5.

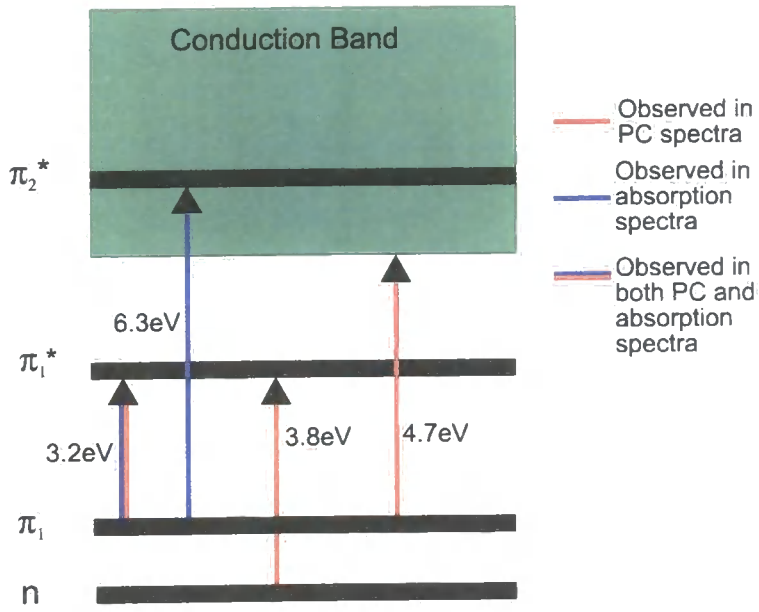


**Figure 6-6** *Energy level diagram for features observed in the absorption spectra and PC spectra of PPY samples.*

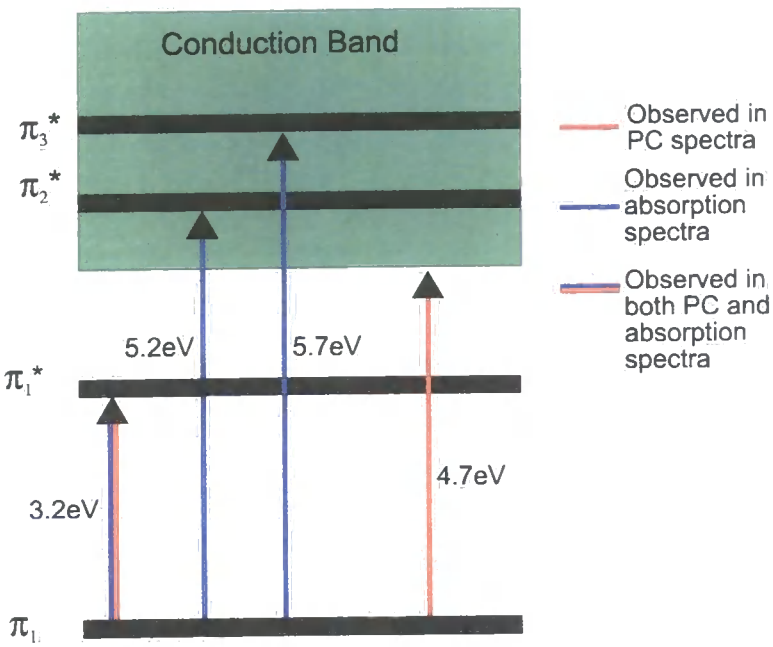


**Figure 6-7** *Energy level diagram for features observed in the absorption spectra and PC spectra of PF2/6 samples.*

| Energy (eV) | Origin of Feature |
|---|---|
| 3.2 | Optical transition from $\pi_1$ to $\pi_1^*$ (absorption of a photon forms an exciton which can be dissociated extrinsically at an electrode to form a free charge carrier and gives rise to a photocurrent) |
| 3.8 | Optical excitation involving the electron lone pair (ascribed to an interchain process resulting in the formation of a free charge carrier giving rise to a photocurrent) |
| 4.7 | Optical excitation perpendicular to the chain from one chain to another resulting in the formation of a free charge carrier and gives rise to a photocurrent |
| 6.3 | Optical transition from $\pi_1$ to $\pi_2^*$ (not able to illuminate the sample at such high photon energy) |

**Table 6-4** *Origin of features observed in the absorption spectrum of PPY and the PC spectra.*

| Energy (eV) | Origin of Feature |
|---|---|
| 3.2 | Optical transition from $\pi_1$ to $\pi_1^*$ (absorption of a photon forms an exciton which can be dissociated extrinsically at an electrode to form a free charge carrier and gives rise to a photocurrent) |
| 4.7 | Optical excitation perpendicular to the chain from one chain to another resulting in the formation of a free charge carrier and gives rise to a photocurrent |
| 5.2 | Optical transition from $\pi_1$ to $\pi_2^*$ (not able to illuminate the sample at such high photon energy) |
| 5.7 | Optical transition from $\pi_1$ to $\pi_3^*$ (not able to illuminate the sample at such high photon energy) |

**Table 6-5** *Origin of features observed in the absorption spectrum of PF2/6 and the PC spectra.*

## 6.6 Summary

The PC spectra of a 6 micron thick PF2/6 film sandwiched between Au and ITO electrodes has been measured. It has been determined that hole mobility is greater than electron mobility. The effects of aggregates and impurities have been observed. A comparison with PPY has been made. Excitations involving the nitrogen atom in PPY have been elucidated due to their absence in the PC spectra in PF2/6 samples. Excitations perpendicular to the chain have been observed in PF2/6 samples and are also seen in PPY samples. Energy level diagrams have been obtained for both PPY and PF2/6 from the PC data obtained.

# References


1. A.J. Cadby, P.A. Lane, H. Mellor, S.J. Martin, M. Grell, C. Giebeler, D.D.C. Bradley, M. Wohlgenannt, C. An, and Z.V. Vardeny, *Physical Review B*, **62** 15604-15609 (2000).
2. M. Redecker, D.D.C. Bradley, M. Inbasekaran, and E.P. Woo, *Applied Physics Letters*, **73** 1565-1567 (1998).
3. A.J. Campbell, D.D.C. Bradley, and H. Antoniadis, *Journal of Applied Physics*, **89** 3343-3351 (2001).
4. L. Bozano, S.A. Carter, J.C. Scott, G.G. Malliaras, and P.J. Brock, *Applied Physics Letters*, **74** 1132-1134 (1999).
5. T. Yamamato, *J. Am. Chem. Soc.*, **116** 4832-4845 (1994).
6. A.J. Epstein, J.W. Blatchford, Y.Z. Wang, S.W. Jessen, D.D. Gebler, L.B. Lin, T.L. Gustafson, H.L. Wang, Y.W. Park, T.M. Swager, and A.G. MacDiarmid, *Synthetic Metals*, **78** 253-261 (1996).
7. M.E. Vaschetto, A.P. Monkman, and M. Springborg, *Theochem-Journal Of Molecular Structure*, **468** 181-191 (1999).
8. M.E. Vaschetto, B.A. Retamal, A.P. Monkman, and M. Springborg, *Journal of Physical Chemistry a*, **103** 11096-11103 (1999).
9. J. Blatchford, *J.Chem.Phys*, **105** 9214-9226 (1996).

# Chapter 7

# Conclusions

## 7.1 MEH-PPV

Samples of thick (7 microns) and thin (170nm) poly(2-methoxy-5-(2'ethylhexyloxy)-1,4-phenylene vinylene) (MEH-PPV) polymer films sandwiched between ITO and semitransparent Au electrodes were fabricated. Photocurrent spectra were obtained for illumination through either the Au or ITO electrode for different bias polarities. The electric field and temperature dependence of the photocurrent was obtained as a function of photon energy.

Between 2eV and 3eV, absorption of a photon in the MEH-PPV film excites an electron from the $\pi_1$ molecular orbital to the $\pi_1^*$ molecular orbital. This electron does not have enough energy to escape the coulombic attraction of the hole. The electron becomes bound to the hole and this entity is known as an exciton. The exciton may find it energetically favourable to transfer the electron to the positive electrode due to the presence of impurities at the polymer/electrode interface. This leaves a hole that will be attracted to the negative electrode under the influence of the electric field and contributes to the photocurrent. Excitons are created throughout the polymer but only those formed at the positive electrode can dissociate to form free charge carriers. From the response of the photocurrent to different directions of illumination and bias polarities, we conclude that the hole mobility is greater than the electron mobility.

Above 3eV, absorption of a photon in the bulk MEH-PPV film excites an electron from either the $\pi_1$ or $\pi_2$ orbital to the $\pi_1^*$ or $\pi_2^*$ orbital. This leaves a hole in either the $\pi_1$ or $\pi_2$ orbital. The electron has enough energy to overcome the coulombic attraction of the hole and free charge carriers are formed. This is known as intrinsic photogeneration of charge carriers.

In thin film MEH-PPV samples, both the electron and hole mobility have no effect on the intrinsic photocurrent since the electron and hole have mobilities large enough for the electron and hole to traverse the polymer layer and reach the positive and negative electrode respectively. If the excited electron is photogenerated near the positively biased electrode (the sample is illuminated through the positively biased electrode), the excited electron has a sufficiently high mobility to reach the positive electrode. The hole will then be able to reach the negative electrode and a photocurrent will be observed.

In thick MEH-PPV film samples, the excited electron does not have a large enough mobility to reach the positive electrode if it is photogenerated near the negative electrode (the sample is illuminated through the negatively biased electrode). The excited electron will travel a certain distance and then become trapped. This has the effect of creating a space charge layer that will decrease the electric field that the hole will observe and the photocurrent will be reduced compared to the photocurrent produced for charge carriers generated near the positively biased electrode.

The intrinsic photocurrent spectra for charge carriers generated at the positively biased Au electrode may be fitted using peaks corresponding to peaks in the optical absorption spectrum of MEH-PPV. Peak fitting suggests that, as the photon energy increases, more electrons are gaining enough energy to avoid the coulombic attraction of the hole.

Aggregates may form in the MEH-PPV solution before it is drop cast or spin coated onto the ITO coated substrate. This is due to the effect of the solvent used to form solutions of MEH-PPV. The solvent chlorobenzene has a preferential interaction with the aromatic backbone of the polymer chain and the

chains adopt a rigid open conformation in solution. With the backbone open and exposed, it is easily possible for the π electrons on one chain to overlap with those on another chain and aggregation of the polymer chains can occur. These aggregates may remain once the solution has been drop cast or spin coated onto the ITO coated substrate. Aggregates may also form as the solvent is evaporating during the drop casting process. These aggregates will have a lower energy than polymer chains that are not aggregated. Excitons formed on these chains will have a lower energy than excitons not formed on aggregates. The energy needed for excitons formed on aggregates to dissociate will therefore be greater than the energy needed for excitons not formed on aggregates to dissociate.

The photocurrent increases exponentially with electric field for excitons dissociated extrinsically at both the Au electrode and the ITO electrode. The temperature dependence of the extrinsic photocurrent for excitons dissociated at the Au electrode is different to the temperature dependence of the extrinsic photocurrent for excitons dissociated at the ITO electrode for thick polymer films. As temperature increases, the photocurrent also increases. The photocurrent increase is very small when the temperature is increased from 200K to 300K for excitons dissociated extrinsically at the Au electrode. The photocurrent increase is much greater when the temperature is increased from 200K to 300K for excitons dissociated extrinsically at the ITO electrode compared to excitons dissociated extrinsically at the Au electrode. We suggest that, during operation of an ITO/MEH-PPV/metal sample, oxygen from the ITO electrode diffuses into the MEH-PPV and forms carbonyl species in the MEH-PPV. Carbonyl formation produces a loss of conjugation in the polymer backbone and an interfacial layer is produced between the ITO and the MEH-PPV. Charge mobility through this

interfacial layer will be lowered and the interfacial layer can be thought of as a barrier to charge transport. Charge transport through this interfacial layer (tunnelling) will then be temperature dependent. There is no loss of conjugation at the Au/MEH-PPV interface so, for excitons photogenerated near the positively biased Au electrode, the exciton is dissociated extrinsically as above.

The photocurrent increases exponentially with electric field for charge carriers intrinsically photogenerated at 4eV near the positively biased Au electrode in the thick MEH-PPV film.

There are two regimes in the temperature dependence of the photocurrent for charge carriers photogenerated at 4eV near the positively biased Au electrode. The photocurrent increases linearly with temperature with a discontinuity at 245K. We suggest that below 245K, the MEH-PPV monomers are frozen with respect to adjacent monomers. The temperature dependence of the photocurrent is similar to the temperature dependence of the electron and hole mobility. We therefore suggest that the mobility of charge carriers photogenerated intrinsically results in the temperature dependence of the observed intrinsic photocurrent.

The electric field and temperature dependence of charge carrier mobility obscures the electric field and temperature dependence of charge carrier generation.

## 7.2 PPY

Samples of thin (120nm) poly(2,5-pyridinediyl) (PPY) films sandwiched between ITO and semitransparent Au electrodes were fabricated. Photocurrent

spectra were obtained for illumination through either the Au or ITO electrode for different bias polarities.

Between 2.5eV and 3.5eV, absorption of a photon in the PPY film excites an electron from the $\pi_1$ molecular orbital to the $\pi_1$* molecular orbital. This leaves a hole in the $\pi_1$ orbital. The electron is bound to the hole as an exciton. The exciton may be dissociated extrinsically at the negative electrode to form free charge carriers. From the response of the photocurrent to different directions of illumination and bias polarities, we conclude that the electron mobility is greater than the hole mobility.

Peak fitting of the extrinsic PC spectra shows that the vibronics have an energy separation of 160meV. This corresponds to C=N vibrations.

Above 3.5eV, absorption of a photon in the bulk PPY film excites an electron from $\pi_1$ to the $\pi_1$* orbital. This leaves a hole in the $\pi_1$ orbital. The electron has enough energy to avoid the coulombic attraction of the hole and free charge carriers are formed. If the free hole is photogenerated near the negatively biased electrode (the sample is illuminated through the negatively biased electrode), the free hole has a high enough mobility to reach the negative electrode. The electron will then be able to reach the positive electrode and a photocurrent will be observed. The free hole does not have a large enough mobility to reach the negative electrode if it is photogenerated near the positive electrode (the sample is illuminated through the positively biased electrode). The free hole will travel a certain distance and then become trapped. This has the effect of creating a space charge layer that will decrease the electric field that the electron will observe and the photocurrent will be reduced compared to the

photocurrent produced for charge carriers generated near the negatively biased electrode.

There is a peak at 4.7eV in the photocurrent spectrum. This does not correspond to a peak in the absorption spectrum of PPY. Based on ellipsometry measurements, we conclude that free charge carriers are being formed from excitations perpendicular to the chain and that all other features of the photocurrent spectra are due to charge carriers being formed from excitations parallel to the chain.

## 7.3 PF2/6

Samples of thick (6 microns) poly(9,9-bis(2-ethyl hexyl)fluorene-2,7-diyl) (PF2/6) films sandwiched between ITO and semitransparent Au electrodes were fabricated. Photocurrent spectra were obtained for illumination through either the Au or ITO electrode for different bias polarities.

The symbatic and antibatic effects were observed for photon energies appropriate to the fundamental absorption peak of PF2/6 . The data confirms that the hole mobility is greater than the electron mobility in PF2/6.

PF2/6 is very similar to PPY and a comparison was made between the PC spectra of PF2/6 samples and the PC spectra of PPY samples. A peak was observed in the PC spectra at 4.7eV. This peak was also observed in the PC spectra for PPY samples. This was therefore ascribed to the effects of excitations perpendicular to the chain. The effect of the electron lone pair associated with the nitrogen atom in PPY was determined from a comparison with PF2/6 since there

is no nitrogen atom in PF2/6. It was determined that excitations involving the nitrogen lone pair occur at ~3.8eV.

## 7.4 What Next ?

It is not possible to determine an accurate value for the exciton binding energy from the experiments performed above due to the presence of extrinsic effects. It would be possible to remove the extrinsic effects from the MEH-PPV spectra by the addition of a thin film of silicon monoxide (SiO) between the polymer and the electrode. Extrinsic dissociation of excitons in MEH-PPV takes place when the negative constituent of the exciton (the electron) is transferred to the positively biased electrode. This is the same as injecting a hole from the positively biased electrode into the polymer. The SiO layer has energy levels that would introduce a barrier to prevent photoinjection of positive charge carriers from the electrode into the polymer while affecting the discharge of charge carriers only weakly. Extrinsic dissociation of excitons cannot, therefore, take place and only intrinsic photogeneration of charge carriers can take place. The addition of an SiO layer between PPY and the electrode will not remove the extrinsic effects since the energy levels in SiO are not conducive to this process.

The experimental method used in this work can be applied to other conjugated polymers and the photon energy, electric field and temperature dependence of the photocurrent can be obtained. The electric field and temperature dependence of the photocurrent can be compared with the temperature and electric field dependence of the charge carrier mobility obtained from current-voltage measurements. Charge carrier photogeneration and transport

mechanisms can then be determined and then modelled. This will allow conjugated polymers to be tailored for such applications as LED's and, perhaps one day, flexible displays.